AD-A118 272 NAVAL POSTGRADUATE SCHOOL MONTEREY CA F/G 11/4
POSTBUCKLING BEHAVIOR OF GRAPHITE/EPOXY CLOTH SHEAR PANELS WITH--ETC(U)
MAR 82 R J HERMAN

UNCLASSIFIED NL

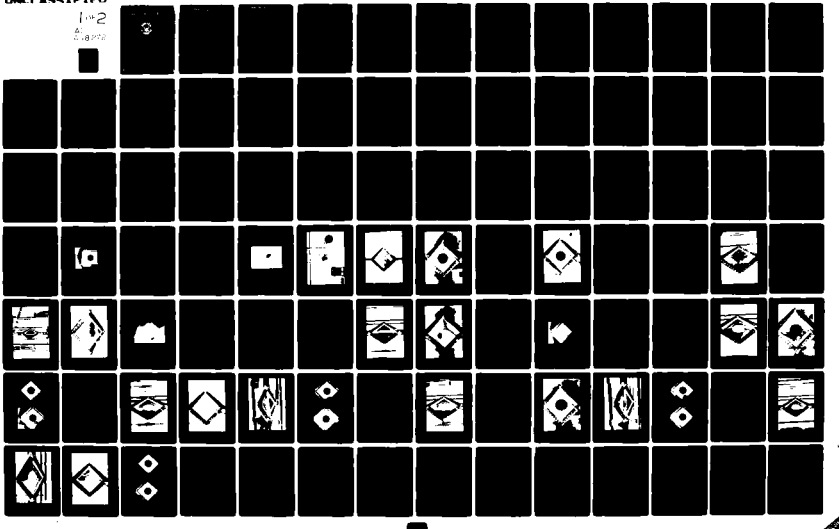

NAVAL POSTGRADUATE SCHOOL
Monterey, California

THESIS

POSTBUCKLING BEHAVIOR
OF GRAPHITE/EPOXY CLOTH SHEAR PANELS
WITH 45°-FLANGED LIGHTENING HOLES

by

Richard John Herman

March 1982

Thesis Advisor: M. H. Bank

Approved for public release; distribution unlimited

UNCLASSIFIED

SECURITY CLASSIFICATION OF THIS PAGE (When Data Entered)

REPORT DOCUMENTATION PAGE		READ INSTRUCTIONS BEFORE COMPLETING FORM
1. REPORT NUMBER	2. GOVT ACCESSION NO. A118272	3. RECIPIENT'S CATALOG NUMBER
4. TITLE (and Subtitle) Postbuckling Behavior of Graphite/Epoxy Cloth Shear Panels with 45°-Flanged Lightening Holes		5. TYPE OF REPORT & PERIOD COVERED Master's Thesis; March 1982
		6. PERFORMING ORG. REPORT NUMBER
7. AUTHOR(s) Richard John Herman		8. CONTRACT OR GRANT NUMBER(s)
9. PERFORMING ORGANIZATION NAME AND ADDRESS Naval Postgraduate School Monterey, California 93940		10. PROGRAM ELEMENT, PROJECT, TASK AREA & WORK UNIT NUMBERS
11. CONTROLLING OFFICE NAME AND ADDRESS Naval Postgraduate School Monterey, California 93940		12. REPORT DATE March 1982
		13. NUMBER OF PAGES 164
14. MONITORING AGENCY NAME & ADDRESS(if different from Controlling Office)		15. SECURITY CLASS. (of this report) Unclassified
		15a. DECLASSIFICATION/DOWNGRADING SCHEDULE

16. DISTRIBUTION STATEMENT (of this Report)

Approved for public release; distribution unlimited.

17. DISTRIBUTION STATEMENT (of the abstract entered in Block 20, if different from Report)

18. SUPPLEMENTARY NOTES

19. KEY WORDS (Continue on reverse side if necessary and identify by block number)

Laminate
Composite Material
Shear Loading
Hole Reinforcement

20. ABSTRACT (Continue on reverse side if necessary and identify by block number)

An experimental and finite-element analysis was performed on graphite/epoxy cloth plates subjected to static shear loading. Two specimens were tested to failure for each of three configurations: a solid panel, a panel with an unreinforced hole and a panel with a 45°-flanged hole. Both a static nonlinear analysis and a bifurcation-buckling analysis were performed for each of the panel configurations. The 45°-flange reinforcement technique

DD FORM 1 JAN 73 1473 EDITION OF 1 NOV 65 IS OBSOLETE
S/N 0102-014-6601

UNCLASSIFIED
SECURITY CLASSIFICATION OF THIS PAGE (When Data Entered)

for cutouts in shear webs was found to be well-suited for use in non-buckling, graphite/epoxy cloth designs. However, an alternate hole-reinforcement technique is required for designs where buckling is allowed.

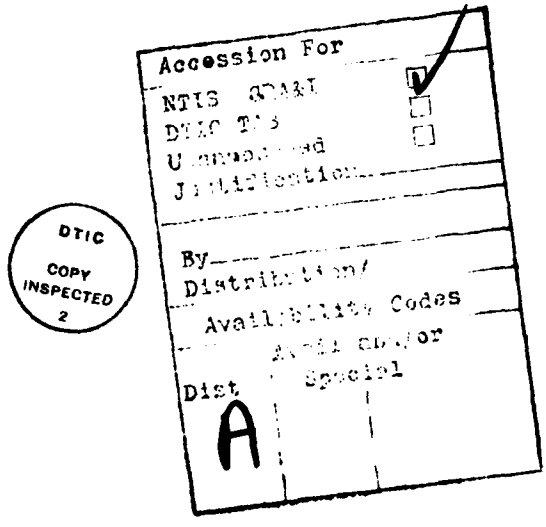

Approved for public release; distribution unlimited

Postbuckling Behavior of Graphite/Epoxy Cloth Shear Panels with 45°-Flanged Lightening Holes

by

Richard John Herman
Lieutenant Commander, United States Navy
B.S., United States Naval Academy, 1973

Submitted in partial fulfillment of the requirements for the degree of

MASTER OF SCIENCE IN AERONAUTICAL ENGINEERING

from the

NAVAL POSTGRADUATE SCHOOL
March 1982

Author: Richard John Herman

Approved by: Milton Vandrey, Thesis Advisor

G. R. Lindsey, Second Reader

Daniel J. Collins, Chairman, Department of Aeronautics

William M. Tolles, Dean of Science and Engineering

ABSTRACT

An experimental and finite-element analysis was performed on graphite/epoxy cloth plates subjected to static shear loading. Two specimens were tested to failure for each of three configurations: a solid panel, a panel with an unreinforced hole and a panel with a 45°-flanged hole. Both a static nonlinear analysis and a bifurcation-buckling analysis were performed for each of the panel configurations. The 45°-flange reinforcement technique for cutouts in shear webs was found to be well-suited for use in non-buckling, graphite/epoxy cloth designs. However, an alternate hole-reinforcement technique is required for designs where buckling is allowed.

TABLE OF CONTENTS

LIST OF FIGURES

TABLE OF SYMBOLS

D	Bending stiffness matrix
E	Modulus of elasticity
G	Shear modulus
K	Buckling constant
N	Force per unit length
P	Testing machine load
a	Panel width
b	Panel hole spacing, center-to-center
c	Panel net width (b-d)
c'	Flat portion of length c
d	Clear hole diameter
h	Panel height
q	Shear flow
t	Panel thickness
ε	Normal strain
γ	Shear strain
ν	Poisson's ratio
σ	Normal stress
τ	Shear stress
[ ]	A square matrix
$\llcorner\!\lrcorner$	A cloth lamina

Subscripts

T	Tangential direction
avg	Average value
c	Value at a given c/t ratio
coll	At collapse
cr	At buckling
h	Value at a given h/t ratio
max	Maximum value
s	A symmetric layup
ult	Ultimate value
x, y	Panel axes

ACKNOWLEDGMENT

The author gratefully acknowledges the enthusiastic support provided by J. A. Bailie and N. A. Cyr of Lockheed Missiles and Space Company, throughout the course of this investigation.

I. INTRODUCTION

Ever since the development of the "Wagner Beam" and the concept of the "diagonal tension field" in the early 1930's, shear panels have been used extensively in the metal semi-monocoque structure of aircraft. After many years of flight experience, analysis and experimental work with aluminum webs, the idea of allowing the web to buckle below ultimate and even limit load is now acceptable in many designs. As a consequence, metal webs that are allowed to buckle offer a weight and cost savings over designs in which buckling is prevented.

Advanced composite materials have been introduced in aircraft manufacturing to achieve weight savings. However, composite shear panel designs are usually thick, with buckling not allowed. Until a sufficient amount of knowledge about the behavior of postbuckled composite structures is developed, the aircraft industry will remain reluctant to incorporate designs permitting routine buckling into future aircraft. Many manufacturers have begun to develop the technology necessary to establish confidence in the ability of composites to perform satisfactorily in the postbuckled regime, but many questions remain.

It has been known for some time that composites provide considerable postbuckling strength in shear web applications.

This strength was demonstrated by Kaminski and Ashton [Ref. 1] for boron/epoxy shear webs and by Bhatia [Ref. 2] for graphite/epoxy shear webs. Just recently, the postbuckling strength of cocured composite-stiffened shear panels has also been shown to be adequate for both static and fatigue loadings [Refs. 3 and 4]. Many other areas of concern, such as the effects of environment, combined loading and curvature remain unexamined. This investigation dealt with another important concern, that is, the possible utilization of lightening/access holes and their effect on the strength and stiffness of composite shear panels.

Frequently the shear webs used in aircraft structures are perforated with regularly-spaced holes to lighten the web or to provide access to the interior of the structure. In some cases it has been found necessary to reinforce the web around these holes. Although many different configurations have been employed to reinforce lightening holes in aluminum shear webs, the integral stamped or beaded flange provides low stress concentration and good stability, and continues to be a common type of reinforcement. This type of hole reinforcement was used in airship girders before the semi-monocoque structure came into general use for airplanes [Ref. 5]. The flange appears particularly well-suited for the unique manufacturing processes required with composite structures. Although the angle at which the flange extends from the plane of the shear web has varied

somewhat in past designs, the 45°-flange appears to be one of the most common.

A 45°-flange has already been shown to be very effective for use with non-buckling, graphite-epoxy tape structures. Tests of the composite aileron rib designed for the Lockheed L-1011 [Ref. 6] resulted in only a slight degradation in strength from that of a solid web and a weight savings of 15 percent. A search of published literature was conducted to find information on any additional applications of composite shear panels with flanged lightening holes. Although it was suspected that this subject had been investigated by several manufacturers, no additional information could be found in the open literature. Therefore, the effectiveness of a 45°-flange for use with non-buckling, graphite/epoxy cloth structures remains unknown.

Accordingly, the purpose of this investigation was to evaluate the effect that a flanged lightening hole has on the behavior of a graphite/epoxy shear web operating well into the postbuckled regime, as well as to evaluate this type of reinforcement technique for use in non-buckling, graphite/epoxy cloth designs. The research was also intended to identify specific failure modes, assess the adequacy of current buckling and strength prediction methodology, and to provide direction for further work.

II. METHOD OF INVESTIGATION

In an effort to answer the questions which have been posed concerning the effectiveness of 45°-flanged reinforcements around holes in graphite/epoxy cloth composite panels, three panel configurations were investigated. First, solid panels (without holes) were considered, to provide baseline data on panel strengths. Panels with unreinforced holes were then investigated, and finally, panels with holes reinforced with 45°-flanges were considered.

The panels were designed as detailed in the following section, and a finite-element structural analysis was then executed for each configuration. Data was generated on diagonal strains, hole stress-concentration patterns, buckling loads and buckling patterns.

Two samples of each panel configuration were then manufactured and subjected to quality control inspections. The panels were instrumented with strain gages, mounted in "picture frame" shear fixtures and tested to destruction. Data was taken using multiple bonded-resistance strain gages throughout the loading process, including the post-buckling regime. Test results were evaluated and compared with the computed data, and conclusions were drawn.

III. PANEL DESIGN

A. PANEL LAYUP

The material utilized for the test specimens was HMF 330/34, a high-modulus woven graphite/epoxy system produced by Hercules Incorporated. The desired panel laminate was to be a symmetric layup, very strong in shear and as thin as possible. These criteria led to the choice of a 5-ply, $(\underline{45}_2/\underline{0})_s$ layup with an approximate cured thickness of 0.07 inches.

The material properties in the transverse direction of a single layer of graphite/epoxy cloth are slightly different from those in the longitudinal direction. The method by which the fibers are woven together produces a greater degree of fiber bending in one direction than the other, which creates this small variation. If this difference is taken into consideration during the construction of a symmetric laminate, virtually all bending-extension and shear-normal coupling would be eliminated. However, since the variation in strength is small and ease of manufacture was deemed a more important concern, no distinction was made between the two directions during panel construction. Therefore, a small degree of coupling was expected to occur.

By averaging the tensile properties given by the manufacturer for the longitudinal and transverse directions, the lamina elastic modulus is 10.75×10^6 psi and the allowable strength is 84.45 ksi at room temperature. This corresponds to an allowable tensile strain in one layer of approximately 0.0078. The inplane shear strength for a laminate constructed with 80 percent of the layers at 45 degrees was also given by the manufacturer. The nominal value is 55 ksi at room temperature, which corresponds to a strain of about 0.0074.

Other properties of the laminate that follow were calculated using manufacturer's data and the "classical laminate theory" presented by Agarwal [Ref. 7]:

$$G = 3.72 \times 10^6 \text{ psi}$$

$$E = 5.54 \times 10^6 \text{ psi}$$

$$\nu = 0.54$$

The bending matrix, D, which is required for buckling computations was calculated to be:

$$D = \begin{bmatrix} D_{11} & D_{12} & D_{16} \\ D_{12} & D_{22} & D_{26} \\ D_{16} & D_{26} & D_{66} \end{bmatrix} = \begin{bmatrix} 197.86 & 138.80 & 2.90 \\ 138.80 & 197.69 & 2.90 \\ 2.90 & 2.90 & 140.43 \end{bmatrix} \text{ lb-in}$$

B. DESIGN CRITERIA

Besides ensuring that the size of the panels would be compatible with available testing machines, the 45°-flanged panel was designed to meet the following criteria:

1. Design limit shear flow of 500 lb/in
2. Withstand a design ultimate shear flow of 1.5 times limit shear flow
3. Buckling onset at 30 percent of limit shear flow, which implies a "buckling ratio" of 5.0; i.e., the ultimate shear flow will be five times that of the shear flow for buckling ($q_{ult}/q_{cr} = 5.0$).

The third criterion of those listed above is unique to a composite shear panel designed to operate in the post-buckled regime. Design studies conducted by Lockheed-California Company indicated that a potential weight savings of about 50 percent (relative to an aluminum structure sized to the same loads) could be achieved when composite panels were allowed to buckle up to a buckling ratio of 5.2 [Ref. 3]. Therefore, if the 45°-flanged panel tests described here resulted in a buckling ratio significantly less than 5.0, then the configuration would be considered unsatisfactory for use in a postbuckled design. If it is assumed that the limit shear flow of 500 lb/in corresponds to the shear flow in a fuselage panel or shear web of a typical fighter/attack aircraft at its limit load factor of 7.33 g's, then the following design reference shear flows are generated:

q = 68 lb/in at basic load (1 g)

q = 150 lb/in at initial buckling (2.2 g's)

$q = 500$ lb/in at limit load (7.33 g's)

$q = 750$ lb/in at ultimate load (11 g's)

The desired critical shear stress, τ_{cr}, for panel buckling is then calculated from the buckling shear flow:

$$\tau_{cr} = \frac{q_{cr}}{t} = 2140 \text{ psi}$$

C. DESIGN APPROACH

A method similar to that used by Fogg [Ref. 6] was employed to size the shear panels. This "pseudo-metallic" approach involves the calculation of an equivalent aluminum thickness which can then be used to size a shear web with a 45°-flanged hole using the empirical relations given by Kuhn [Ref. 8]. Since Kuhn's formulas were developed from the results of tests utilizing aluminum webs loaded with a rail-shear type of fixture rather than the "picture frame" fixture used here, it was not expected that the test results would agree precisely with these design calculations. The pseudo-metallic method was utilized as an aid in design, since no other design tool is known to exist other than a "full-blown" finite-element analysis. Once the test specimen design had been chosen utilizing the pseudo-metallic method, a complete finite-element analysis was made for comparison with test results.

In a pseudo-metallic design analysis the equivalent aluminum thickness is found by equating the critical

buckling shear force expressions given for the composite layup to those for an aluminum panel. These two expressions can be written for either simply-supported or clamped boundary conditions and for any web width-to-height ratio, so long as consistency is maintained. In this analysis a width-to-height ratio of infinity and simply-supported boundary conditions were used; other combinations could have been chosen and would have led to the same equivalent thickness. The term "height" used in the following discussion is defined as the distance measured in the plane of the panel from one rivet line to the other, whereas "thickness" is the distance measured perpendicular to the plane of the panel from one surface of the material to the other. The following calculations are for all sides simply-supported and, to correspond with Kuhn's rail-shear data, a width-to-height ratio (a/h) of infinity.

The expression for the critical buckling load for orthotropic plates used in the Advanced Composites Design Guide [Ref. 9] is

$$N_{xy_{cr}} = \left(\frac{2}{h}\right)^2 \sqrt{D_{22}(D_{12} + 2D_{66})}\,(11.7 + 0.532\theta + 0.938\theta^2)$$

where $\theta = \dfrac{\sqrt{D_{11}\,D_{22}}}{D_{12} + 2D_{66}}$

and D_{16} and D_{26} are assumed to be zero. Solving for $N_{xy_{cr}}$ with the values for the chosen composite layup yields

$$N_{xy_{cr}} = \frac{14008.79}{h^2} \text{ lb/in}$$

The buckling expression for isotropic plates is given by Peery [Ref. 10] as

$$N_{xy_{cr}} = KE \frac{t^3}{h^2}$$

Again, for all sides simply-supported and a width-to-height ratio of infinity,

$$K = 4.8$$

and $E = 10.5 \times 10^6$ psi for aluminum. Thus

$$N_{xy_{cr}} = 5.04 \times 10^7 \frac{t^3}{h^2} \text{ lb/in}$$

Equating the two and solving for the equivalent aluminum thickness yields

$$5.04 \times 10^7 \frac{t^3}{h^2} = \frac{14008.79}{h^2}$$

$$t = 0.0653 \text{ inches}$$

Figure 3 of Kuhn [Ref. 8] was then utilized to determine an appropriate panel height, h, knowing that $\tau_{cr} = 2140$ psi and t = 0.0653 inches. The appropriate height-to-thickness ratio, h/t, was found to be 153 which dictates a panel height of approximately 10 inches.

The tests presented in Kuhn's paper cover a range of parameters approximately as follows:

$$0.15 < \frac{d}{h} < 0.75$$

where d is the clear hole diameter. Therefore, to facilitate comparison with Kuhn's results a hole diameter of 4.5 inches was chosen, placing the tests described here exactly in the middle of Kuhn's range. Initial buckling and collapse loads were then predicted utilizing Kuhn's empirical expressions. For initial buckling, Kuhn's Eq. (3) reads:

$$q_{cr} = t\left[\tau_{h_{cr}}\left(1 - \frac{d}{h}\right) + \tau_{c_{cr}}\left(\frac{d}{h}\right)\right]\frac{c'}{b}$$

where t = 0.0653 inches

d = 4.5 inches

h = 10 inches

b = 10 inches (hole spacing, taken as width of test specimen)

c = b - d = 5.5 inches (net width)

c' = c - 2 x (flange width) = 5 inches (net flat web)

Again from Figure 3 of Kuhn, the critical stress for h/t = 153 is $\tau_{h_{cr}}$ = 2140 psi, and for c/t = 84 is $\tau_{c_{cr}}$ = 7200 psi. Substitution of values yields

$$q_{cr} = 146 \text{ lb/in}$$

which for a 10-inch shear panel equates to

$$P_{cr} = 2065 \text{ lb}$$

Although the failure load of an equivalent aluminum panel cannot be expected to correspond well to that of a composite panel due to differing failure modes, the

predicted postbuckling collapse load was computed for purposes of comparison. Kuhn's Eq. (4) is

$$q_{coll} = t\left[1 - 3.5\left(\frac{h}{1000t}\right)^2\right]\left\{\tau_h\left[1 - \left(\frac{d}{h}\right)^2\right] + \tau_c\sqrt{\frac{d}{h}}\right\}\frac{c'}{b}$$

where the collapse stresses read from his Figure 3 are τ_h = 7400 psi and τ_c = 14200 psi. Substitution of values yields

$$q_{coll} = 462 \text{ lb/in}$$

which for a 10-inch shear panel equates to

$$P_{coll} = 6535 \text{ lb}$$

Based on this analysis, the test specimen configuration was then designed for fabrication as is detailed in Section V.

IV. PANEL ANALYSIS

A. FINITE-ELEMENT PROGRAMS

Panel analysis was accomplished by utilizing a system of program modules designed for structural analysis, known as "DIAL" [Ref. 11], at Lockheed Missiles and Space Company. Both a static nonlinear analysis utilizing a modified Newton-Raphson technique and a bifurcation-buckling analysis were performed for each of the three panel configurations shown in Figures 1 through 3. The panels were represented with 3-dimensional, isoparametric shell elements of the parabolic form with a layered-wall configuration of orthotropic material. The steel frame members of the test fixture were modeled with 3-dimensional shell stiffeners composed of conventional straight-beam elements that essentially create clamped boundary conditions. Unlike the actual test fixture, the beam elements were purposely attached to the corners of the panel model to induce high stress concentrations. These areas of high stress concentration were reported to be a characteristic problem of "picture frame" fixtures used previously, even with special precautions employed to reduce these concentrations [Ref. 4].

At each corner node of the panel, the adjacent beams were connected with a pin joint which equivalences only the

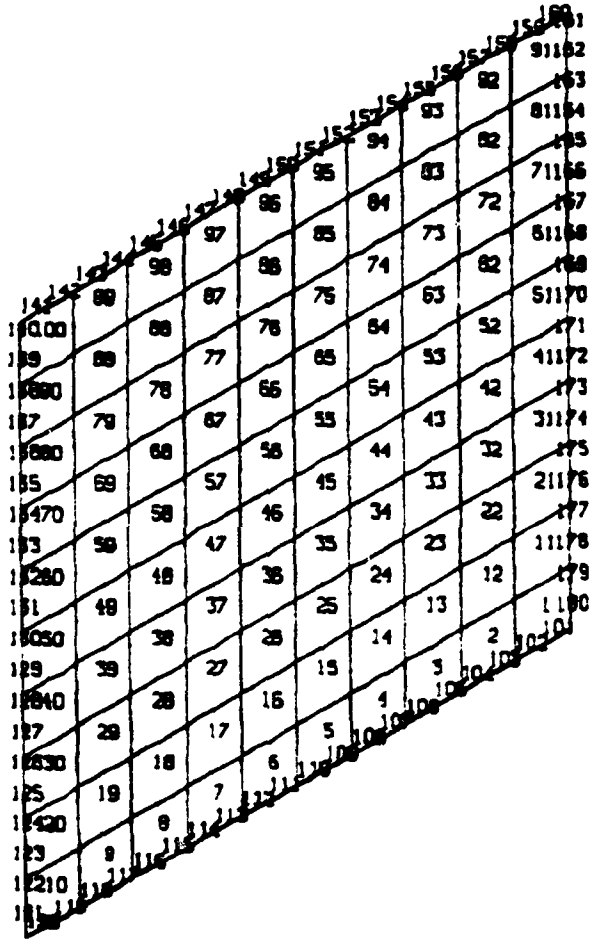

Fig. 1. Shell and Beam Elements of the First Model

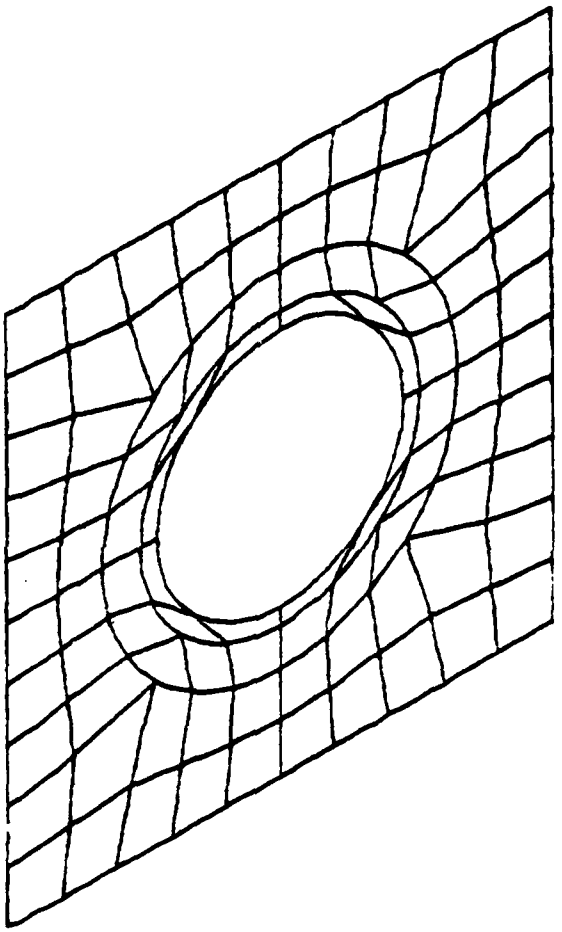

Fig. 2. Shell Elements of the Second Model

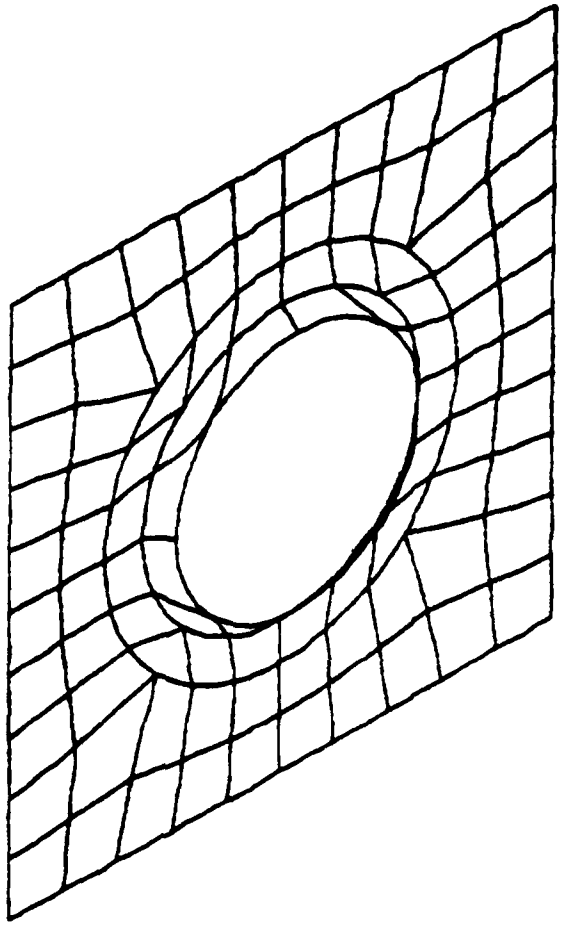

Fig. 3. Shell Elements of the Third Model

translational freedoms. Out-of-plane rotations were also equivalenced at the two diagonally opposite corners of the panel where load is not applied. The panel was then loaded at the other two corners by suppressing all translational freedoms at one corner and allowing only one translation (45° to the panel global axis) at the other. All six degrees of freedom were allowed for all other nodes in the model.

The computer program for the static loading of each of the computer models was intended to produce results beyond the buckling load. This had never been attempted with "DIAL" before and the capability of the system to do this was unknown. Since "DIAL" was not specifically designed to operate in this regime, the severe nonlinearities encountered at buckling could not be resolved by the system without employing special programming techniques. Several of these techniques were attempted to "help" the computer provide solutions beyond buckling. This proved to be a very tedious and time-consuming process. For example, a single computer run for the flanged panel from 1300 to 4400 pounds required 23 hours of CPU time. Although these techniques were successful in that some postbuckled results were obtained, significant solutions near the ultimate load could not be achieved in the time frame of this investigation.

Consequently the single nodal load was applied in increments until reaching a load near the eigenvalue identified

during the buckling analysis. At each load increment a contour plot of diagonal stresses and out-of-plane displacements was obtained. A computer printout containing all nodal point displacements and all centroidal shell-element stresses and strains at each load step was used for direct comparison with experimental results.

B. FINITE-ELEMENT RESULTS

1. Solid Panel

Bifurcation-buckling analysis of the solid panel predicted instability at a load of 3785 pounds. The computer model was then loaded to 3500 pounds in steps of 500. Figure 4 shows the distribution of the inplane forces (lb/in) for the solid panel at 3500 pounds which is close to buckling. Each line on the plot represents a line of constant N_{xy}. The nodal load is being applied in the upper corner of the right side and the diagonally opposite corner is fixed. Stress concentrations can be seen in the corners where the load is applied to the panel. The displacements normal to the plane of the panel at 3500 pounds are illustrated in Figure 5. Each line on the contour plot represents a constant value of normal displacement in inches. In this and all subsequent contour plots, the nodal load is again being applied in the upper right corner. As can be seen in this figure, the solid panel is beginning to bow down a line connecting the two corners where load is applied

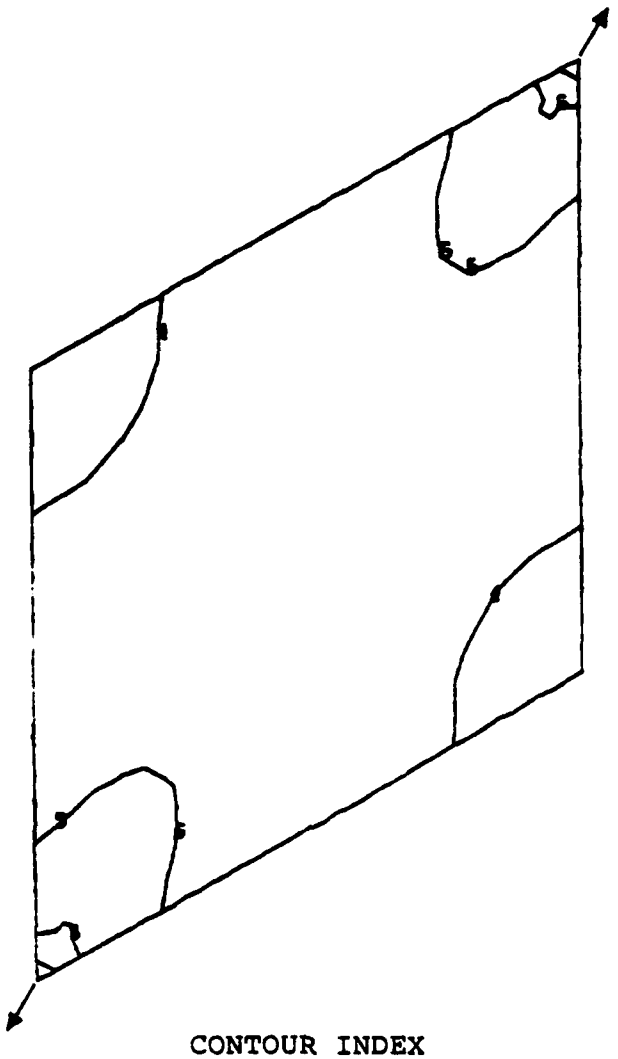

CONTOUR INDEX	
1	0.0
2	1.0×10^2
3	2.0×10^2
4	3.0×10^2
5	4.0×10^2
6	5.0×10^2
7	6.0×10^2
8	7.0×10^2

Fig. 4. N_{xy} Contours for Solid Panel at 3500 lb

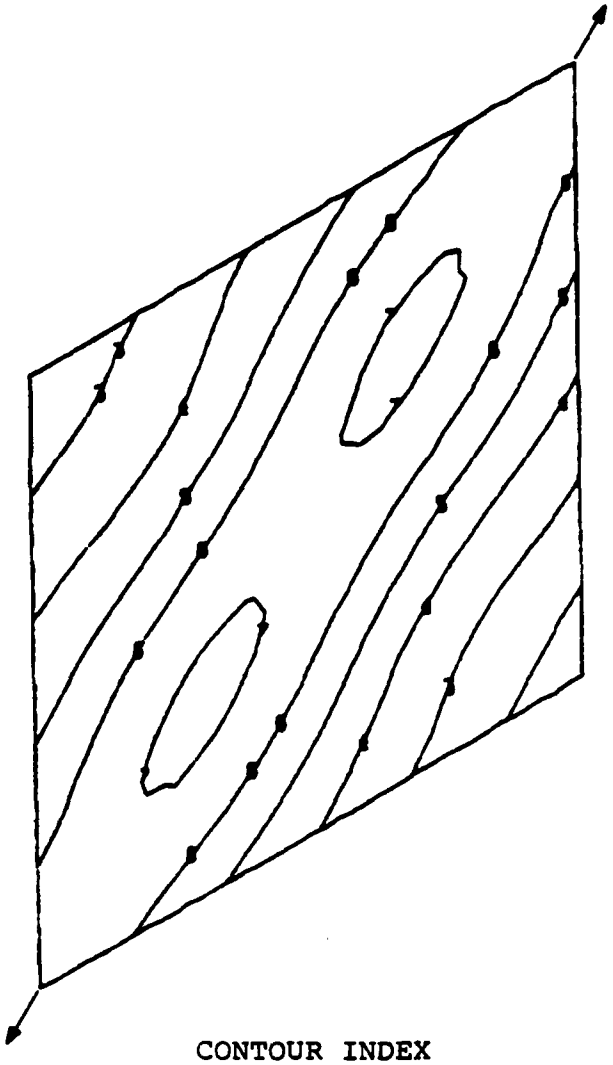

CONTOUR INDEX	
1	-3.0×10^{-7}
2	-2.5×10^{-7}
3	-2.0×10^{-7}
4	-1.5×10^{-7}
5	-10.0×10^{-8}
6	-5.0×10^{-8}
7	0.0

Fig. 5. Normal Displacement Contours for Solid Panel at 3500 lb

(diagonal tension axis). Appendix A contains the contour plots for all of the load steps.

2. Panel with Unreinforced Hole

Predicted buckling for this configuration was 2478 pounds. Output was therefore obtained at every 250 pounds up to 2500 pounds. Figure 6 displays the contours of N_{xy} at 2500 pounds which is immediately after buckling, and Figure 7 shows the corresponding normal displacements. Appendix B contains the contour plots for all of the load steps.

3. Panel with Flanged Hole

Bifurcation-buckling analysis revealed panel instability at 4228 pounds. During the subsequent static loading of the computer model, a smaller nonlinearity was found to occur at approximately 1300 pounds which probably indicates the beginning of significant flange movement. Computer output was obtained up to 4000 pounds in steps of 500 pounds and also at 250, 4250 and 4400 pounds. Figure 8 shows the contours of N_{xy} and Figure 9 displays the out-of-plane displacement distribution at 4250 pounds which is just after buckling (flange is pointing towards the reader). Contour plots for all of the load steps are contained in Appendix C.

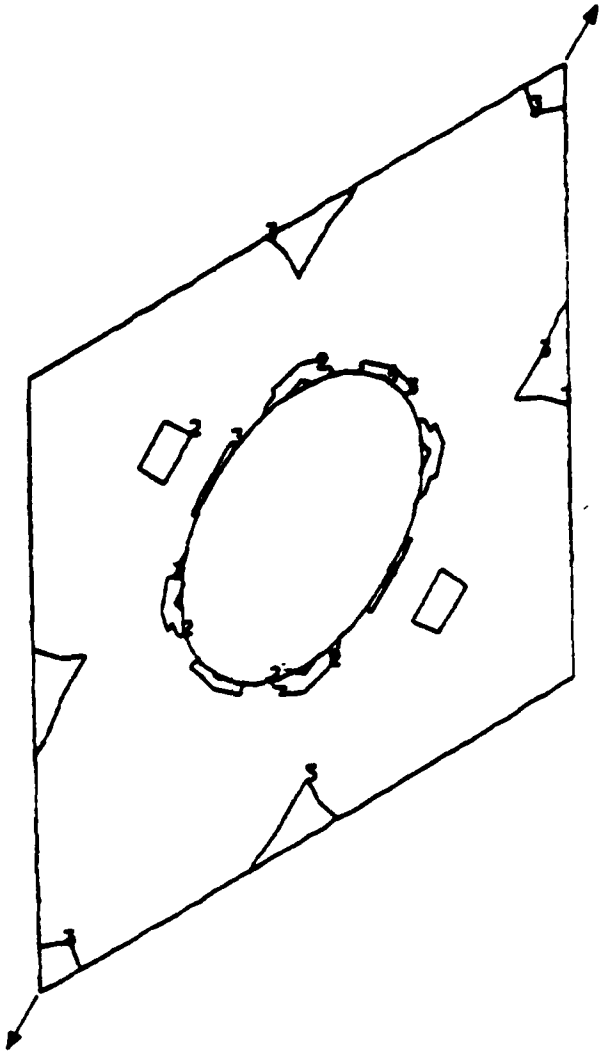

CONTOUR INDEX	
1	-1.5×10^{-5}
2	2.0×10^{2}
3	4.0×10^{2}
4	6.0×10^{2}

Fig. 6. N_{xy} Contours for Panel with Unreinforced Hole at 2500 lb

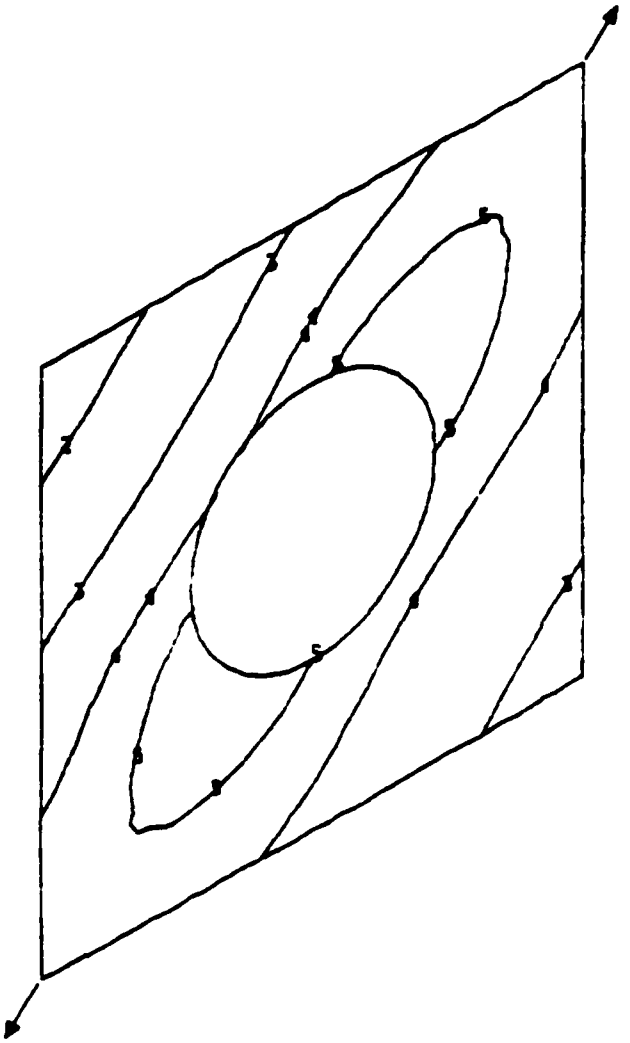

CONTOUR INDEX	
1	-8.0×10^{-7}
2	-6.0×10^{-7}
3	-4.0×10^{-7}
4	-2.0×10^{-7}
5	0.0
6	2.0×10^{-7}

Fig. 7. Normal Displacement Contours for Panel with Unreinforced Hole at 2500 lb

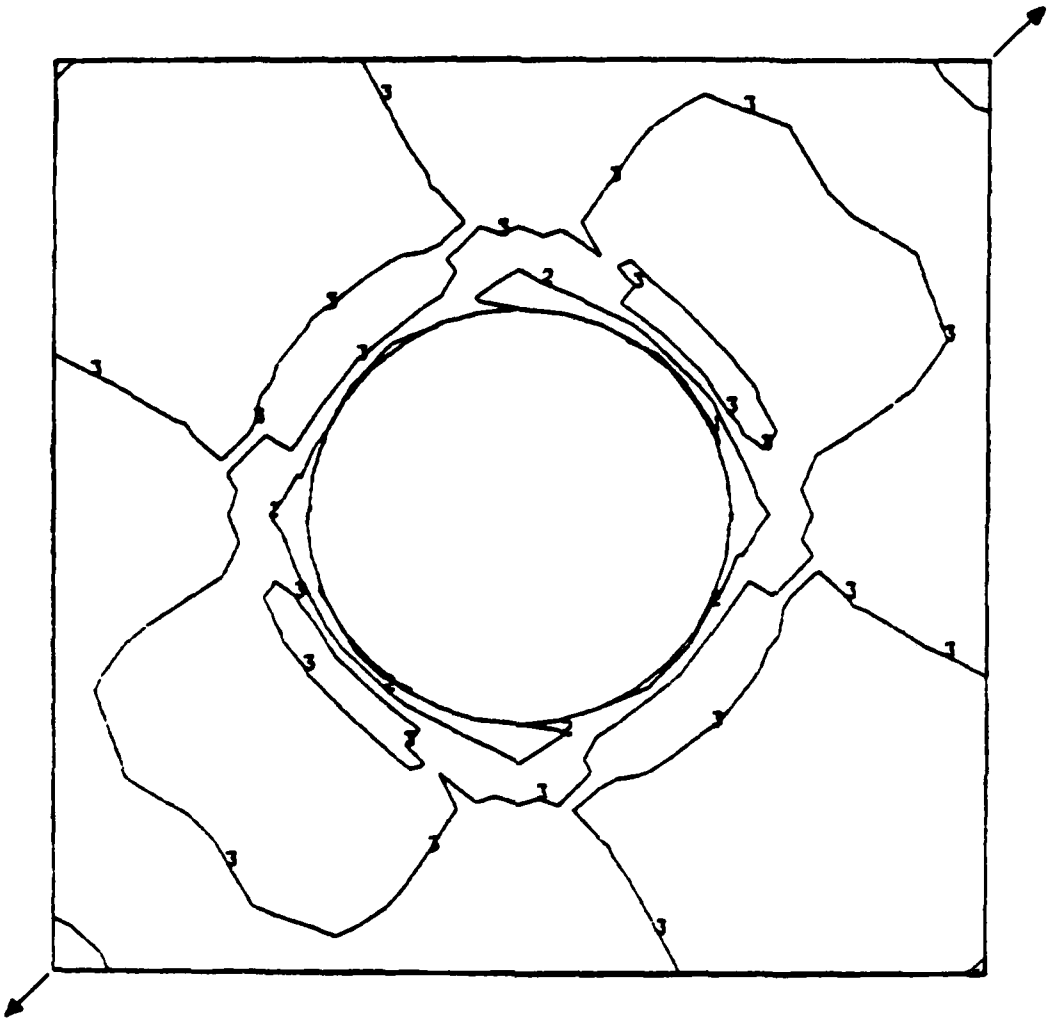

CONTOUR	INDEX
1	-5.0×10^2
2	0.0
3	5.0×10^2
4	1.0×10^3
5	1.5×10^3

Fig. 8. N_{xy} Contours for Panel with Flanged Hole at 4250 lb

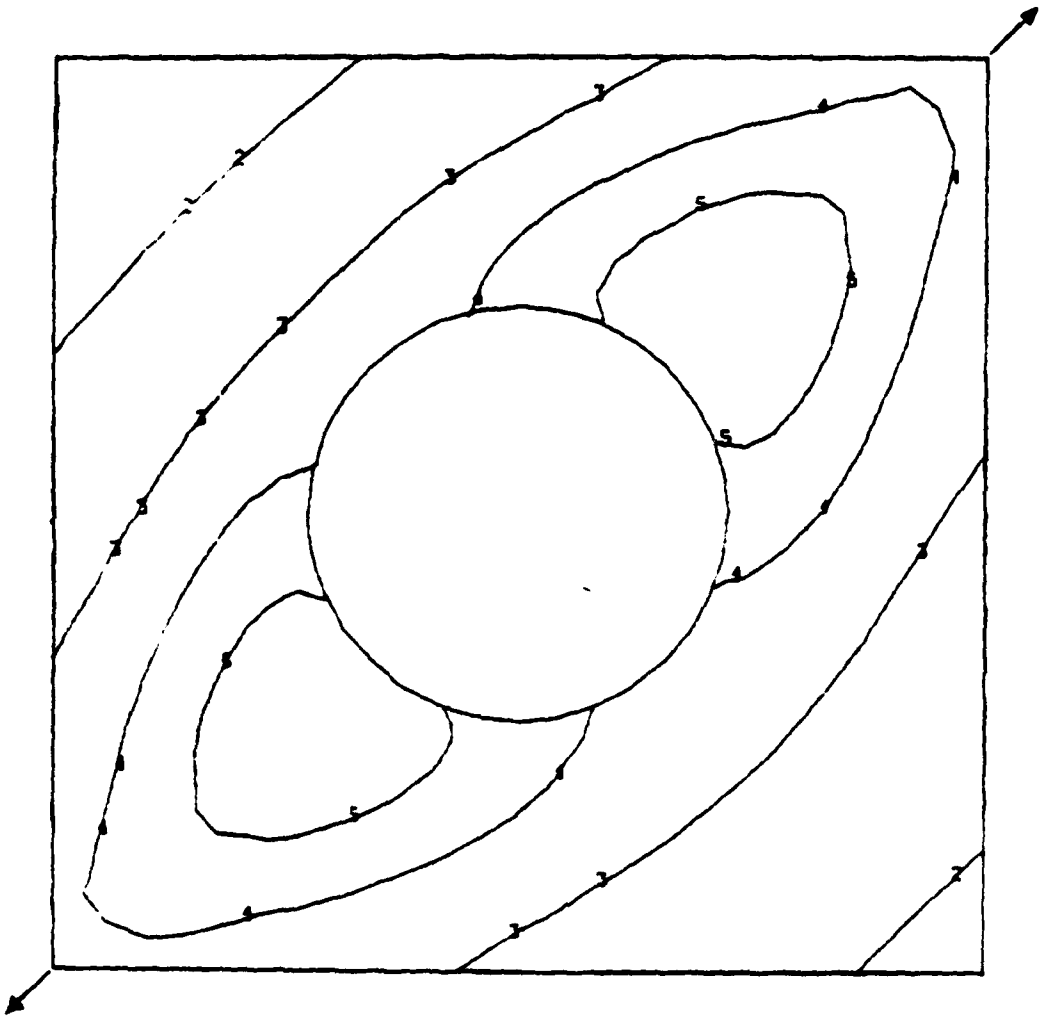

CONTOUR INDEX	
1	-1.5×10^{-1}
2	-10.0×10^{-2}
3	-5.0×10^{-2}
4	0.0
5	5.0×10^{-2}
6	10.0×10^{-2}

Fig. 9. Normal Displacement Contours for Panel with Flanged Hole at 4250 lb

V. EXPERIMENTAL APPARATUS AND PROCEDURES

A. PANELS

Figure 10 shows the drawing to which all three panel configurations were fabricated. The corners of the panels were removed in an attempt to remedy the problem of high stress concentrations mentioned previously. A clear diameter of 4.5 inches was used for both the unreinforced-hole configuration (panels 2A and 2B) and the flanged-hole configuration (panels 3A and 3B). The bend diameter for the flanged panels is approximately 1.14 times the clear diameter. The cocured tabs on both sides of the panel perimeter were constructed from glass/epoxy cloth prepreg. Each panel was subjected to both ultrasonic C-scan and X-ray inspections after manufacture, which revealed no significant defects.

Each of the test panels also was subjected to dimensional checks after fabrication. Skin and tab thicknesses, hole diameter, hole location and panel bowing were noted. Since each cloth lamina was placed in the layup without regard to the stronger weave direction, some bowing of the panels did occur due to thermal contractions during cure. This resulted in a normal displacement difference of the middle of the solid panels and the hole edge of the unreinforced panels of approximately 0.060 inches from that of

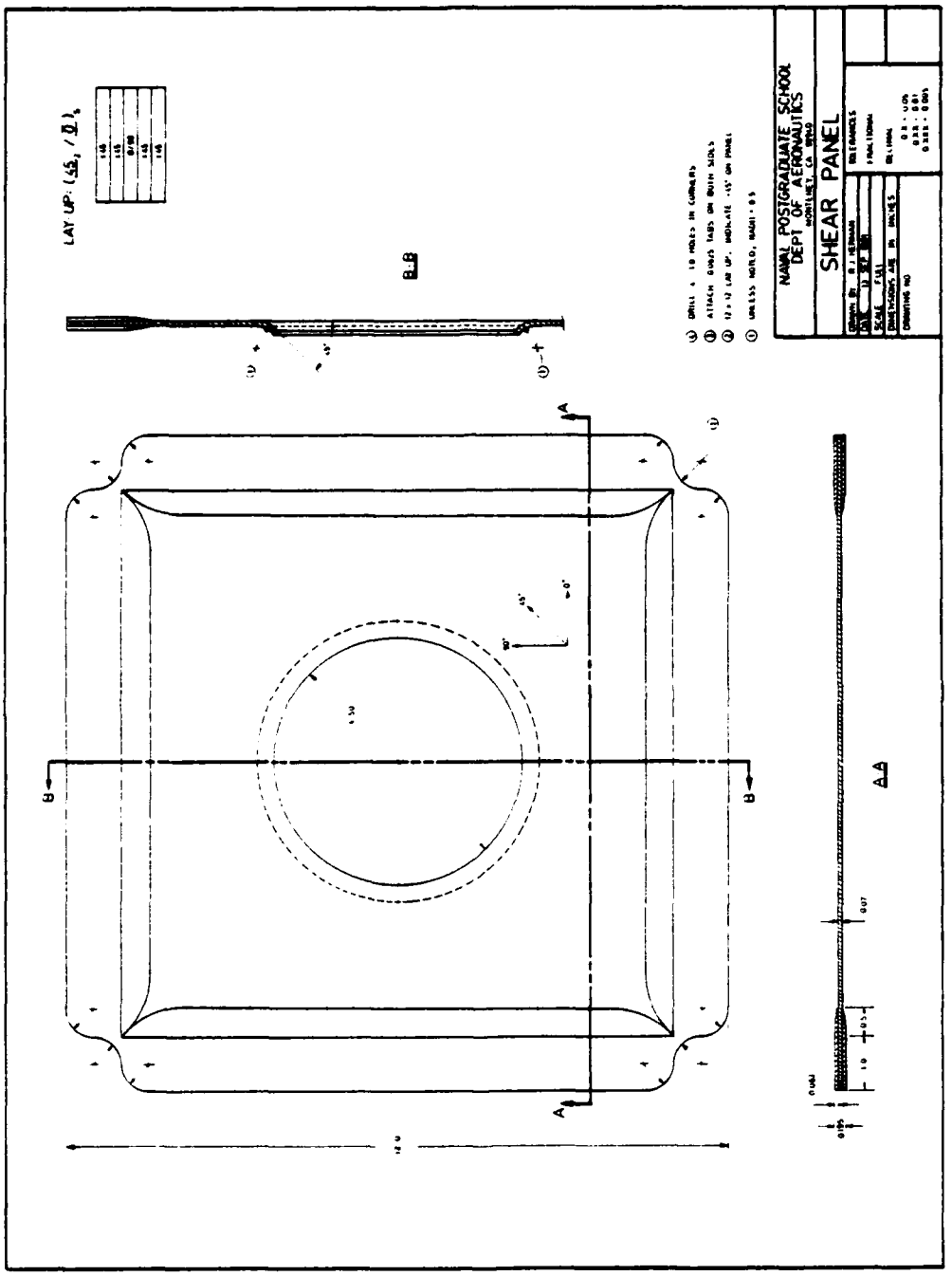

Fig. 10. Shear Panel Drawing

the panel perimeter. The normal displacements of both flanged panels were within 0.010 inches over the entire surface.

Figure 11 illustrates one of the flanged panels after fabrication. The weight of this configuration was not measurably different from that of the unreinforced-hole configuration. The panels with cutouts weighed approximately 1.3 ounces less than the solid panels.

B. FRAMES

The drawing to which the frames of the test fixture were fabricated is illustrated in Figure 12. The frames were tapered in another attempt to create a uniform distribution of stress throughout the panel. Straight-beam designs in the past have resulted in high stress concentrations in the diagonal tension corners [Ref. 4]. The applied load causes local bending of the frames near these corners which introduces higher stresses into the panel. Although the bending moment of the frames cannot (by practical methods) be held constant along the entire length, the taper serves to reduce its rate of change.

Sixteen of these pieces were machined from cold-rolled mild steel for the two fixtures used for testing. All of the panels were placed in the fixture with the same orientation and clamped-up with 3/16-inch bolts which were

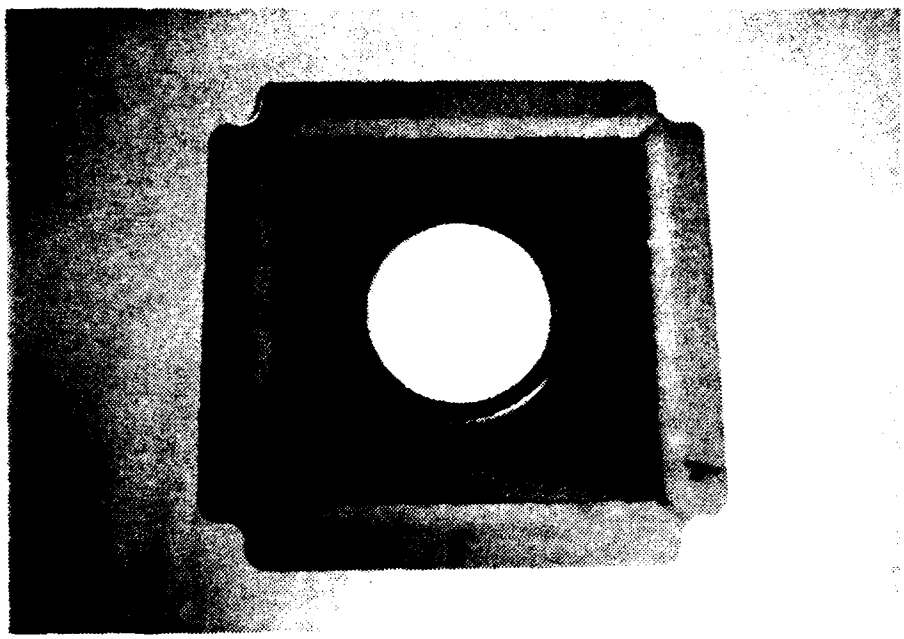

Fig. 11. Panel with Flanged Hole After Fabrication

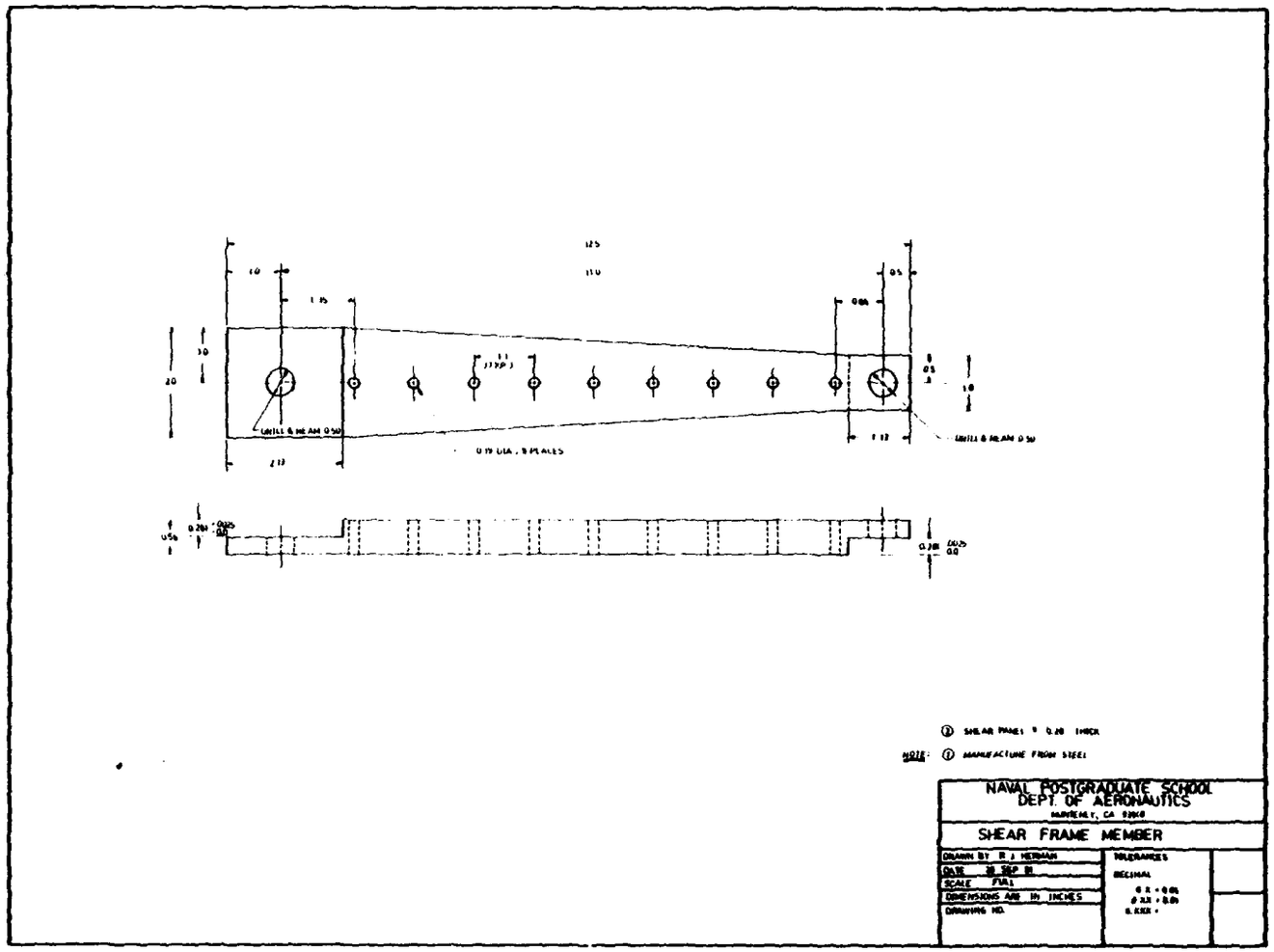

Fig. 12. Drawing of Steel Frame Member

torqued to 50 inch-pounds. A solid panel with a set of frames attached is shown in Figure 13.

C. EXPERIMENTAL SETUP

Figure 14 displays the equipment used for testing. A 300-kip capacity Riehle Testing Machine was used to apply load to the "picture frame." Readings from an array of bonded-resistance strain gages on each panel were recorded by utilizing a Micro-Measurements System 4000 (strain gage scanner with computer keyboard). An additional strain gage mounted on a separate piece of graphite/epoxy material was used to compensate for any variations in temperature during the experiments.

The rosette strain gage pattern for panel 1A is shown in Figure 15. For each strain gage shown in the photograph, an identical strain gage was mounted on the other side in the same orientation, "back-to-back." Four rosettes were mounted around the central rosette at a distance of 2 3/8 inches. An additional rosette was placed 4 3/8 inches above center. The same pattern was used for panel 1B except that the bottom and two side rosettes were deleted.

Figure 16 illustrates panel 2A just prior to loading. The back-to-back strain gage orientation displayed in this photograph was used for all four of the panels with holes. The top rosette is again 4 3/8 inches above the panel center. Nine back-to-back axial gages were then positioned

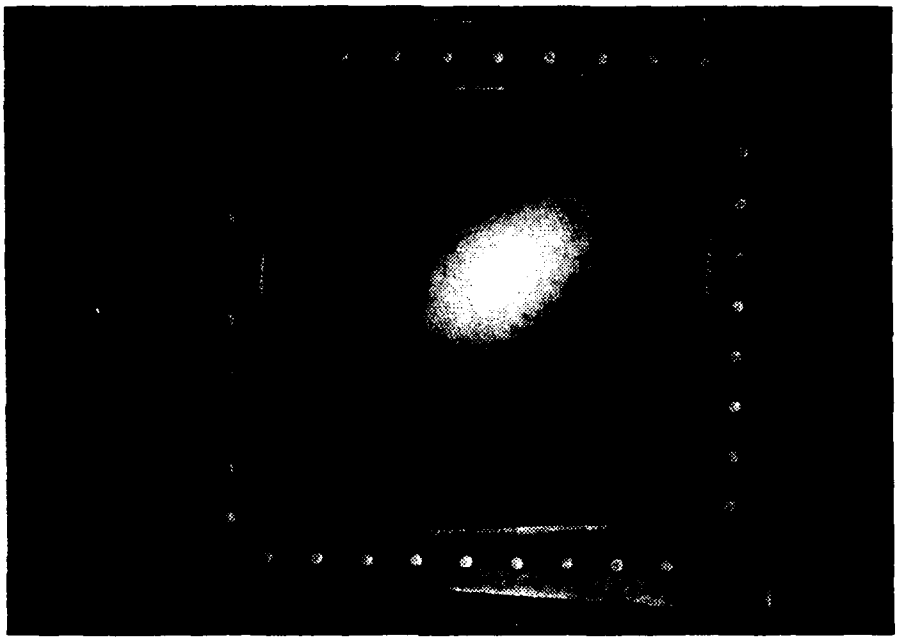

Fig. 13. Solid Panel with Frames Attached

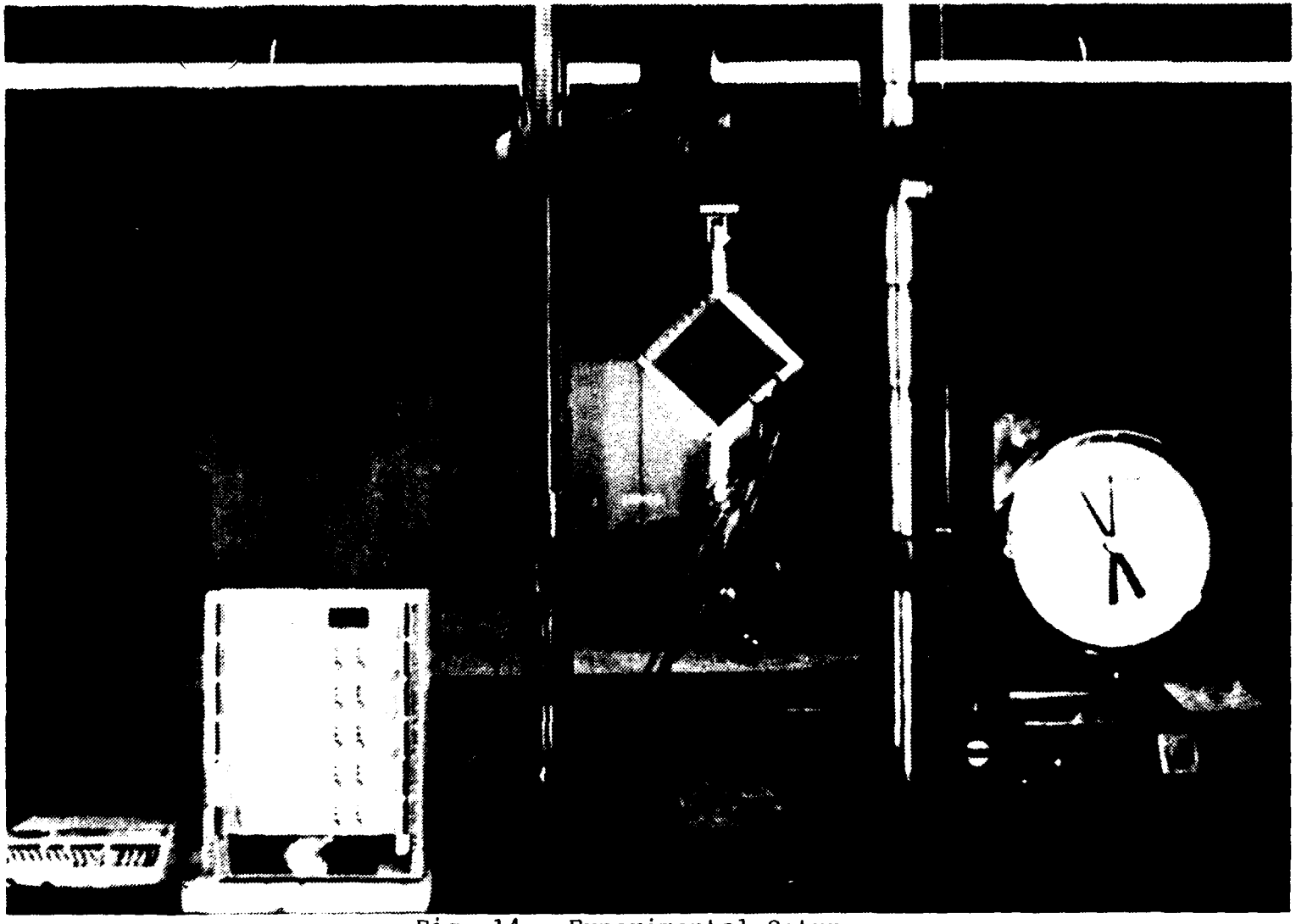

Fig. 14. Experimental Setup

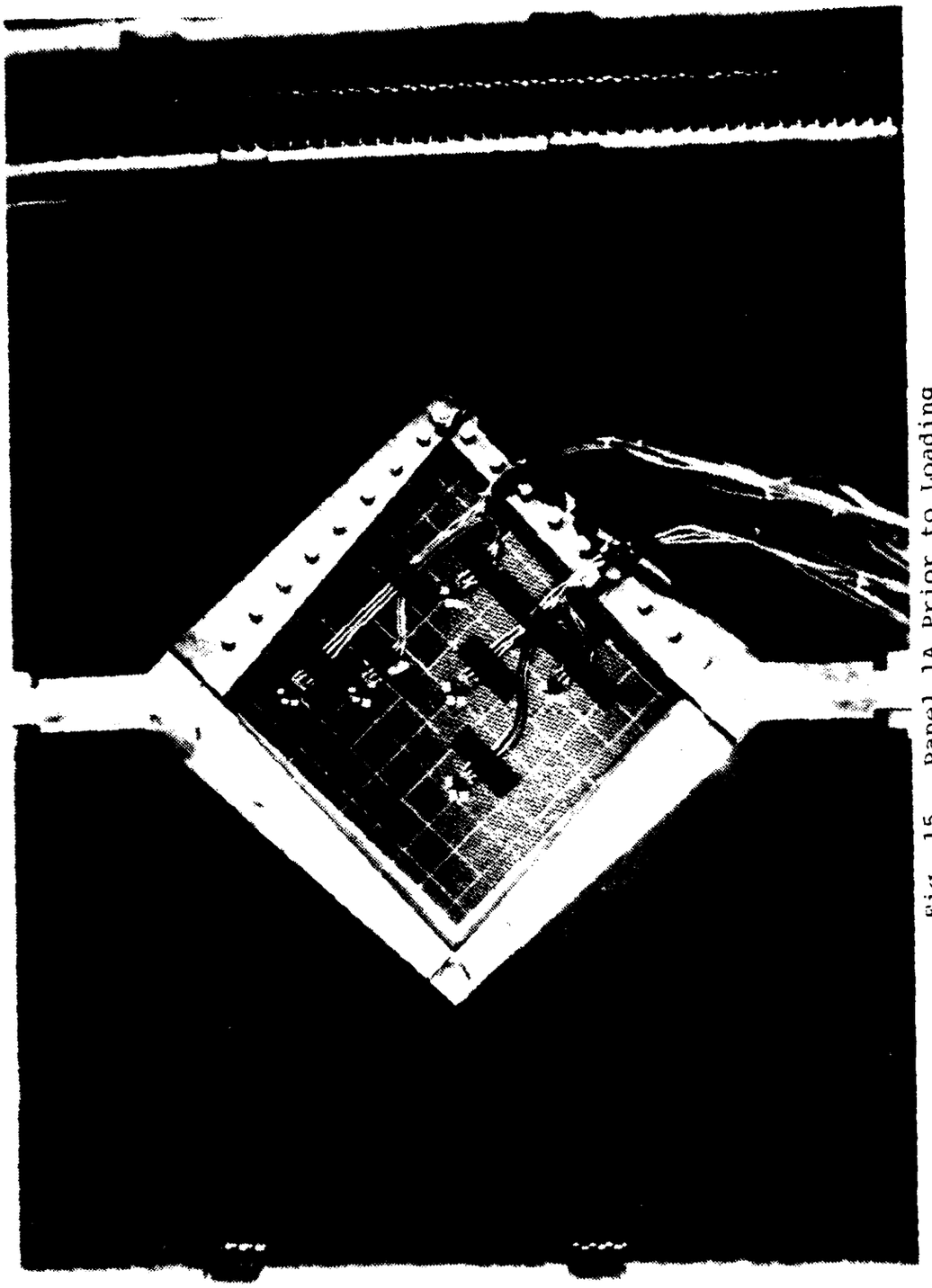

Fig. 15. Panel 1A Prior to Loading

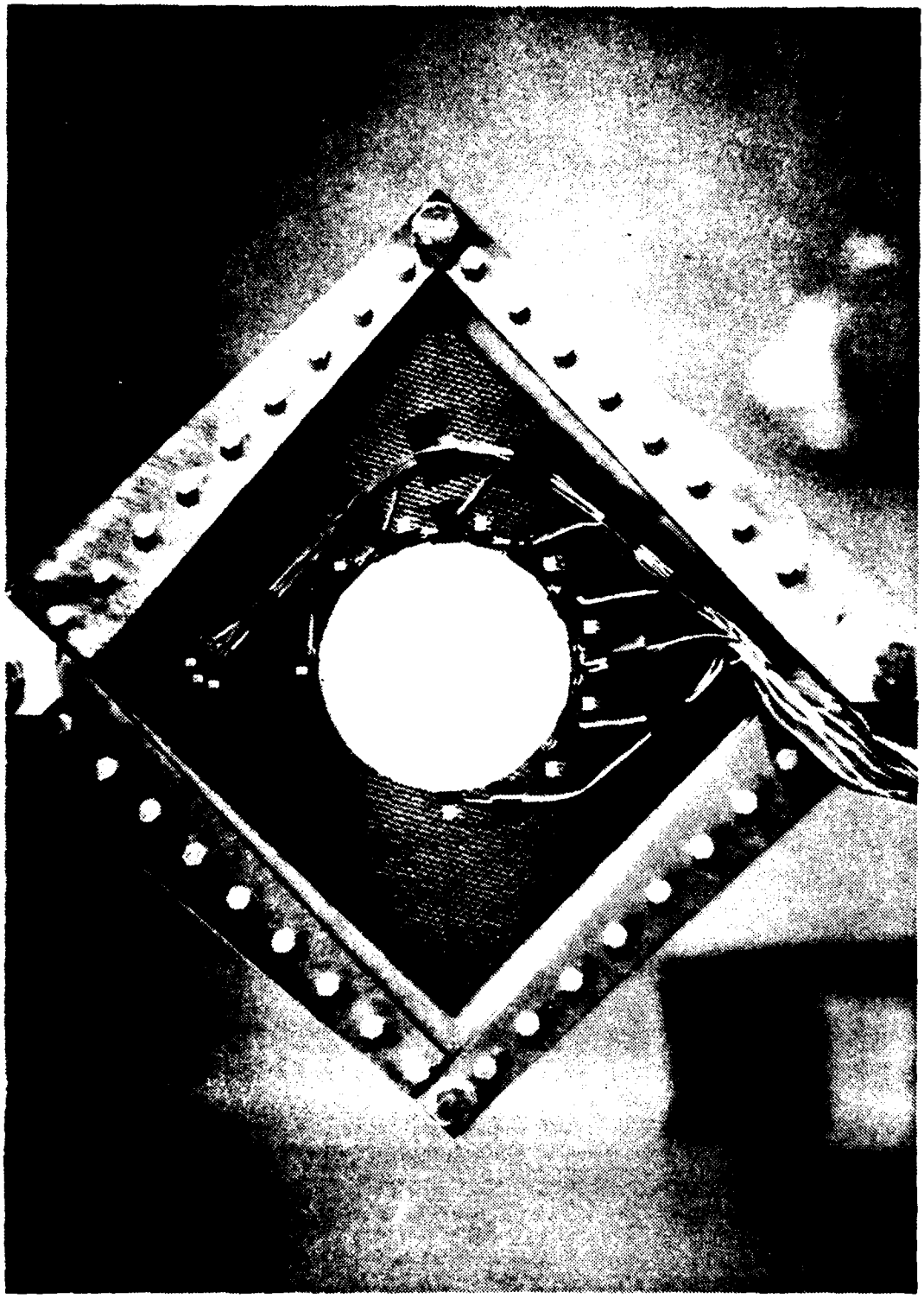

Fig. 16. Panel 2A Prior to Loading

as close to the hole as possible, oriented so that the tangential stress distribution around the cutout could be determined. Figure 17 displays a flanged panel as it appeared in the test fixture immediately prior to testing.

D. TEST PROCEDURES

Prior to loading them to failure, each of the solid panels was twice loaded to 1000 pounds, and each of the panels with cutouts was twice loaded to 500 pounds for various system checks. The bottom clevis of the fixture was then detached from the Riehle machine, the load indicator was re-zeroed and the strain gages were zeroed and calibrated again. With the fixture then reattached, the load was slowly increased and stopped at predetermined load levels for the recording of strains. All six panels were stopped at the same load levels even if a recording was not taken for a particular panel configuration at that load. The failure load was defined as the load at which any macroscopic evidence of damage to the layup could be observed, regardless of whether or not the panel could continue to carry load.

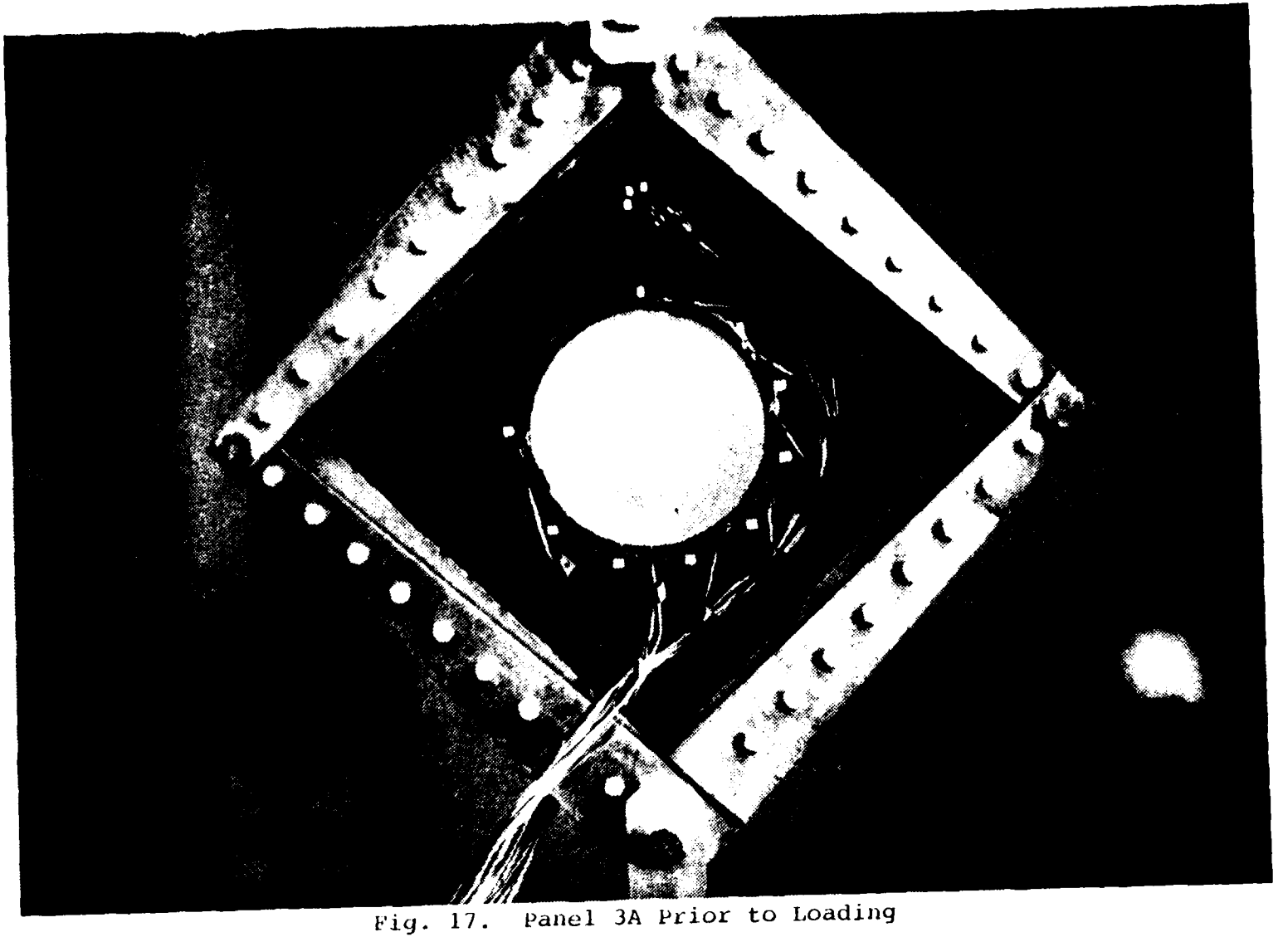

Fig. 17. Panel 3A Prior to Loading

VI. EXPERIMENTAL RESULTS

A. SOLID PANELS

1. Panel 1A

In order to describe the out-of-plane displacement directions of the shear panels, the side of the panel facing the front of the Riehle machine will be termed the "front" and the opposite side will be called the "back." In the case of panel 1A, the direction of original panel warp was towards the front. Figure 18 illustrates a sample of the procedure used to define the buckling load for all of the test specimens. Buckling was determined by the intersection of the prebuckling and postbuckling slopes of the curve of bending strain versus machine load. This strain is the difference in readings from gages positioned back-to-back in the compression direction of the panel. The bending strain curve for each of the four rosettes positioned down the center of panel 1A indicated the occurrence of buckling at 3850 pounds.

At 6000 pounds, a buckle towards the front and down the center of the panel could be easily seen. Figure 19 shows the front of the panel at 9000 pounds where small "crackle" sounds were first heard. At 25000 pounds, two smaller buckles became visible on each side of the large center bow. Upon reaching 28000 pounds, a loud "pop" was

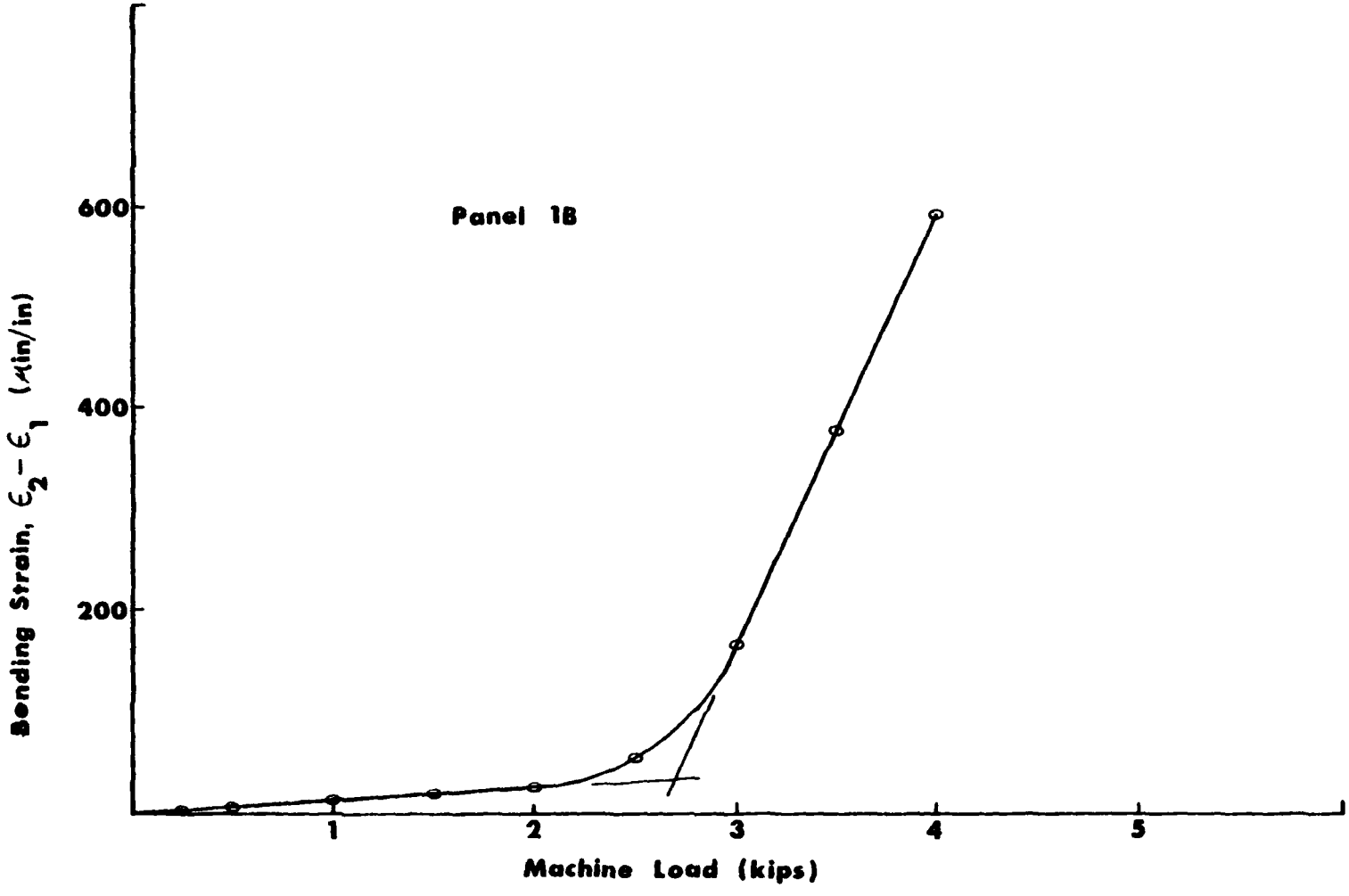

Fig. 18. Procedure for Determination of Buckling

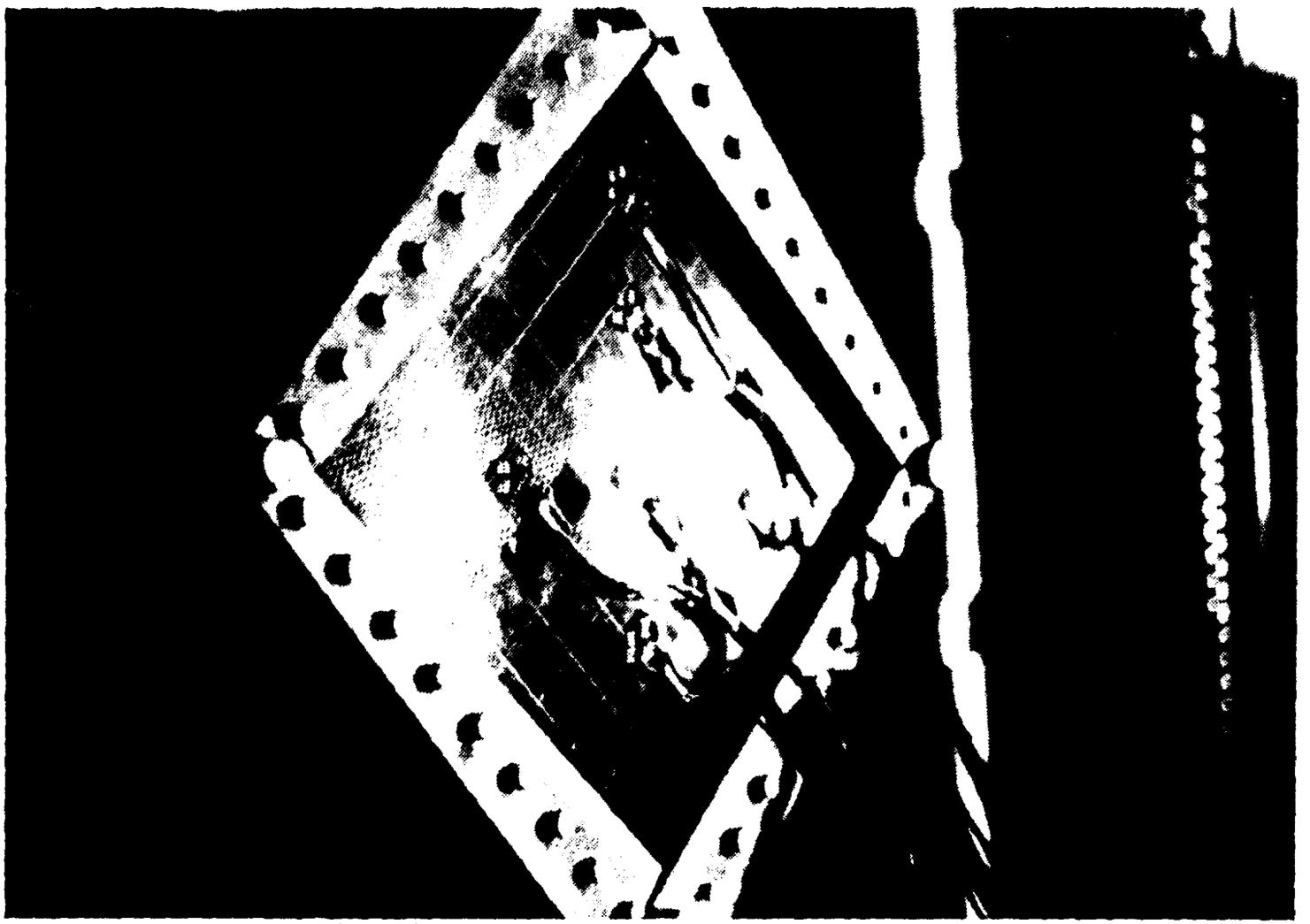

Fig. 19. Front Side of Panel 1A at 9000 lb

heard and a two-inch crack was discovered on the left side of the center buckle. There was no significant decrease in load after the failure occurred. Figures 20 and 21 display the front side of the panel after failure. The crack which was caused by bending of the skin can be seen near the top of the panel.

After the panel was unloaded and removed from the "picture frame," almost no evidence of skin curvature could be found to remain. The crack was observed to extend through only the outer 45°-layer of cloth on the front side of the panel. Minute compression cracks due to bending were also discovered in the diagonal tension corners of the back side. No panel delamination or any damage to the bolt holes could be found. Figure 22 illustrates the front side of the panel after disassembly. In this photograph, and all subsequent ones that display panels after removal from the test fixture, the cracks have been highlighted with a grease pencil for clarity.

The maximum shear strain was found by averaging the values calculated from readings of a front rosette and the corresponding rosette on the back. This maximum shear strain at each of the six rosette positions is plotted versus machine load in Figure 23. The direction of principal strain at all locations was within three degrees of the panel diagonal. As shown in the figure, the shear distribution appears to be symmetric about both diagonal axes,

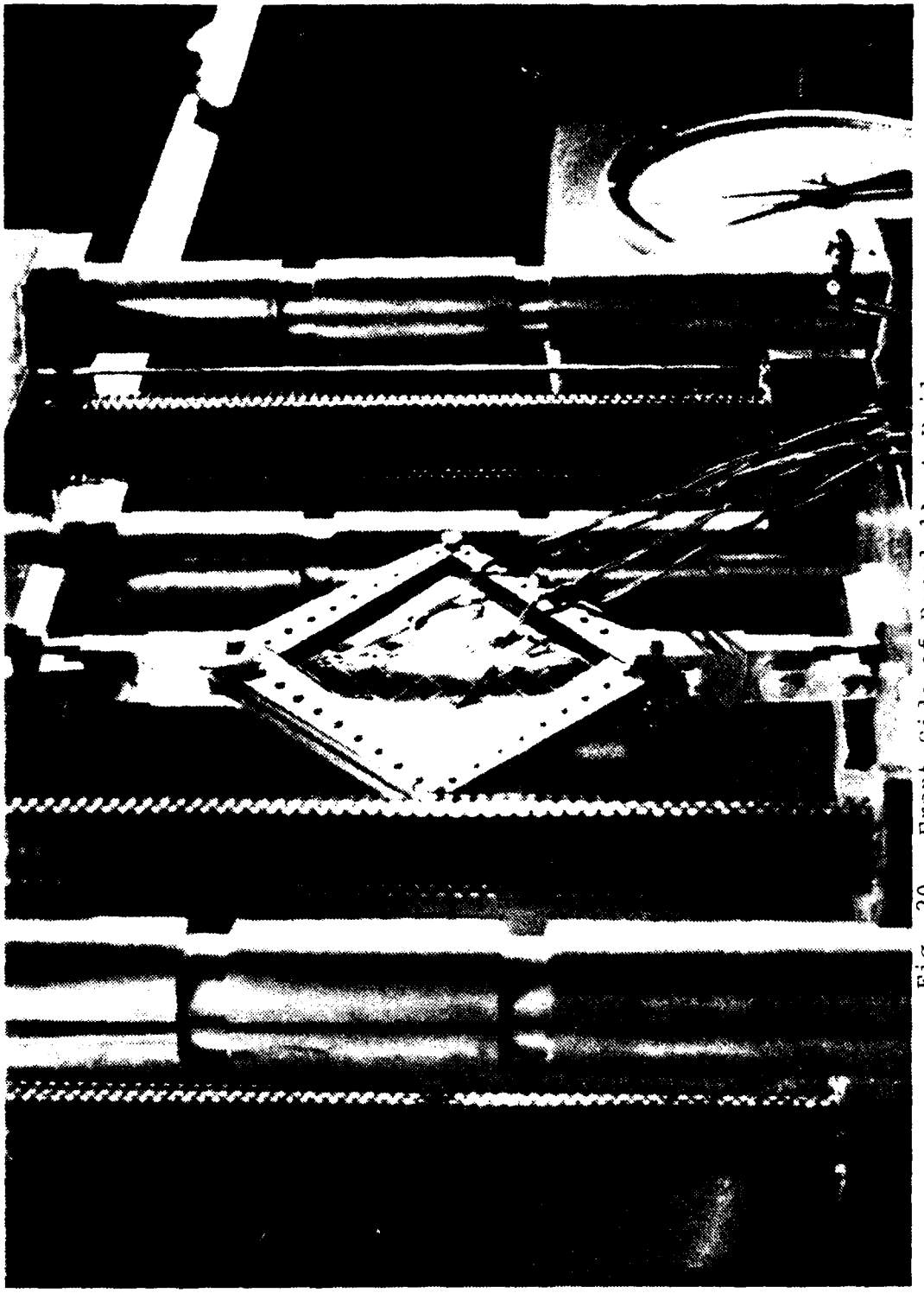

Fig. 20. Front Side of Panel 1A at Failure

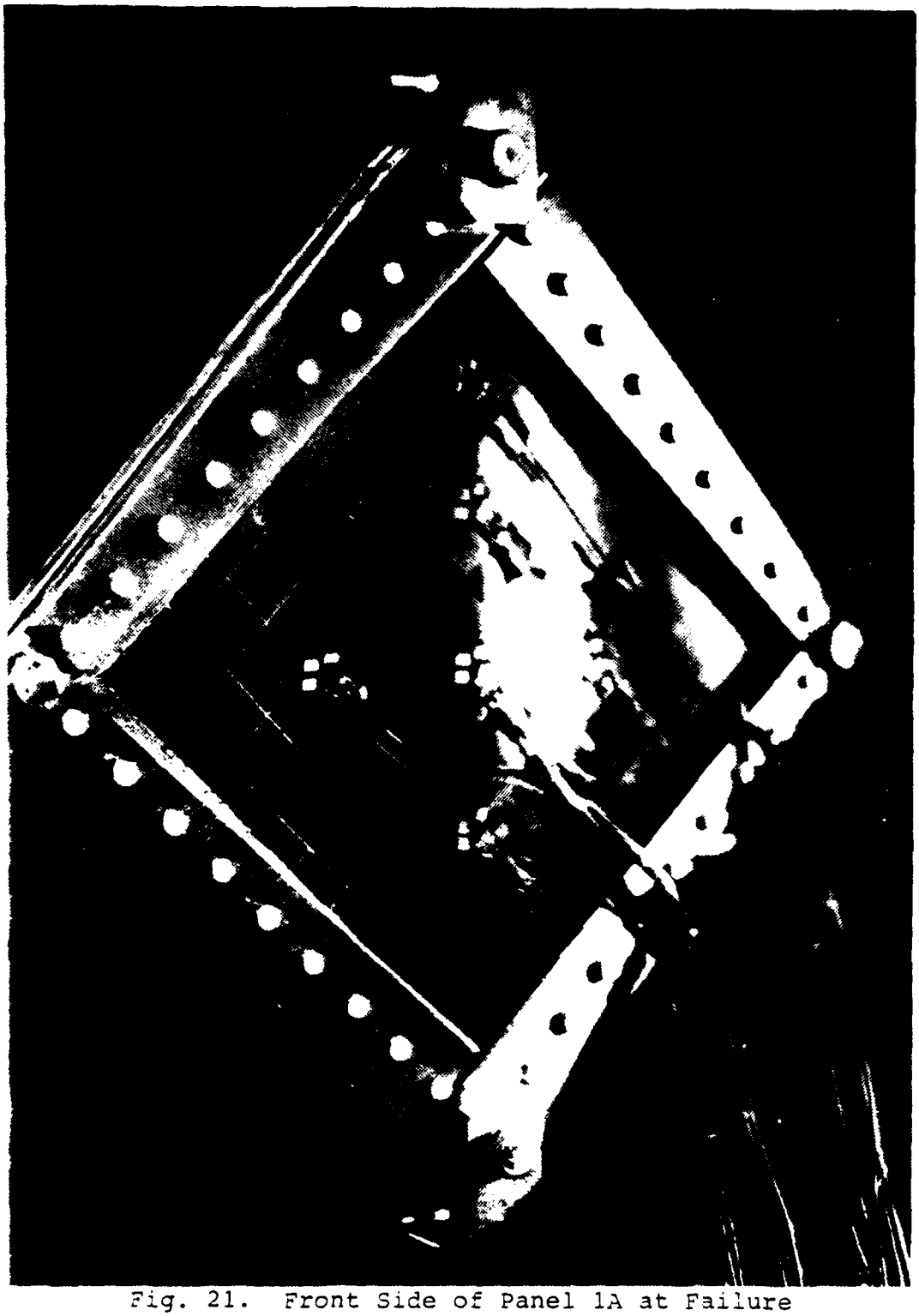

Fig. 21. Front Side of Panel 1A at Failure

Fig. 22. Front Side of Panel 1A After Disassembly

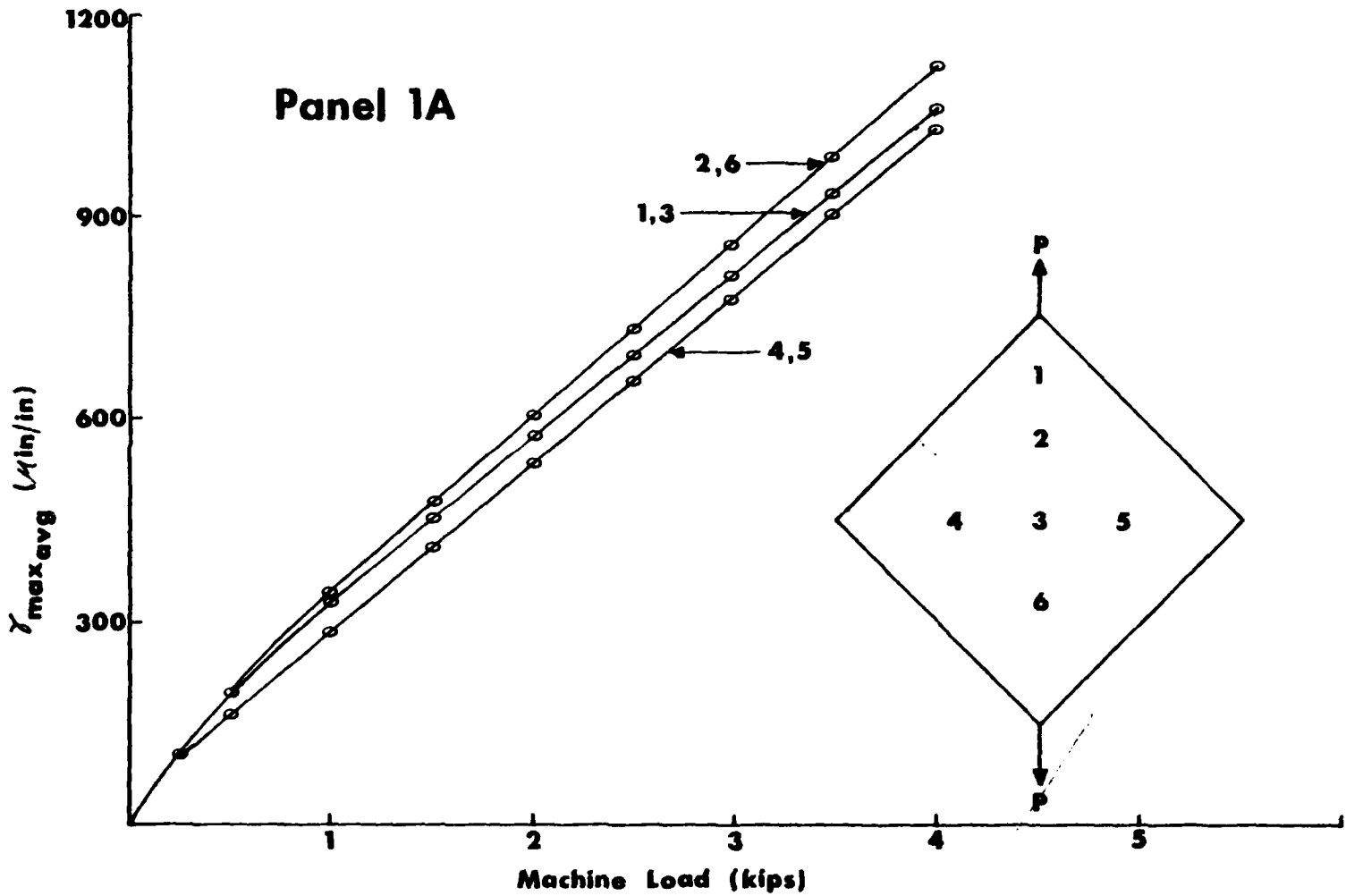

Fig. 23. Shear Distribution for Panel 1A

but varies as much as five percent down the panel as buckling becomes imminent. Figure 24 shows the maximum shear strain values recorded for the center rosette plotted against the calculated shear stress introduced by the test fixture at each load-level. The shear modulus, G, was found to be approximately 4.03×10^6 psi.

2. Panel 1B

Although panel 1B was originally bowed in the same direction and to the same extent as panel 1A, this specimen began to buckle down the center towards the back. The load for buckling was determined to be 2700 pounds. Buckling was visually detectable at approximately 5000 pounds. Small "crackle" sounds were not heard until the load reached a level of 12000 pounds. No secondary buckles were ever seen as this panel approached failure. At 26000 pounds, the specimen instantaneously split completely through the layup on the diagonal tension axis, due to bending. Figure 25, taken during testing, shows the front of the panel as the applied load fell to 24500 pounds immediately after failure. After approximately two minutes at this load-level, the layup failed along the two top sides, load carrying capability was lost completely, and the load fell to zero. The condition of the panel at this point is illustrated in Figure 26, which again shows the front of the panel.

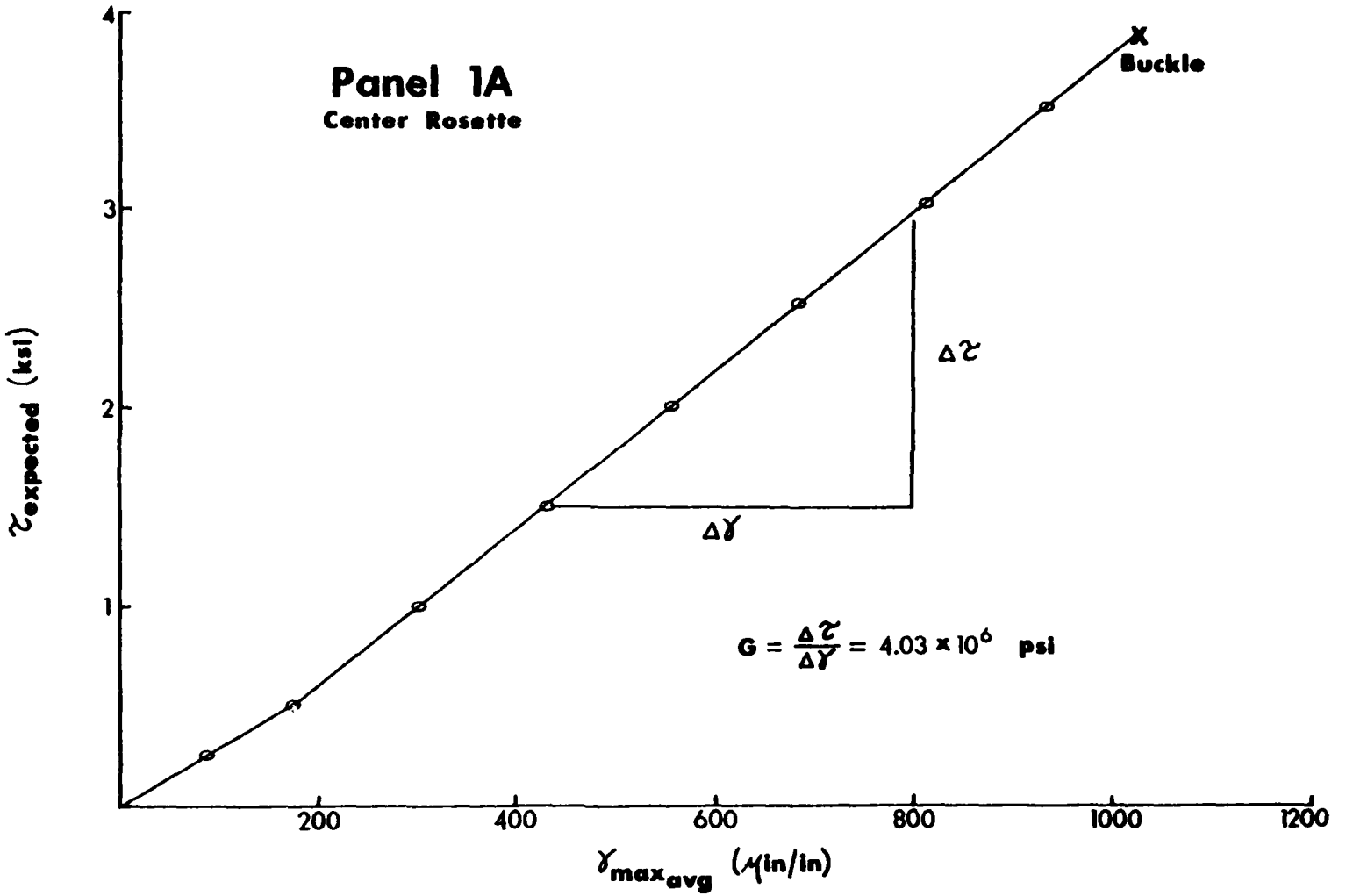

Fig. 24. Shear Modulus Calculation for Panel 1A

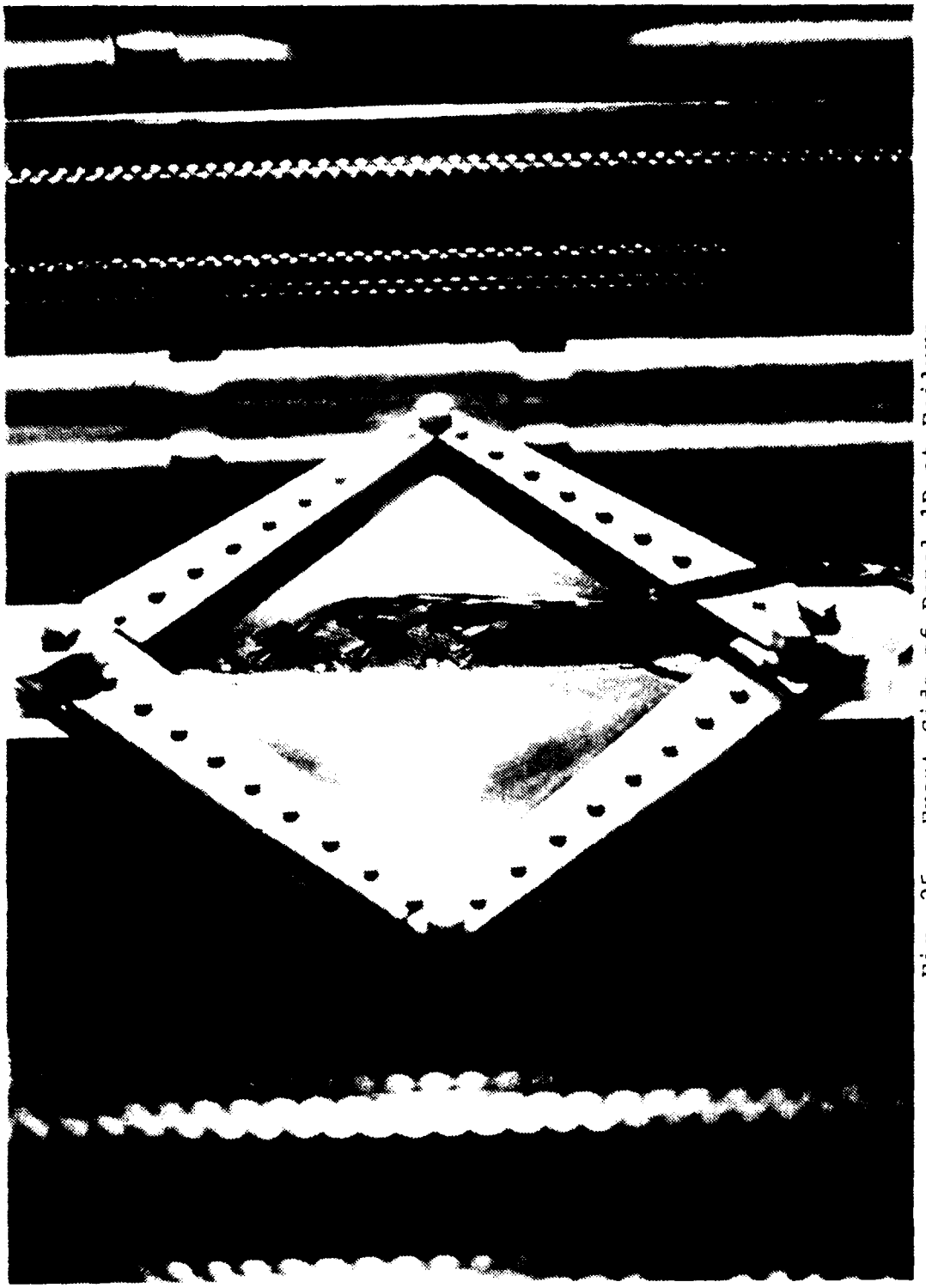

Fig. 25. Front Side of Panel 1B at Failure

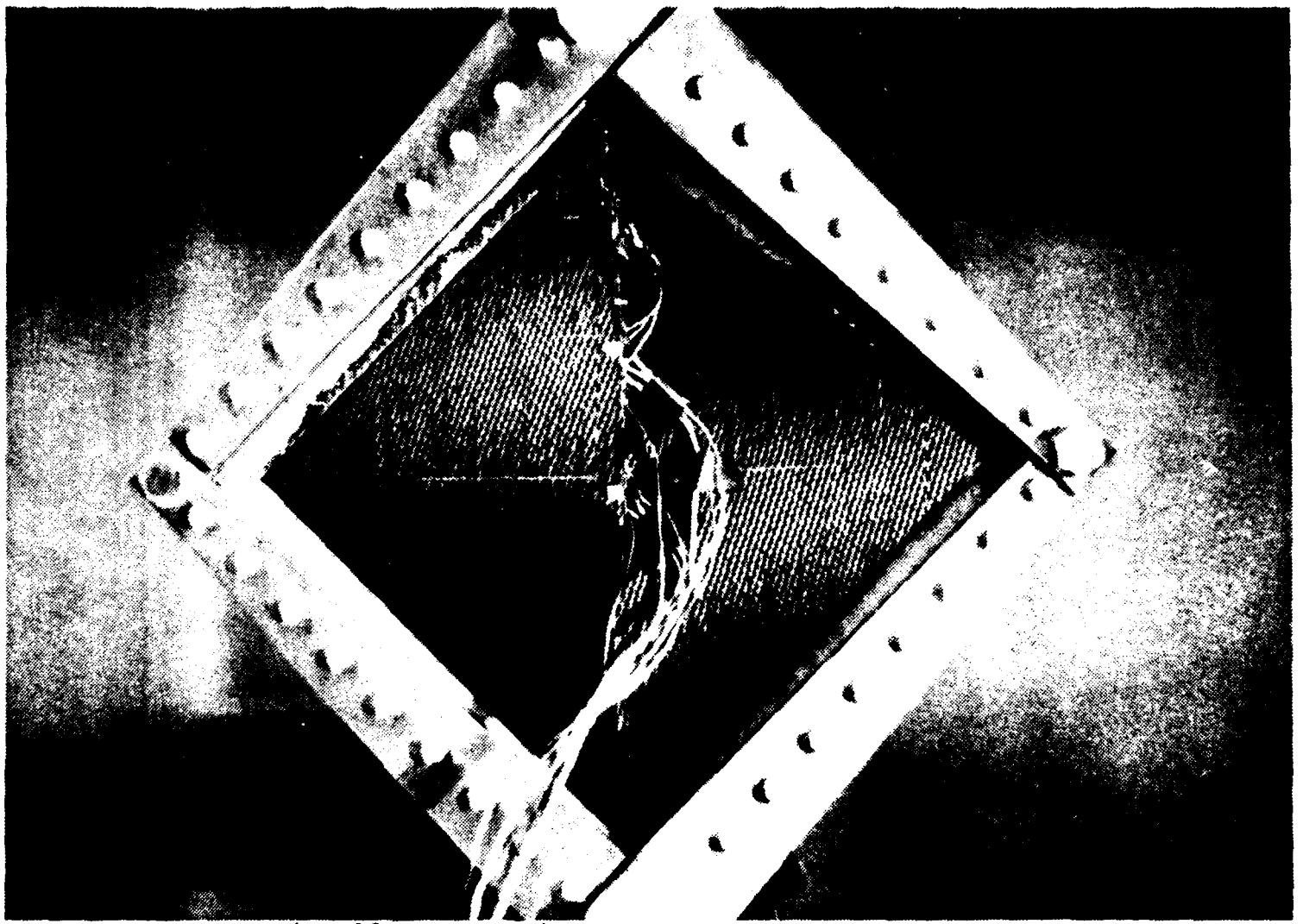

Fig. 26. Front Side of Panel 1B After Collapse

After the panel was removed from the load frame, it returned almost completely to its original flat shape. The extent of panel damage as viewed from the back side of the panel is shown in Figure 27. Visual inspection revealed no damage to the bolt holes and no areas of delamination of the layup.

The distribution of the maximum shear strain in the panel was determined in the same fashion as that for panel 1A. The strain at all three rosette positions down the diagonal tension axis was equal in magnitude and direction up to a load of 2000 pounds. At this point, the maximum shear strain values diverged in the same manner as panel 1A (see Figure 23). A plot of calculated shear stress versus the maximum shear strain at the center of the panel is presented in Figure 28. The shear modulus value for panel 1B determined from this graph was 3.93×10^6 psi.

B. PANELS WITH UNREINFORCED HOLE

1. Panel 2A

The direction of original warp for this specimen was towards the back. The buckling load determined at the position of the rosette was 1000 pounds, although local deformation at the hole began at approximately 650 pounds. This local distortion around the hole could be detected visually at a load-level of 1000 pounds. Both the top and bottom of the hole (as mounted in the test fixture) buckled

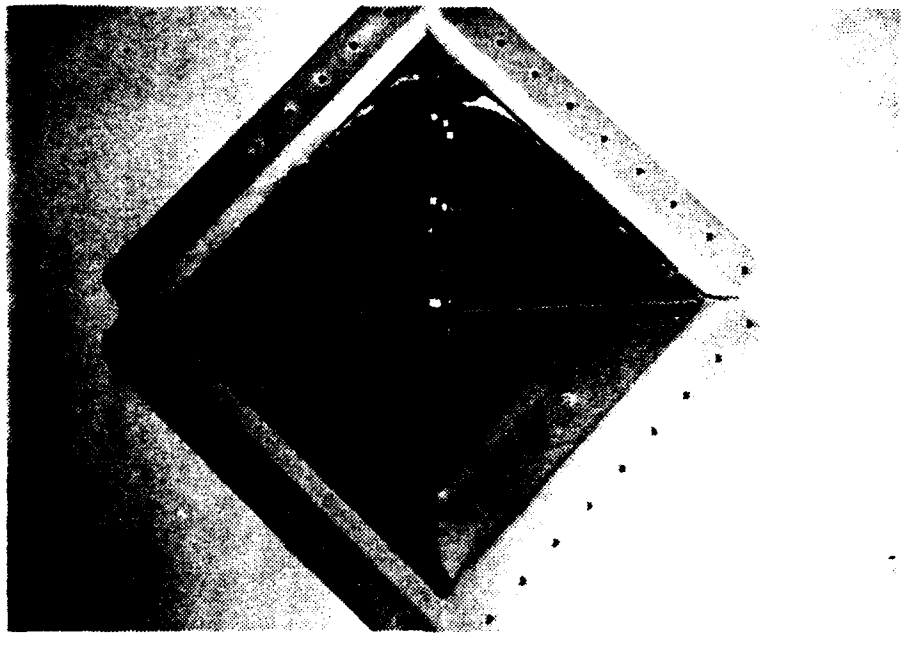

Fig. 27. Back Side of Panel 1B After Disassembly

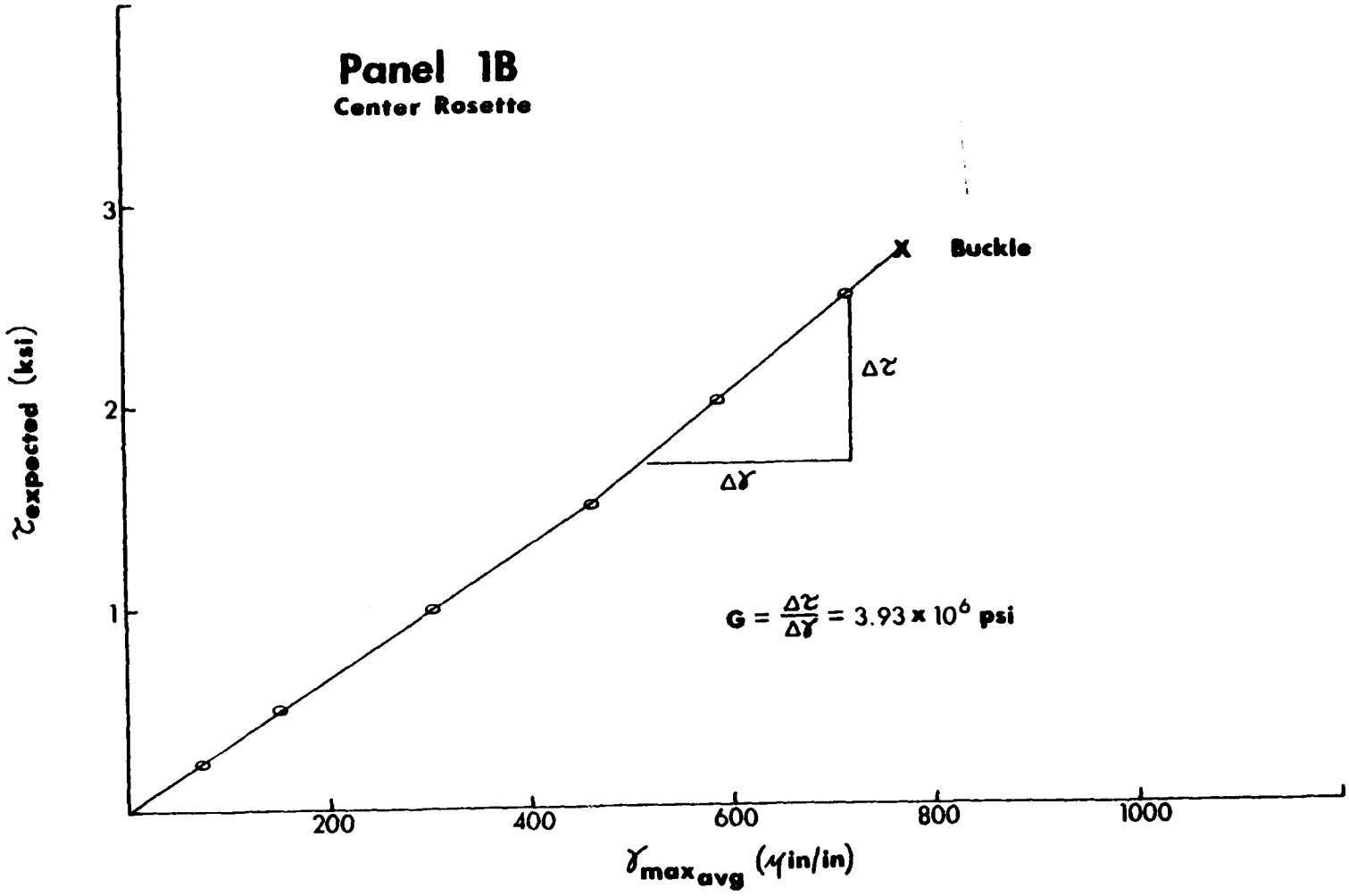

Fig. 28. Shear Modulus Calculation for Panel 1B

towards the back. The edge of the hole at the two positions 90 degrees from the top (or bottom) of the hole remained basically flat. The intermediate positions (45 degrees from the top and bottom) began to bow towards the front. The entire perimeter of the hole subsequently displaced towards the back as buckling of the entire panel commenced.

Small "crackle" sounds were first heard as the machine load reached 5000 pounds. Figure 29 shows the deep buckle down the center of the panel as viewed from the front at 8000 pounds. Immediately after reaching 11000 pounds, a brittle failure with fiber pullout occurred completely through the layup and horizontally across the entire panel. Figure 30 illustrates the front of the specimen immediately after failure. The residual load capability of the panel was only 2000 pounds.

Figure 31 displays the front side of the panel after removal from the frame. The small branch of the crack to the left of the hole was found to extend through only the surface layer. Small compression cracks in the front surface layer were also found in the diagonal tension corners, due to bending. The path of the cracks on the back side of the panel is shown in Figure 32. Once again, the panel resumed a basically flat shape and no skin delaminations or bolt-hole damage could be detected.

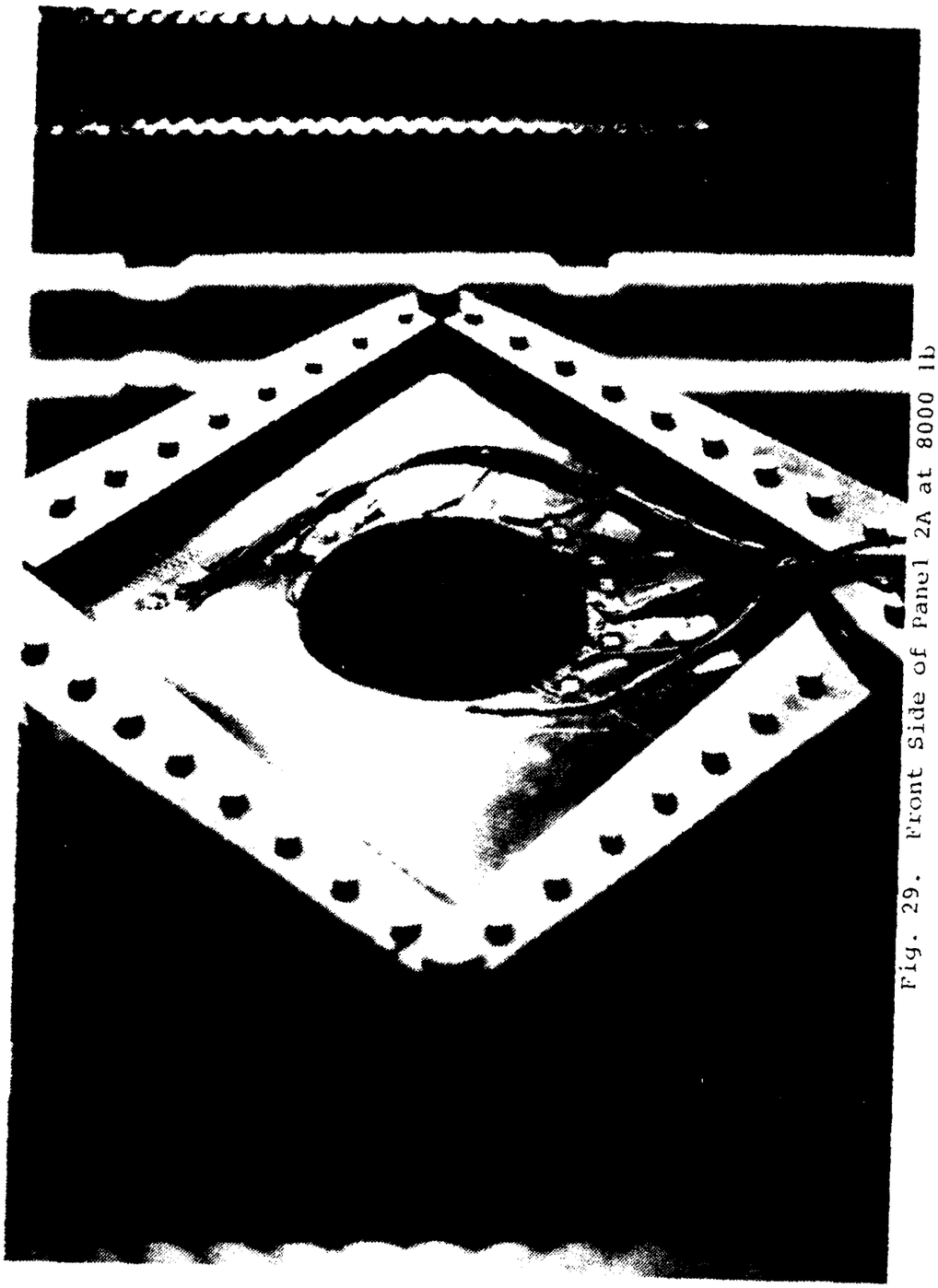

Fig. 29. Front Side of Panel 2A at 8000 lb

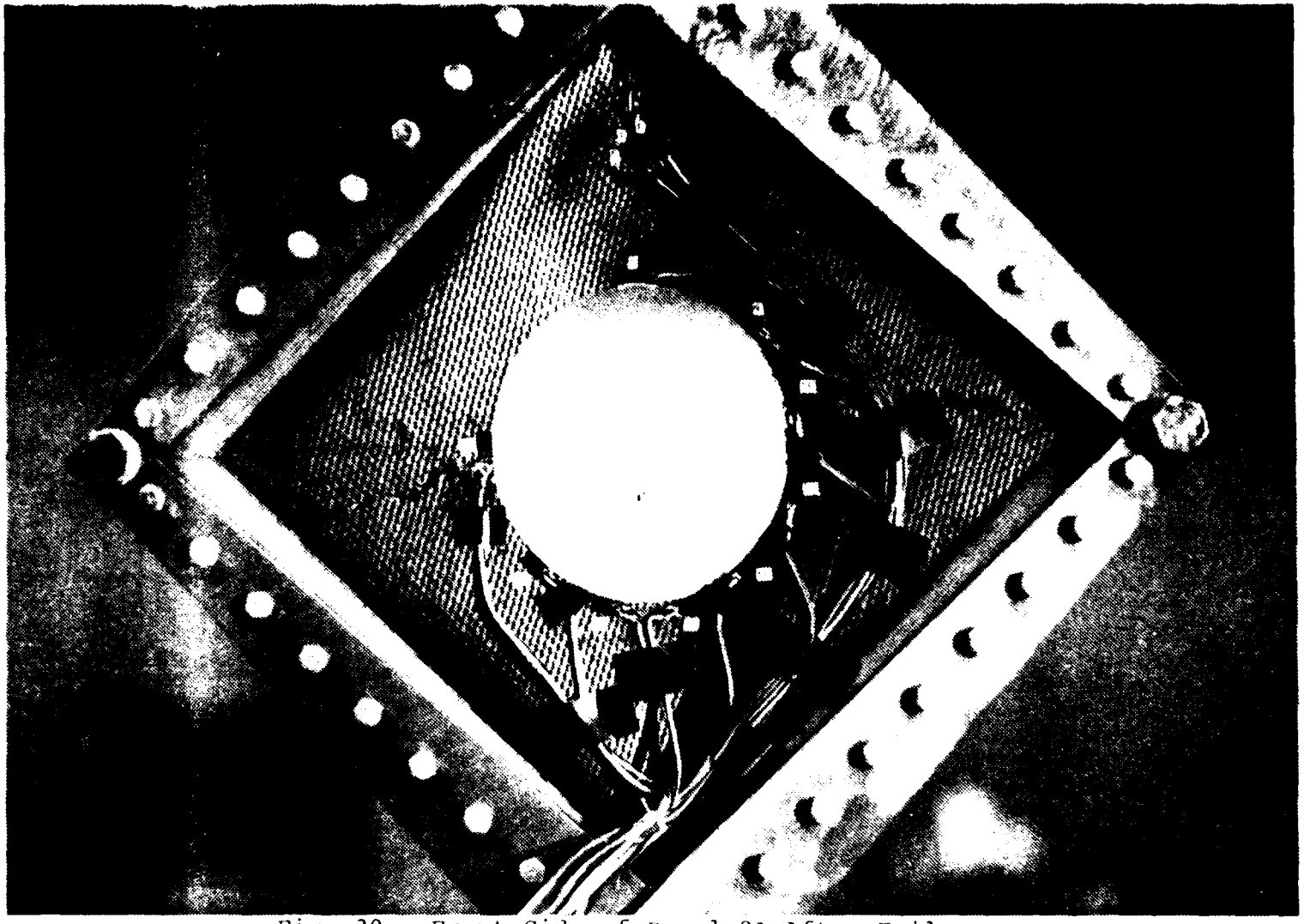

Fig. 30. Front Side of Panel 2A After Failure

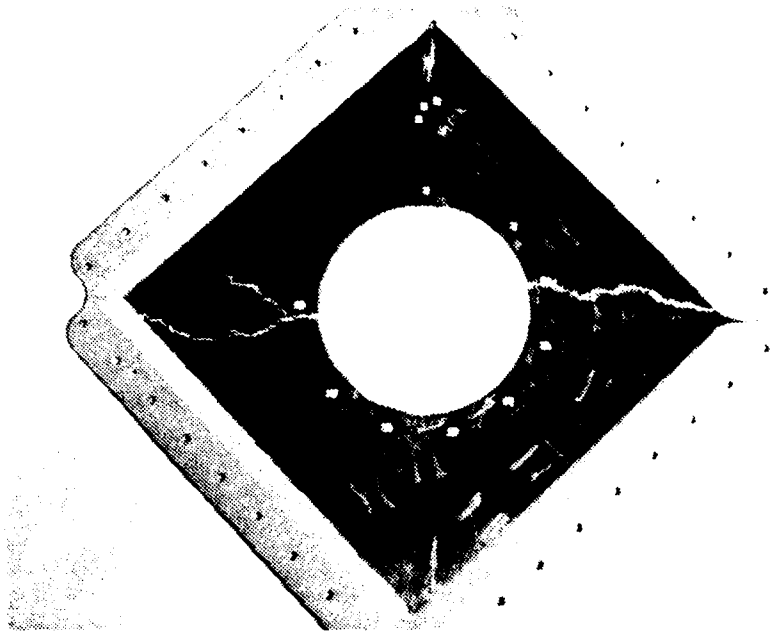

Fig. 31. Front Side of Panel 2A After Disassembly

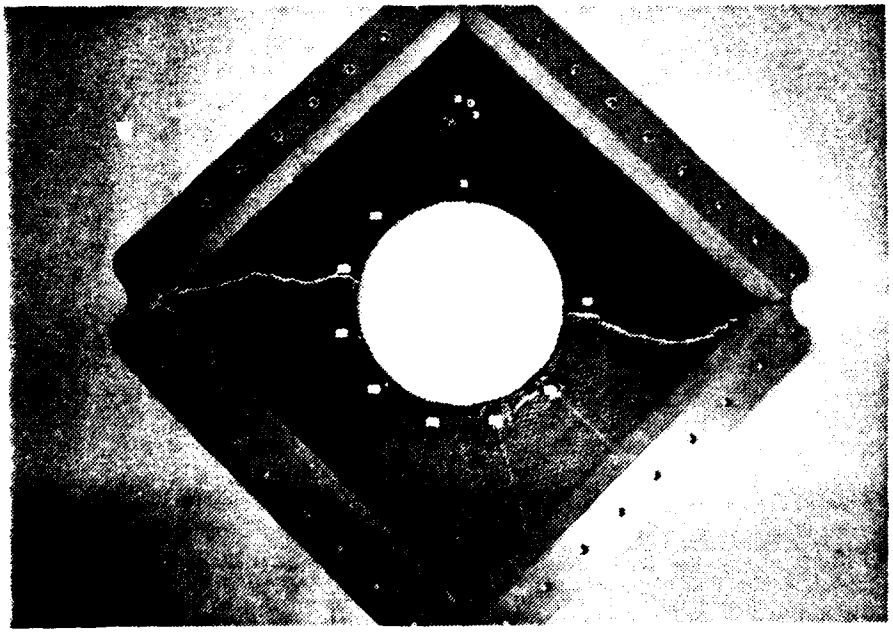

Fig. 32. Back Side of Panel 2A After Disassembly

2. Panel 2B

This specimen was originally warped towards the front side. The panel subsequently buckled in the direction of warp, as did panel 2A. The buckling load was determined to be 1150 pounds from readings obtained from the back-to-back rosettes. The out-of-plane displacement pattern in the postbuckled regime was the same as described for panel 2A.

Audible evidence of initial fiber failures was not detected until approximately 6000 pounds. The front side of panel 2B at 8000 pounds is illustrated in Figure 33. As was the case for the previous unreinforced-hole configuration, failure occurred upon reaching the 11000-pound load-level. The test machine load dropped immediately to 3000 pounds. Figure 34 shows the front of the panel subsequent to failure. An appreciation of the tremendous out-of-plane displacements that occur during buckling can be gained by viewing Figure 35, which shows the back of the panel under load after failure.

Figure 36 displays the path of the brittle tensile fracture with fiber pullout on the front side of the panel. No other damage could be detected on this side. The propagation of the cracks on the back side of the panel can be seen in Figure 37. Again, small compression cracks in the surface layer of the side opposite the buckling direction occurred in the diagonal tension corners due to bending.

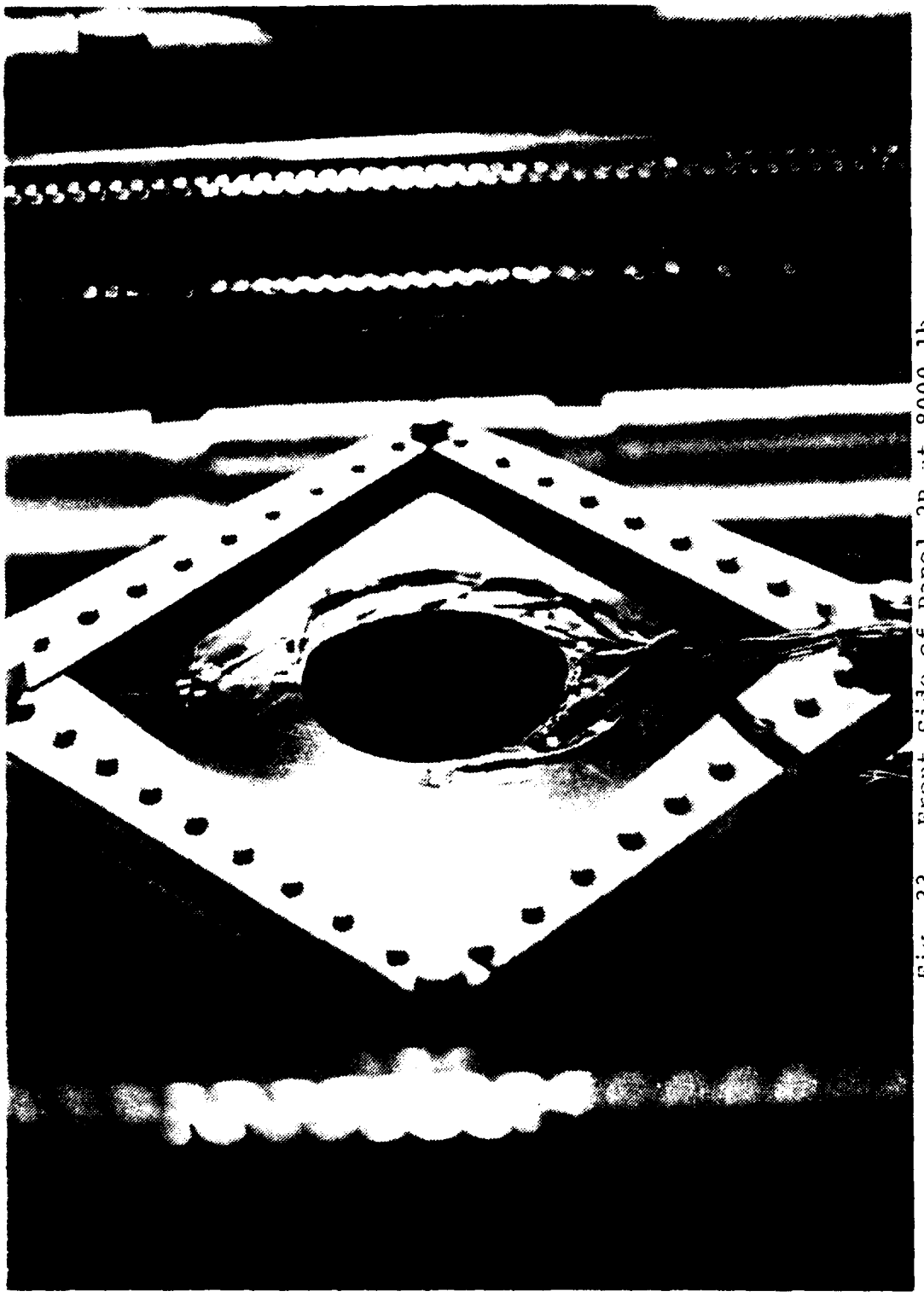

Fig. 33. Front Side of Panel 2B at 8000 lb

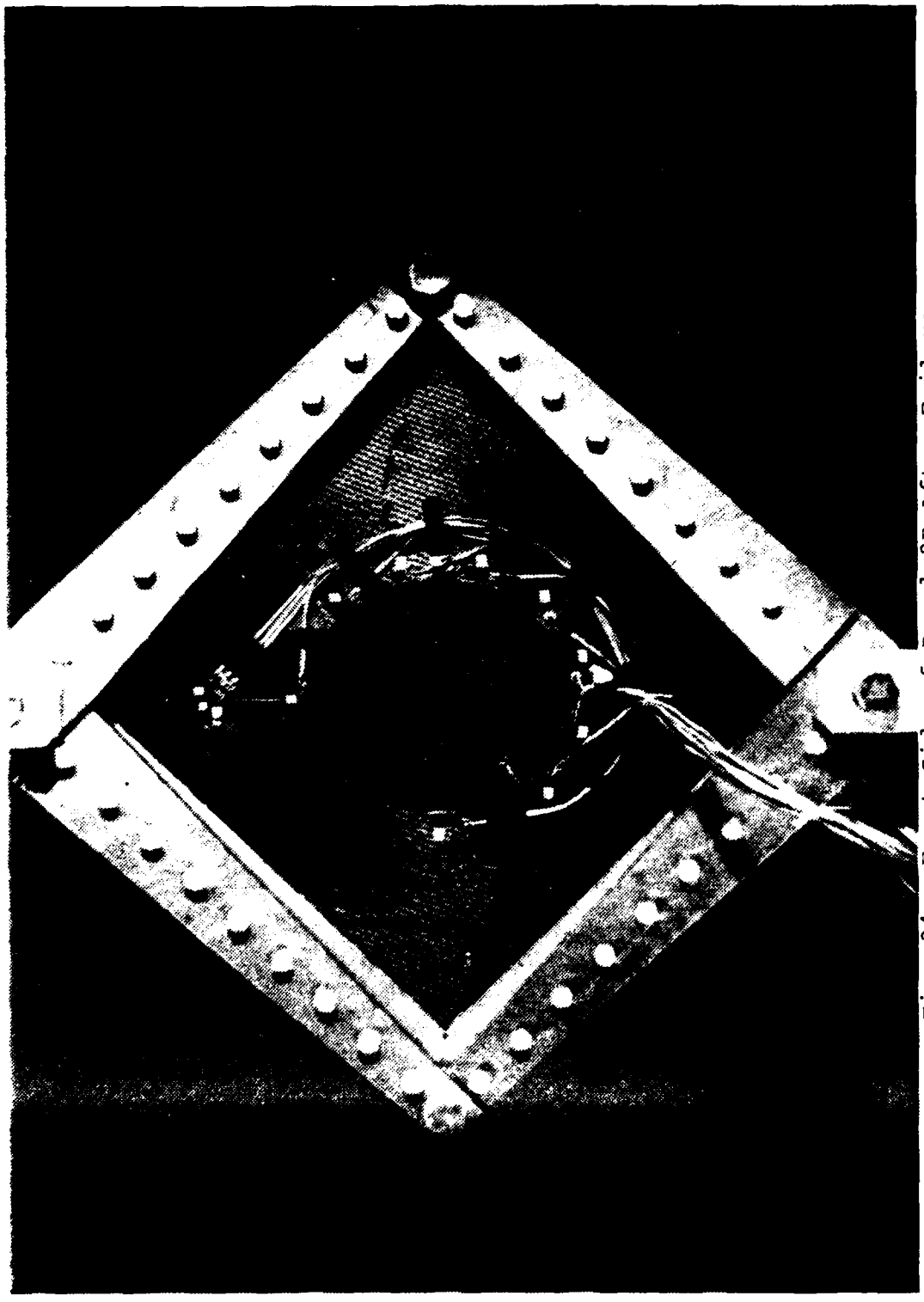

Fig. 34. Front Side of Panel 2B After Failure

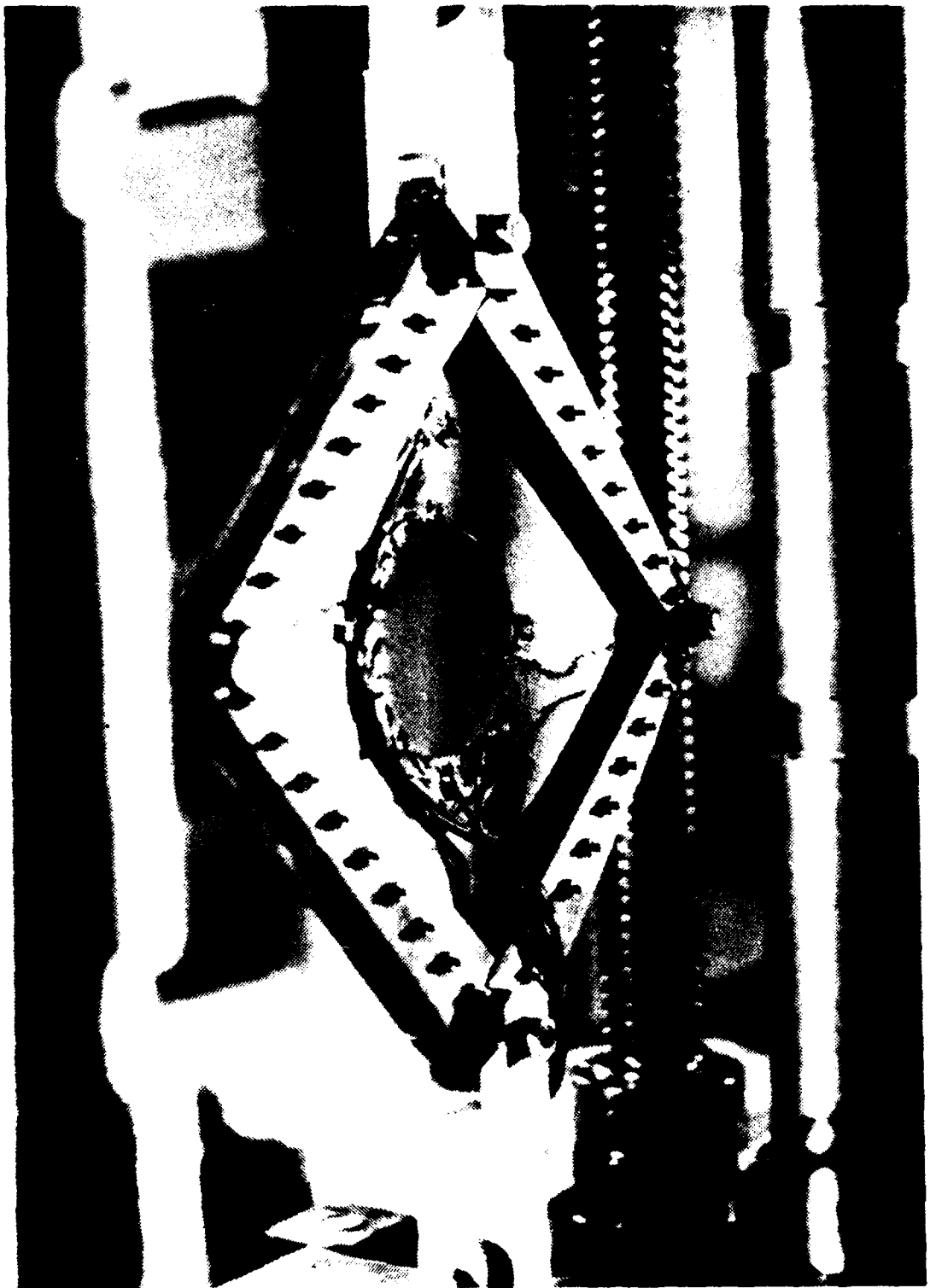

Fig. 35. Back Side of Panel 2B After Failure

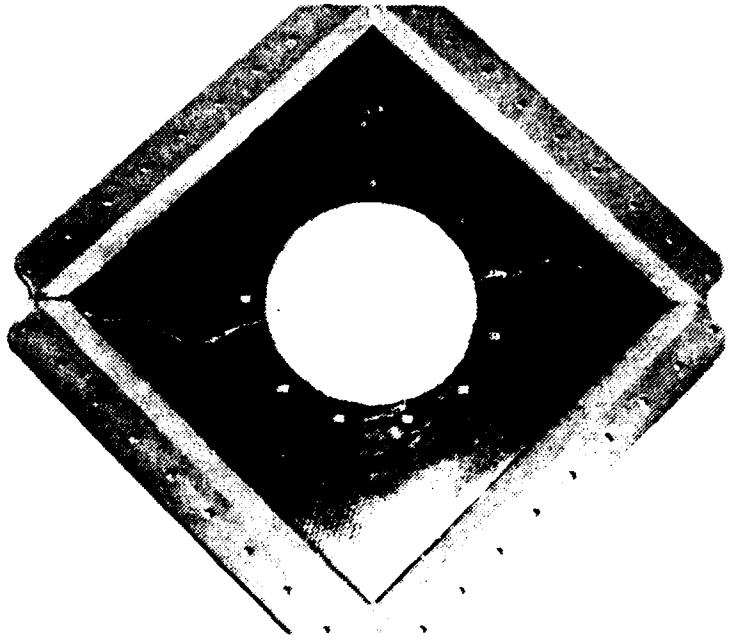

Fig. 36. Front Side of Panel 2B After Disassembly

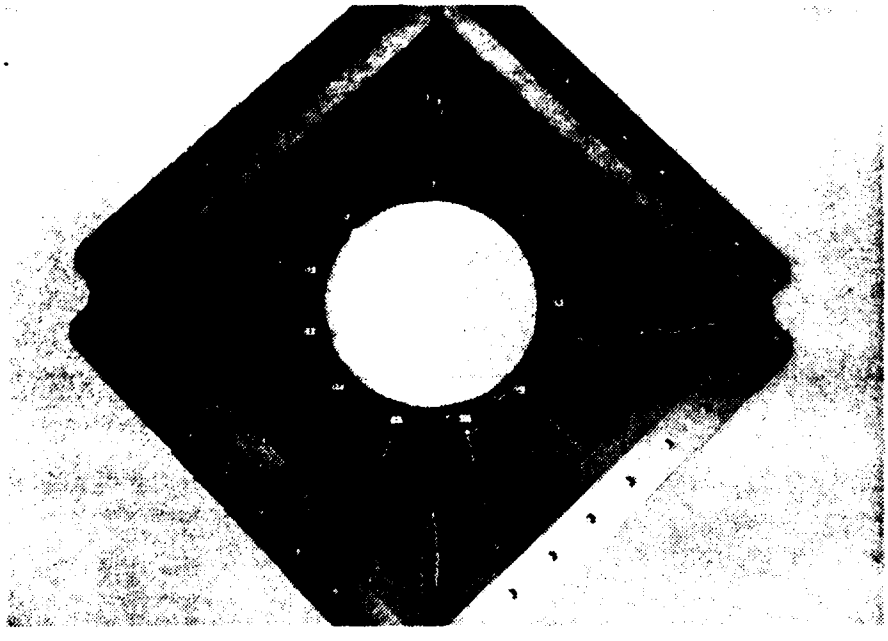

Fig. 37. Back Side of Panel 2B After Disassembly

The areas of this damage are outlined at the top and bottom of the photograph.

C. PANELS WITH FLANGED HOLE

1. Panel 3A

Both of the panels with flanged holes were mounted in the test fixture with the flange extending towards the front of the Riehle machine. The buckling load for panel 3A was determined at the rosette position to be 2600 pounds. Movement of the flange towards the front at the top and bottom of the hole (as mounted in the test fixture) could not be detected visually until 3000 pounds. Unlike the unreinforced configuration, the entire flange began to displace towards the front as the load was increased. The movement of the flange was greatest at the top and bottom of the hole and decreased uniformly to the sides. Simultaneously, the 45°-flange angle was forced to decrease at the top and bottom and increase on the sides. As a result, the tangential stress in the flange at the two positions along the diagonal compression axis was found to be a combination of tension and bending.

Small "crackle" sounds were heard beginning at a load of approximately 6000 pounds. Figure 38 shows the buckling pattern at 8000 pounds as viewed from the front side. At 10500 pounds, a loud "pop" was heard and a small crack through the flange at the top of the hole was

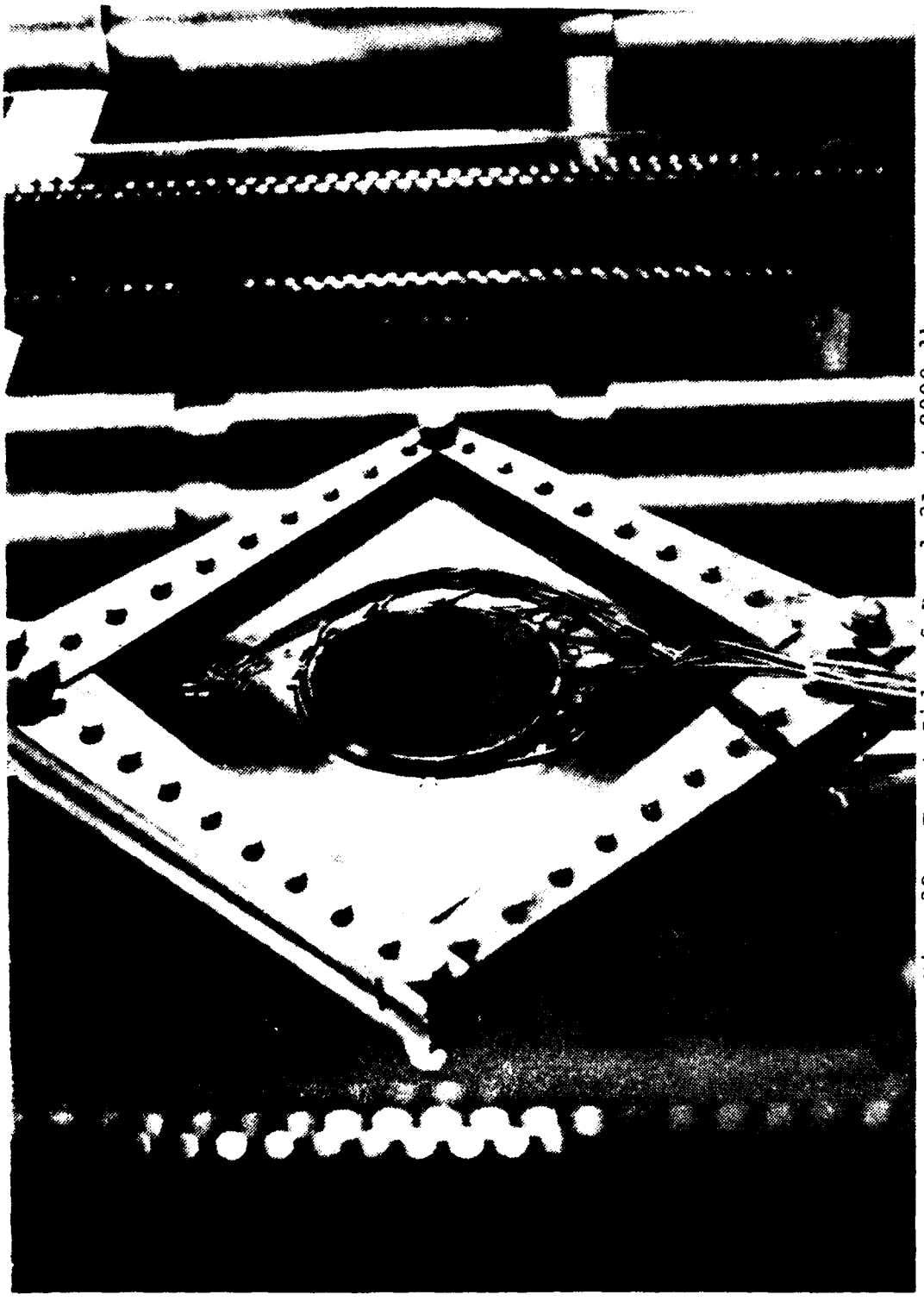

Fig. 38. Front Side of Panel 3A at 8000 lb

discovered. No significant loss of load-carrying capability occurred as a result of this failure. Additional load was applied to the fixture and at 12000 pounds, the bottom of the hole cracked in a similar fashion. After approximately 30 seconds at this load-level, the panel failed completely along the diagonal compression axis and the load dropped to 1250 pounds. The front of the panel at this load is displayed in Figure 39 and the back in Figure 40.

The panel returned to its original flat shape after removal from the "picture frame." Neither any delamination of the laminate nor any bolt-hole damage could be found. The two small bending cracks at the top and bottom of the hole can be seen in Figure 41 which shows the front side of the panel. The path of the brittle fracture along the compression axis can also be seen. The small branch of the crack on the left side of the hole was found to extend only through the outer 45°-ply. Damage to the back side of panel 3A is illustrated in Figure 42. The extent of surface compression cracking along the diagonal tension axis was found to be much more extensive than that of the unreinforced-hole configuration. These areas of damage are outlined in the photograph.

2. Panel 3B

The buckling load for this specimen was determined to be 2550 pounds. The buckling pattern developed in

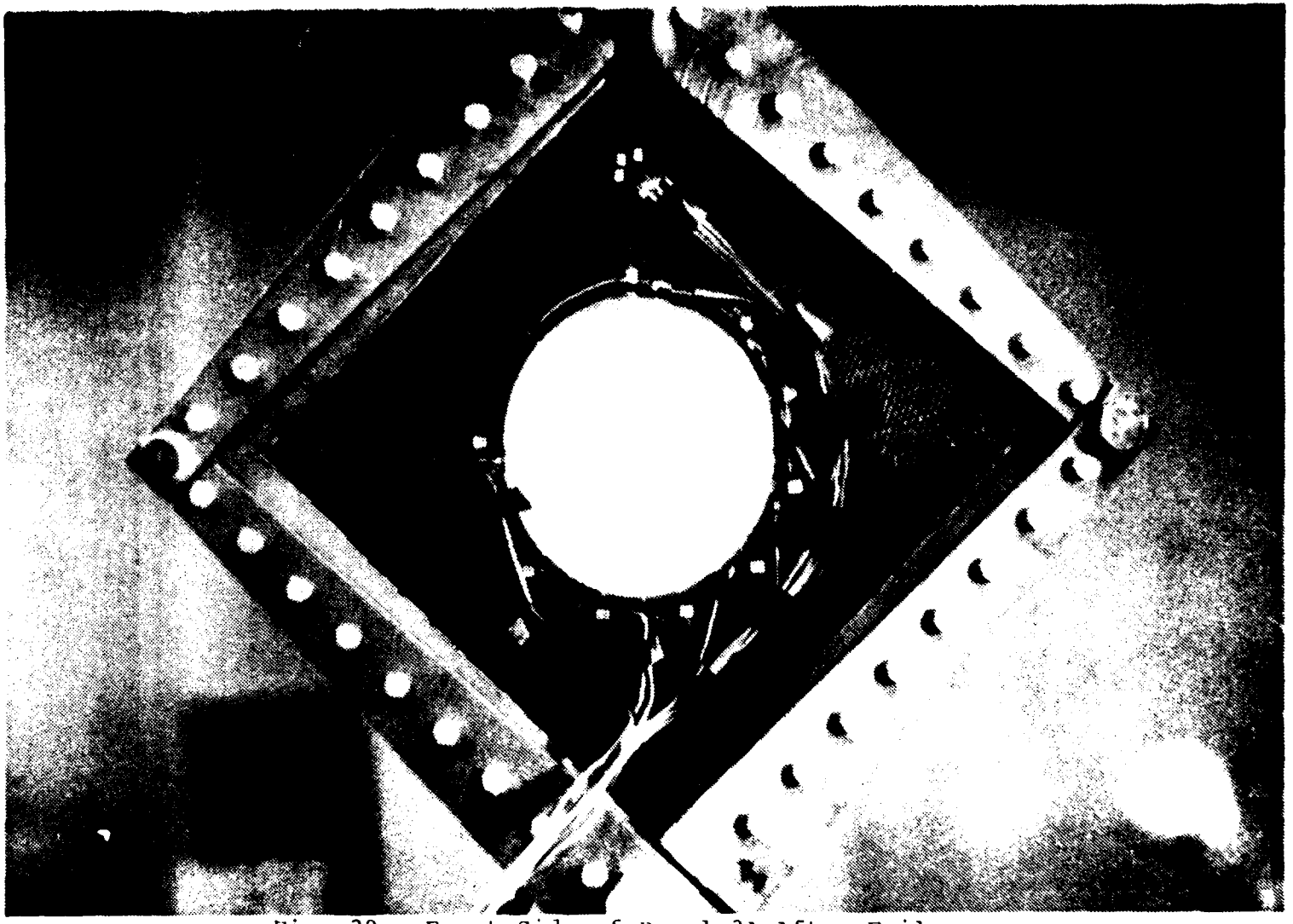

Fig. 39. Front Side of Panel 3A After Failure

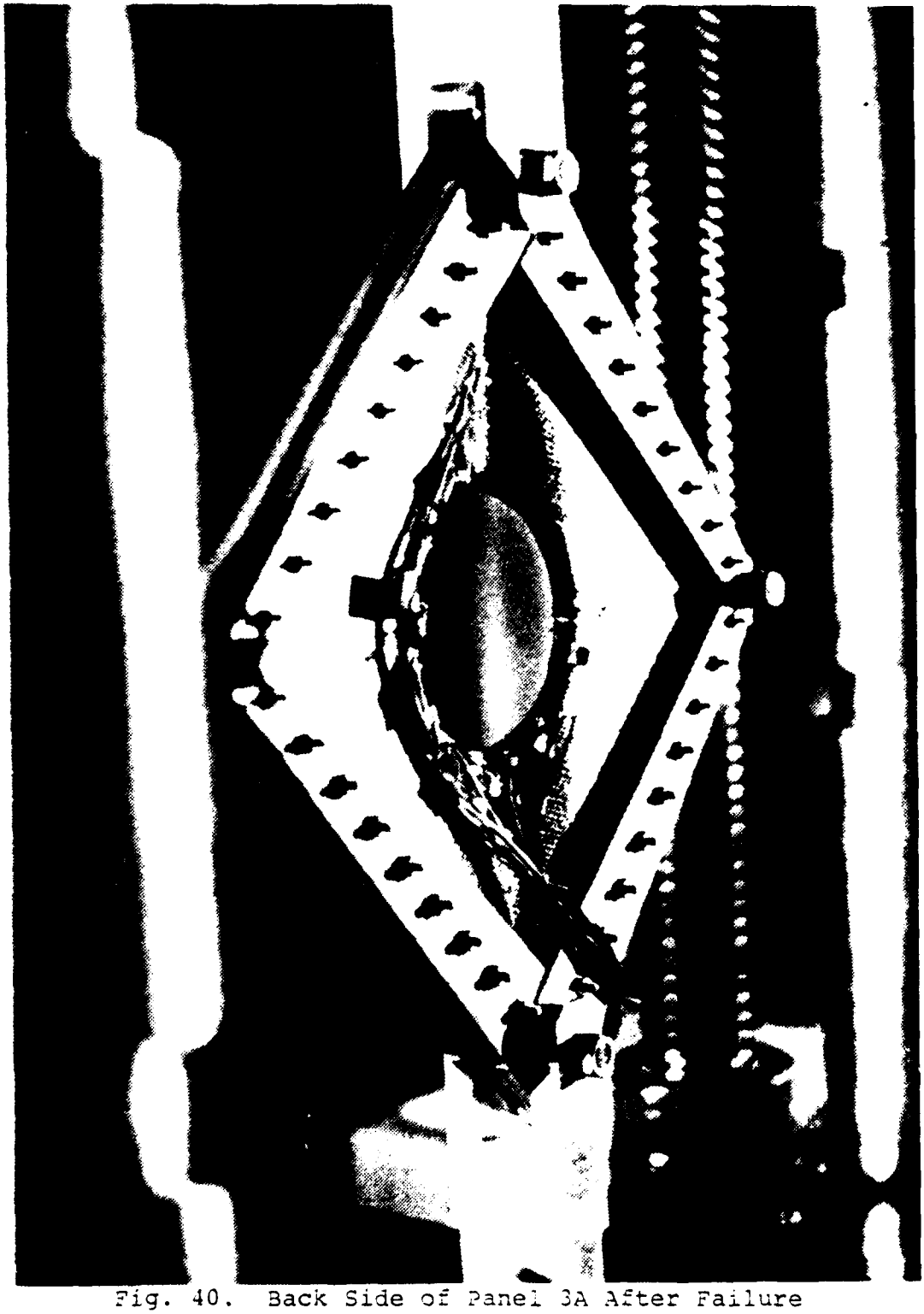

Fig. 40. Back Side of Panel 3A After Failure

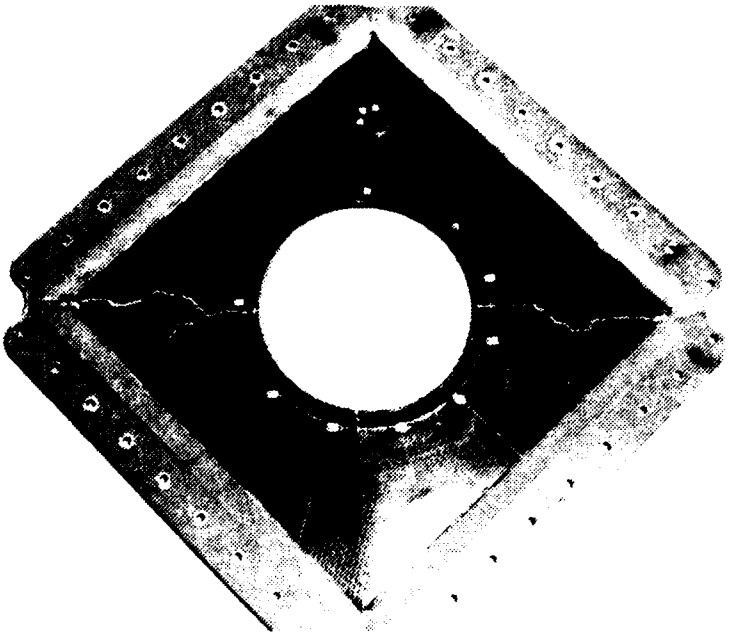

Fig. 41. Front Side of Panel 3A After Disassembly

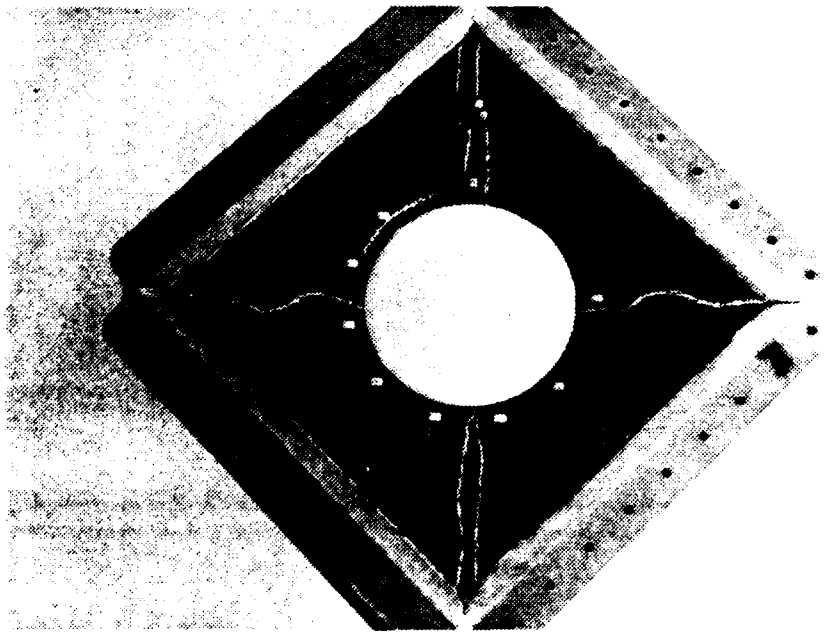

Fig. 42. Back Side of Panel 3A After Disassembly

exactly the same manner as described for panel 3A. At 10750 pounds, a 3/4-inch crack extending completely through the layup occurred at the top of the hole due to bending. After approximately three minutes had passed with the test machine stopped at this load, an identical crack propagated at the bottom of the hole. Figure 43 shows the front side of the panel while maintaining 10500 pounds of load after the failure. Additional load was applied until reaching 12400 pounds. At this time, the panel failed completely along both diagonal axes and the machine load dropped to 750 pounds. Figures 44 and 45 show the front of the panel after this complete collapse.

The propagation of the brittle fracture with fiber pullout along the compression axis can be seen in Figure 46 which shows the front side of the specimen. Unlike panel 3A, vertical cracks caused by high tensile stresses in the surface layer due to bending can be seen to extend completely down the panel. Again, surface compression cracking was extensive along the diagonal tension axis on the side opposite the buckling direction, which was the back side in this case. These areas of damage are outlined on the back of the specimen in Figure 47.

D. SUMMARY OF RESULTS

The results of the shear panel tests are presented graphically in Figure 48 (the set of steel frames used to

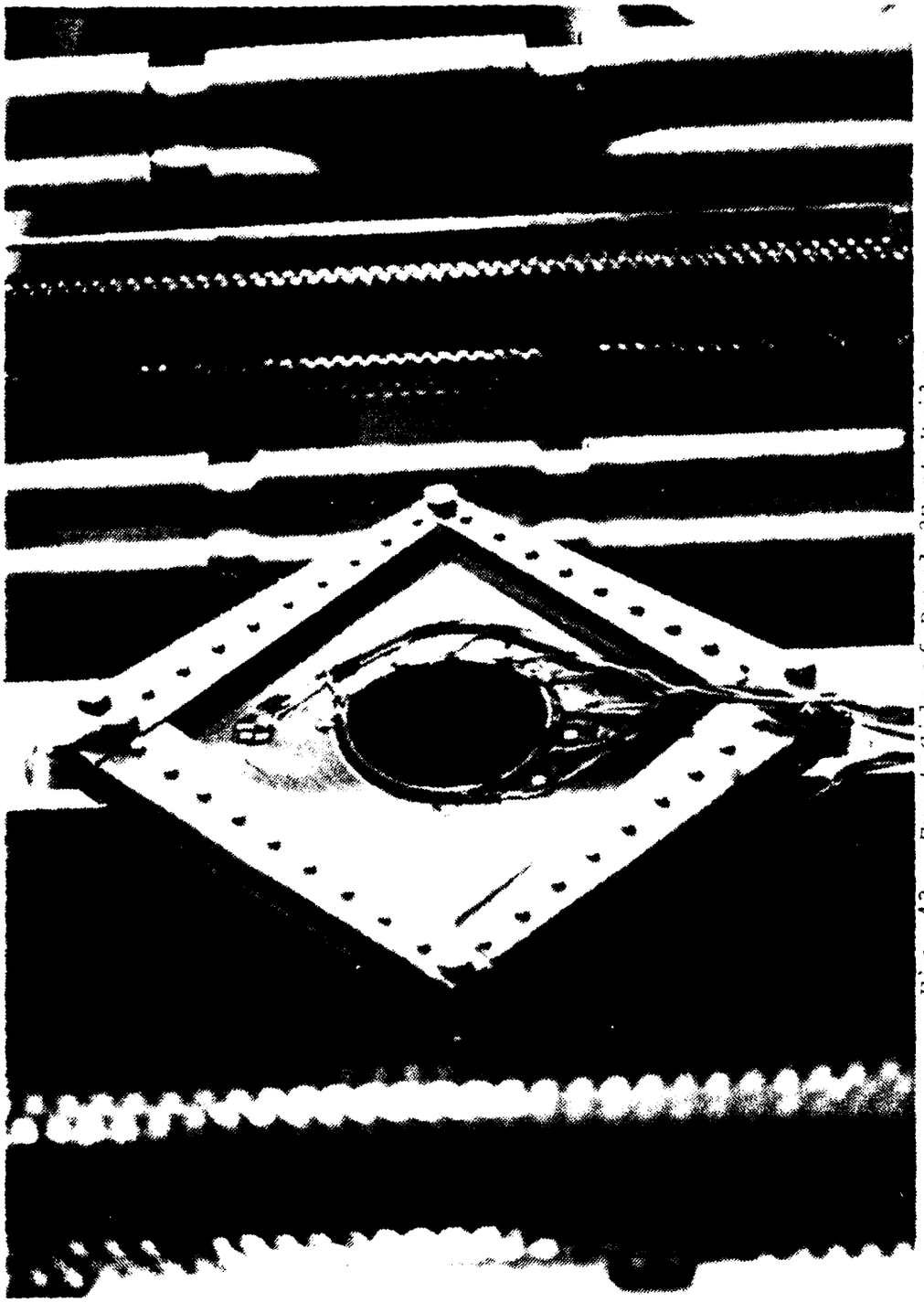

Fig. 43. Front Side of Panel 3B at Failure

Fig. 44. Front Side of Panel 3B After Collapse

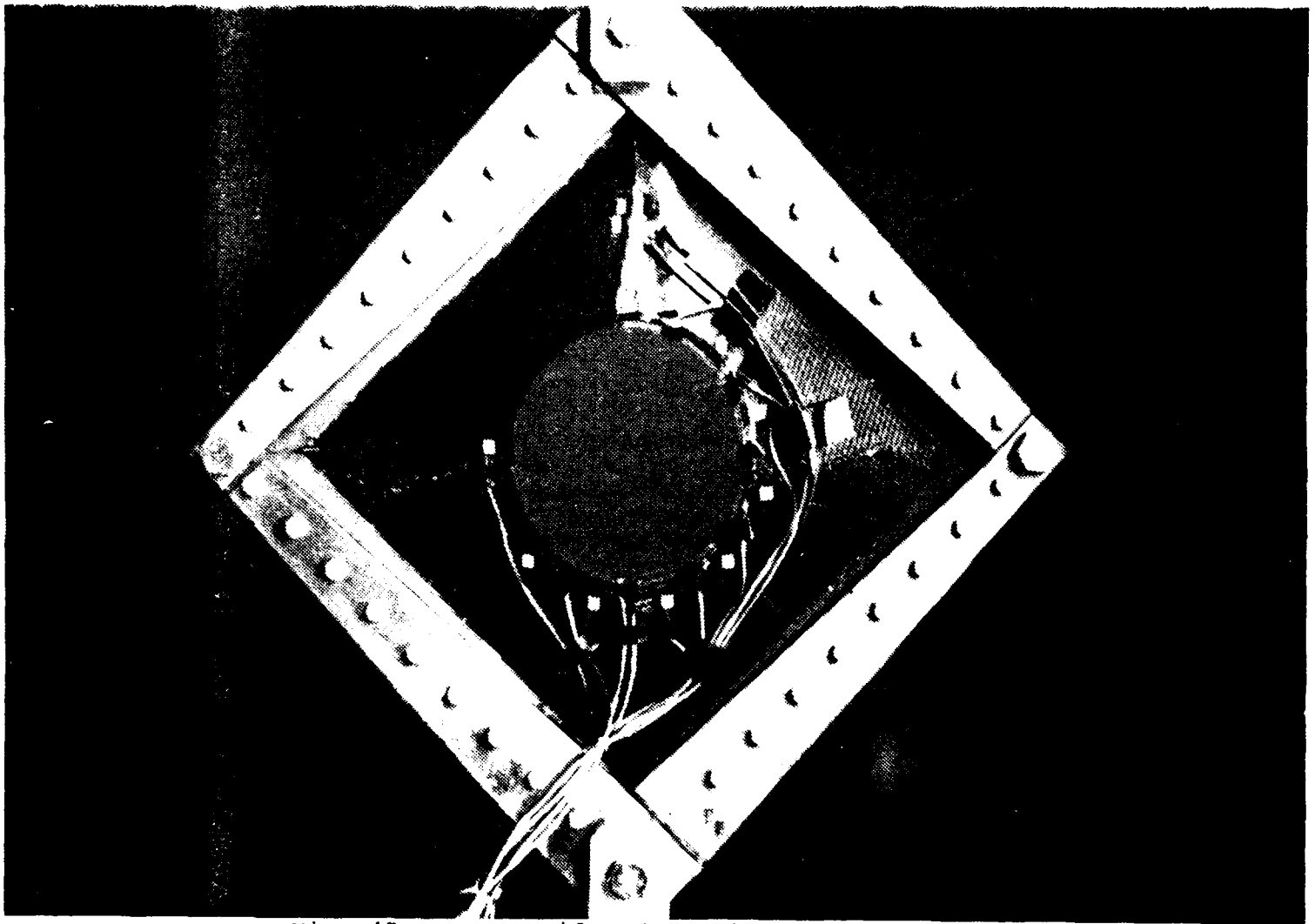

Fig. 45. Front Side of Panel 3B After Collapse

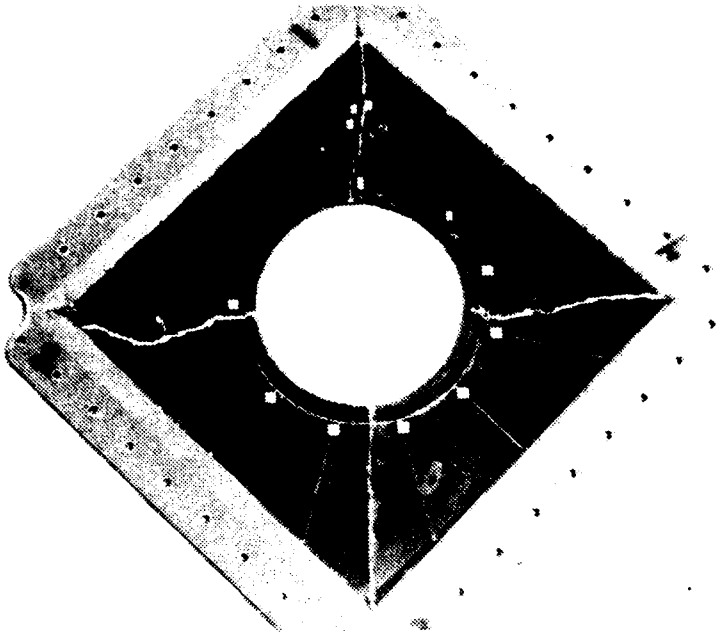

Fig. 46. Front Side of Panel 3B After Disassembly

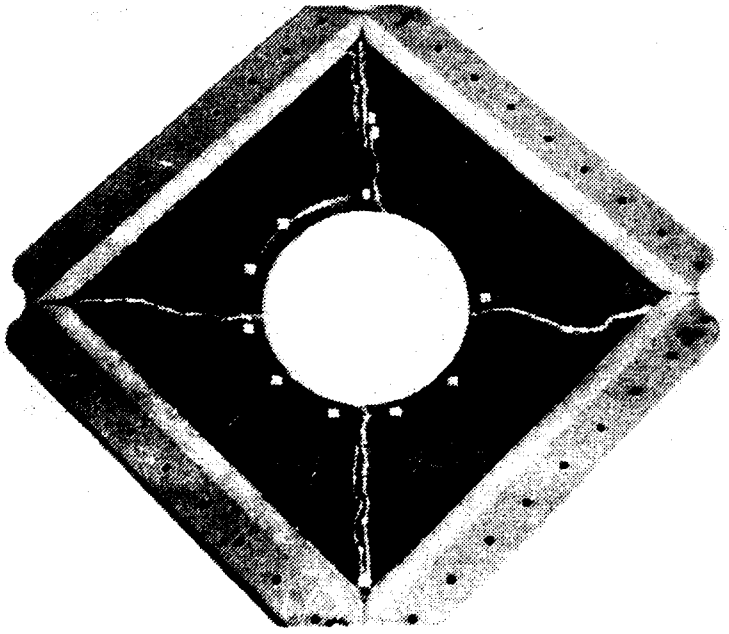

Fig. 47. Back Side of Panel 3B After Disassembly

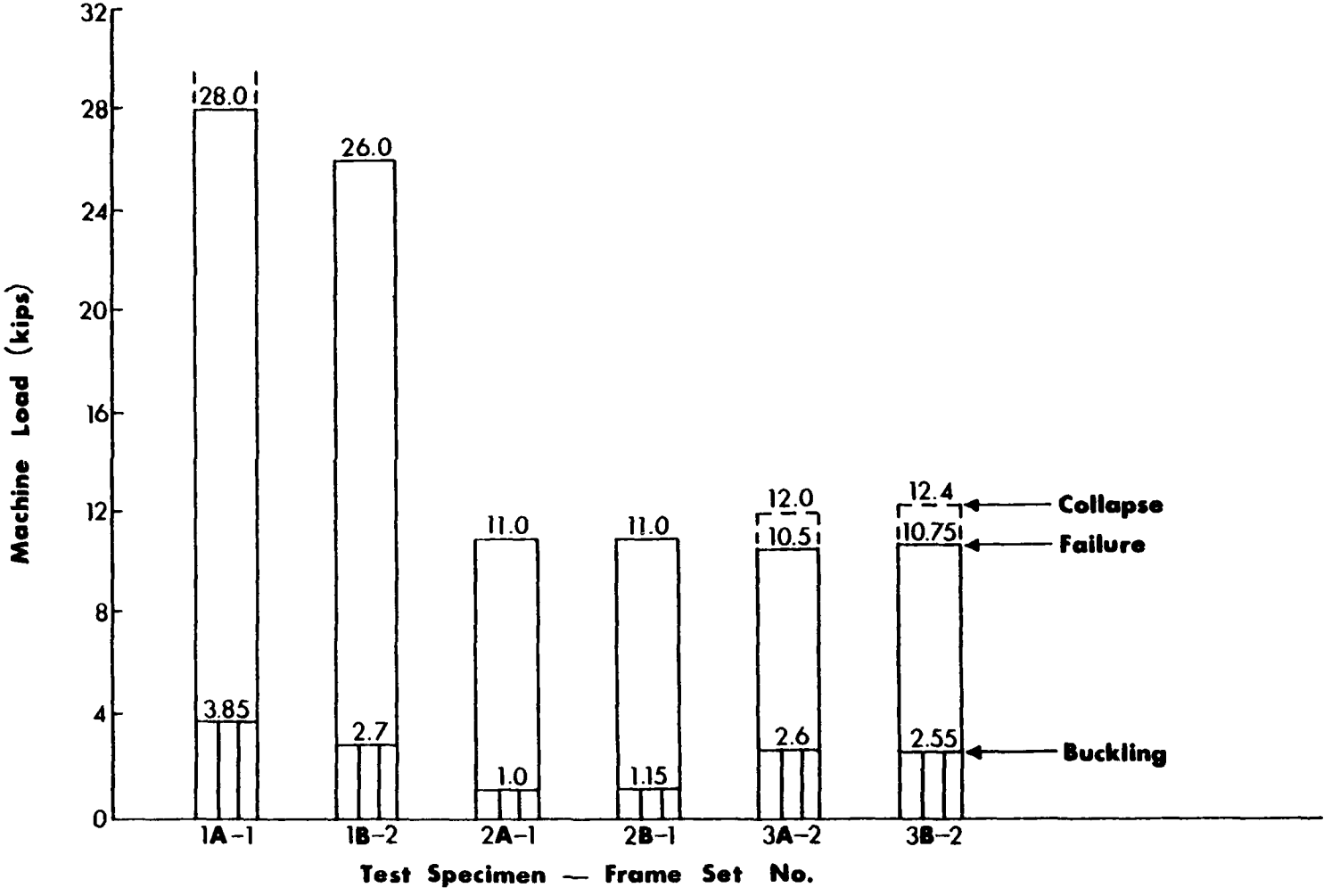

Fig. 48. Experimental Results

load each specimen is indicated as a hyphenated post-script). The load values for failure and collapse are accurate to within ±25 pounds.

The load values for the onset of buckling were based solely on the method described previously. Since the pre-buckling and postbuckling portions of the bending strain versus load curve for the solid panels were very linear, it is felt that these loads are accurate to within ±25 pounds. However, the panels with holes displayed a some-what nonlinear postbuckling curve. As a result of this phenomenon, it was difficult to determine the slope in the postbuckling region. Therefore, an approximation technique was employed to define the postbuckling slopes of all of the panels with cutouts in the same way. Therefore, the buckling loads should relate well amongst the panels, but the actual buckling load could be as much as 50 pounds in error.

Another important aspect affecting these results is the location of the strain gage utilized to compute buckling. Since all of the rosettes positioned down the diagonal ten-sion axis of the solid panels indicated buckling simulta-neously, a problem does not arise in this case. However, in the case of a panel with a hole (especially unrein-forced), stress concentrations cause local buckling defor-mations to appear first near the hole. As the load is increased, the area of deformation spreads from the hole

to the diagonal tension corners. The load for buckling can vary greatly depending on where the strain gage is placed along the diagonal tension axis. A position half-way between the edge of the cutout and the diagonal tension corner was deemed as an appropriate position to determine panel instability. Therefore, it is felt that no additional error was introduced in the calculation of buckling loads for the panels with flanged holes, but an additional error of approximately ±50 pounds should be added for the unreinforced panels.

VII. DISCUSSION OF RESULTS

A. ASSESSMENT OF TEST FIXTURE

The particular "picture frame" design utilized for testing was found to be quite adequate in subjecting panels to shear loading. Although the load introduced in tension was slightly higher than in compression, the direction of principal strain was reasonably aligned with the panel diagonal axes. Furthermore, the magnitude of the maximum shear strain was relatively uniform throughout the panel. The problem of high tensile stress concentrations in the diagonal tension corners, associated with many "picture frame" designs in the past, appears to have been remedied.

The existence of initial warp in the panels did not seem to affect the direction of buckling for the solid configuration. Although both of these panels were initially warped, they seemed to behave as flat plates during testing. Both panel 1A and panel 1B were bowed in the same direction as assembled in the load frame, but they buckled in opposite directions. It should be noted, however, that the buckling loads and modes for these two panels were quite different. The buckling load for panel 1B was 30 percent less than that for panel 1A. Unlike panel 1A, the development of small secondary buckles was not observed during the testing of panel 1B, and the failure mode was also somewhat

dissimilar. The difference in experimental G values for the two panels was only 2.5 percent (see Figures 24 and 23). Both of these values indicate that the laminates were slightly stiffer than predicted.

Although a problem in correlating solid-panel results arose, both of them displayed adequate strength. It will be shown that the test fixture created boundary conditions which were closer to simply-supported than clamped. Both solid panels buckled at a load close to, although somewhat higher than, that predicted for simply-supported boundary conditions. In addition, sufficiently high buckling ratios (on the order of eight) were demonstrated. Using results presented by Kuhn [Ref. 8], the graphite/epoxy cloth panels displayed approximately four times the ultimate strength of an equivalent aluminum web.

The failure load for the two solid panels was based on the first visual indication of any damage. Closer inspection after testing revealed the very small areas of compression cracking in the diagonal tension corners mentioned previously. These cracks were found in the surface layer of the side opposite the direction of buckling. This damage is believed to have commenced simultaneously with the beginning of the small "crackle" sounds. These sounds were first detected for the solid panels at approximately 10000 pounds. It is not known what effect, if any, this damage would have on panel strength during repeated loading. This

cracking may result only from the particular test fixture utilized. If indeed these cracks are a cause for concern, then the ultimate failure loads presented must be reduced.

Experimental and predicted loads for the solid panel configuration are presented graphically in Figure 49. The same method which was utilized to design the panels with flanged holes was used to predict the buckling load for a solid web. The shear flow for buckling was calculated to be 140 lb/in.

A method outlined by Housner and Stein [Ref. 12] was also employed to compare the buckling load for a solid panel. Expressions for the critical buckling load are provided for both simply-supported and clamped, linear-elastic, orthotropic plates. The critical shear flow for simply-supported edges was calculated to be 158 lb/in. This value closely corresponds to the results presented by Kuhn, whose tests involved webs that were basically simply-supported. The critical shear flow for clamped edges was determined to be 253 lb/in. As shown in Figure 49, this value compares well with the buckling load predicted by the finite-element model with clamped edges.

B. ASSESSMENT OF FINITE-ELEMENT ANALYSIS

Predicted and experimental buckling loads are also compared in Figure 49. The loads determined by bifurcation-buckling analysis are seen to be significantly higher than

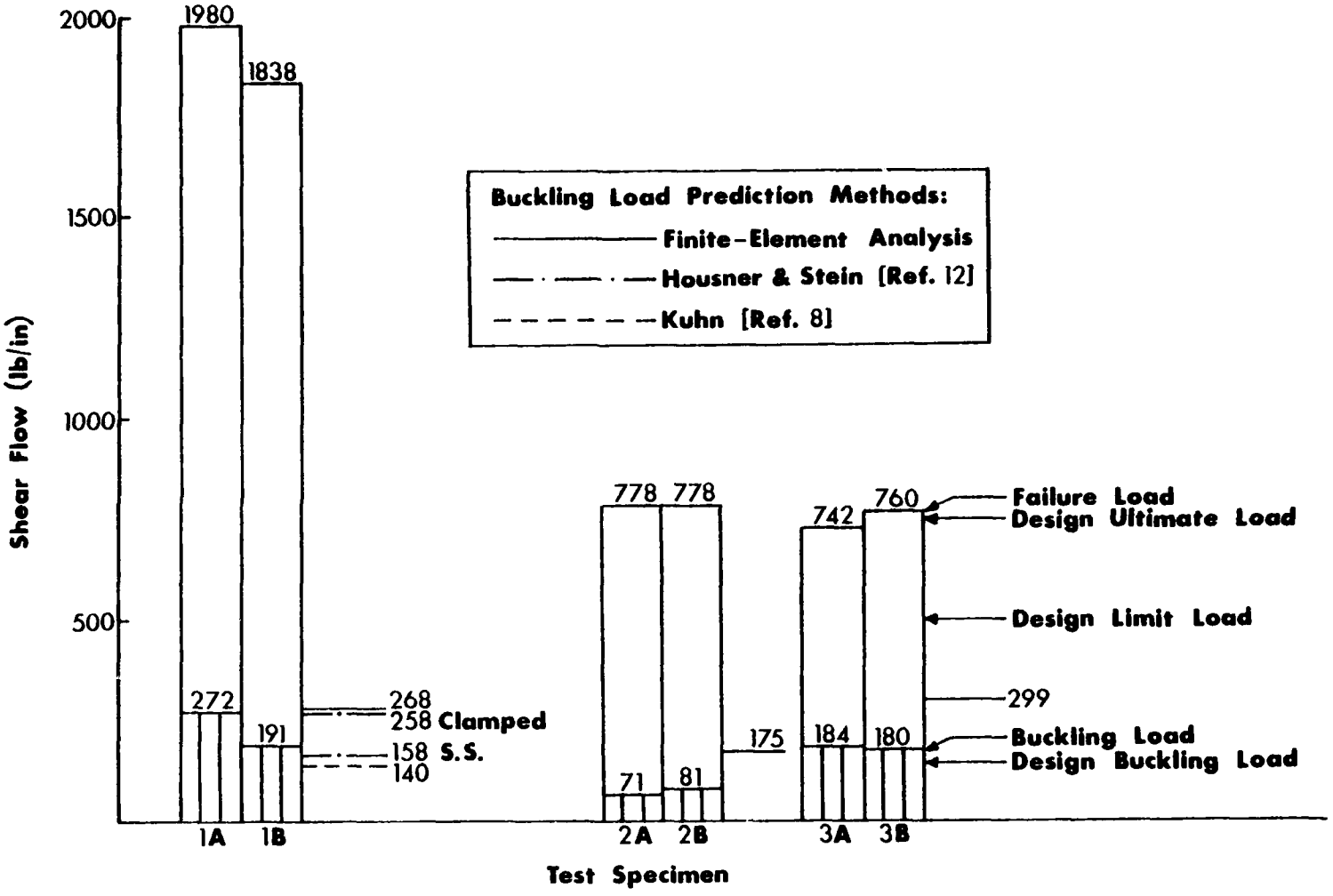

Fig. 49. Static Strength versus Design/Predicted Loads

the experimental results for five of the six specimens. It is felt that the high buckling load achieved by panel 1A probably resulted from an unusual residual-stress distribution in the skin, due to thermal contractions during cure. The buckling loads for panel 1B and for the flanged panels indicated that the boundary conditions of the test fixture tended to be closer to those of a simple-support. This disparity of boundary conditions was responsible for the predicted buckling loads being consistently high throughout this investigation.

The way in which the computer model of the skin was loaded produced a different stress distribution in the shear web from that observed experimentally. Since the beams of the computer model were attached to and introduced load into the corners of the panel, high stress concentrations resulted there. The corners of the actual shear panels were not attached to the frames and thus were not loaded; consequently, the resulting distribution of tensile stresses along the diagonal tension axis was much better than expected. These high concentrations of stress can be seen in all of the contour plots of the predicted inplane forces, N_{xy}, contained in the appendices.

A comparison of the predicted and experimental strains along the tension field direction for panel 1A is presented in Figure 50. The analytical strain values are seen not only to be higher, but they vary with position along the

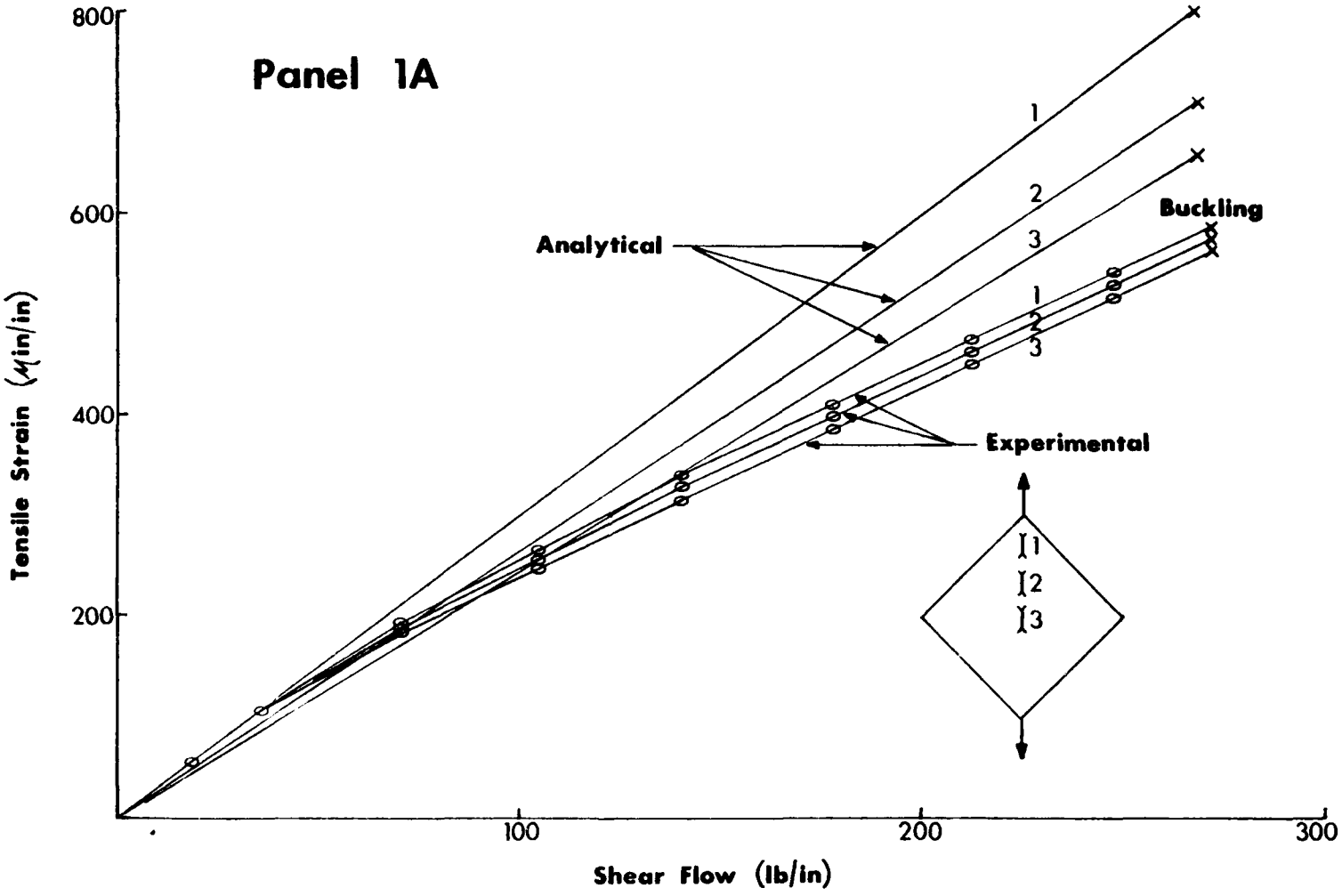

Fig. 50. Experimental and Analytical Strain Along Tension Field for Panel 1A

panel diagonal. In contrast, the measured values remained fairly constant down the diagonal. The plot for panel 1B, which shows similar results, is displayed in Figure 51. The tensile strain is seen to be approximately linear up to buckling for the solid panel configuration.

Experimental and analytical strain on the diagonal tension axis for the panels with unreinforced holes and with flanged holes are presented in Figures 52 and 53 respectively. The presence of the cutout is seen to immediately affect the state of stress in the panel. The measured tensile strain at the rosette location was found to be nonlinear even at the lower load-levels. However, the cutout had little influence on the tensile strain of the computer models until a much higher load-level was reached.

Despite these deficiencies of the particular computer model utilized, a good representation of buckling patterns was obtained. The normal-displacement contour plots contained in the appendices depict the movement of the panel skin through the prebuckling range. The patterns seen developing in these plots are very similar to those observed during the postbuckling phase of the actual tests.

C. PANEL FAILURE

Experimental tensile strains recorded at the position on each panel nearest the point of failure were compared to

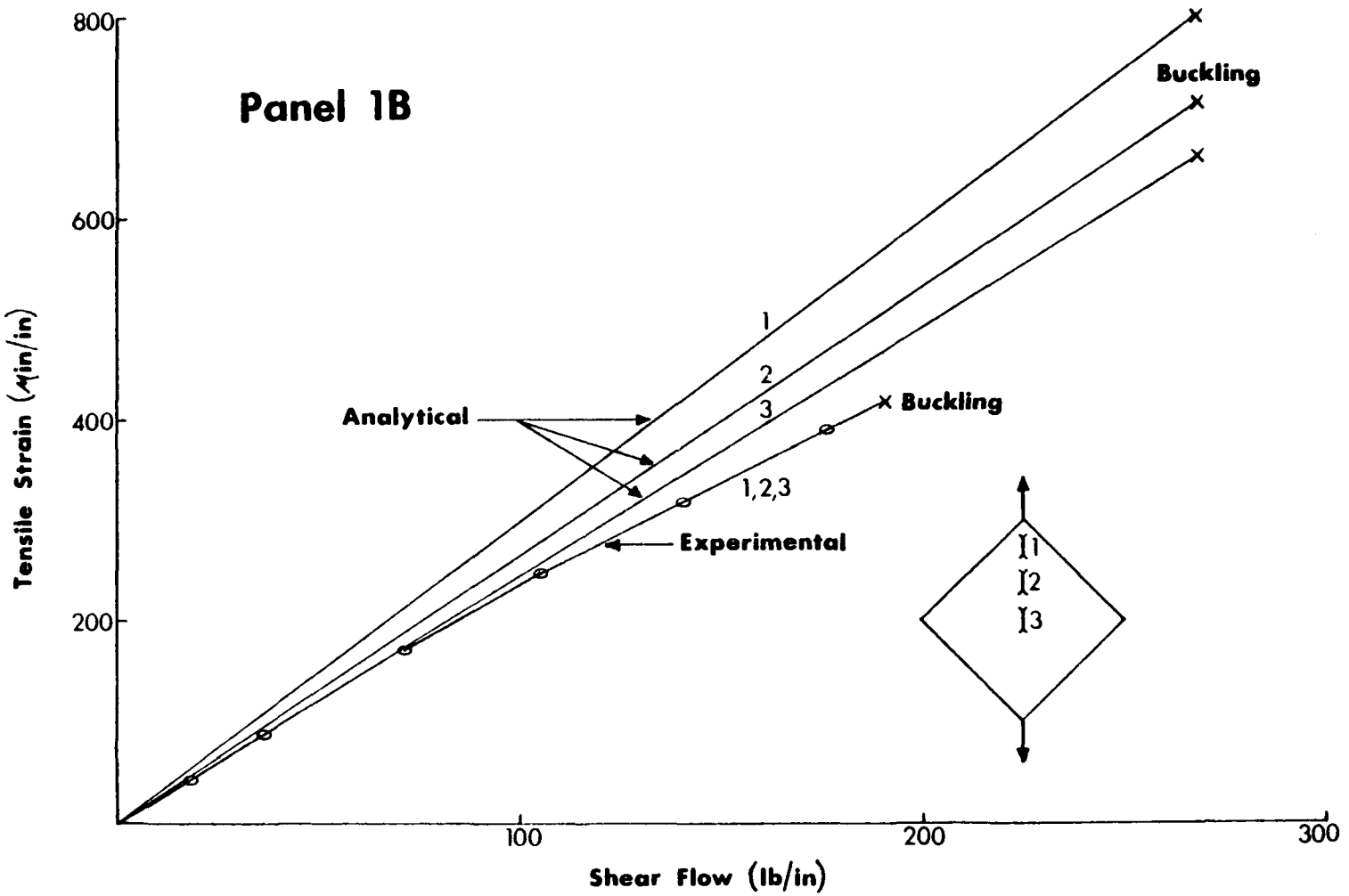

Fig. 51. Experimental and Analytical Strain Along Tension Field for Panel 1B

AD-A118 272 NAVAL POSTGRADUATE SCHOOL MONTEREY CA F/G 11/4
POSTBUCKLING BEHAVIOR OF GRAPHITE/EPOXY CLOTH SHEAR PANELS WITH--ETC(U)
MAR 82 R J HERMAN

UNCLASSIFIED NL

2 of 2
AD A118272

END
DATE FILMED
8-82
DTIC

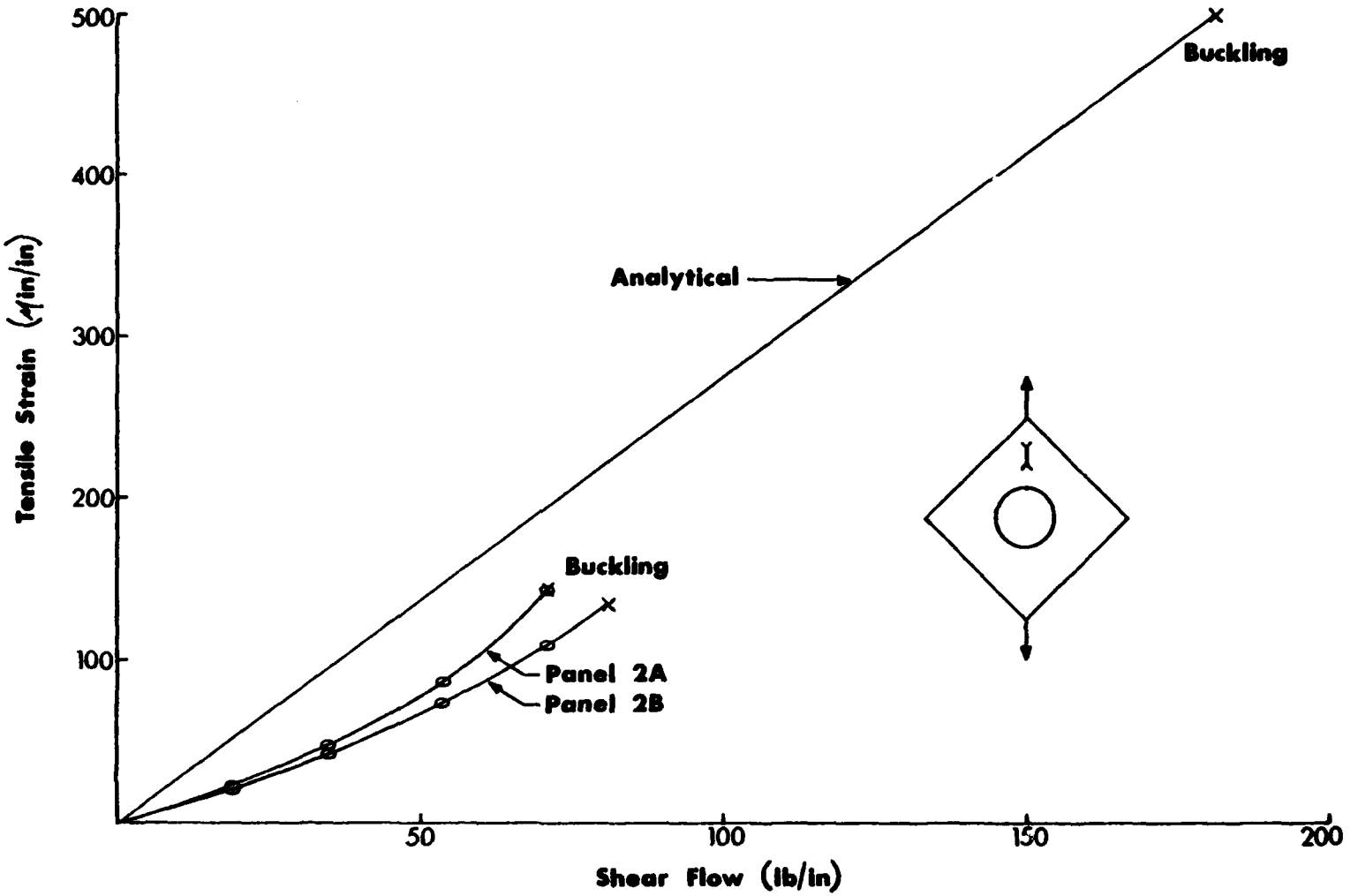

Fig. 52. Experimental and Analytical Strain on Tensile Axis for Panels with Unreinforced Holes

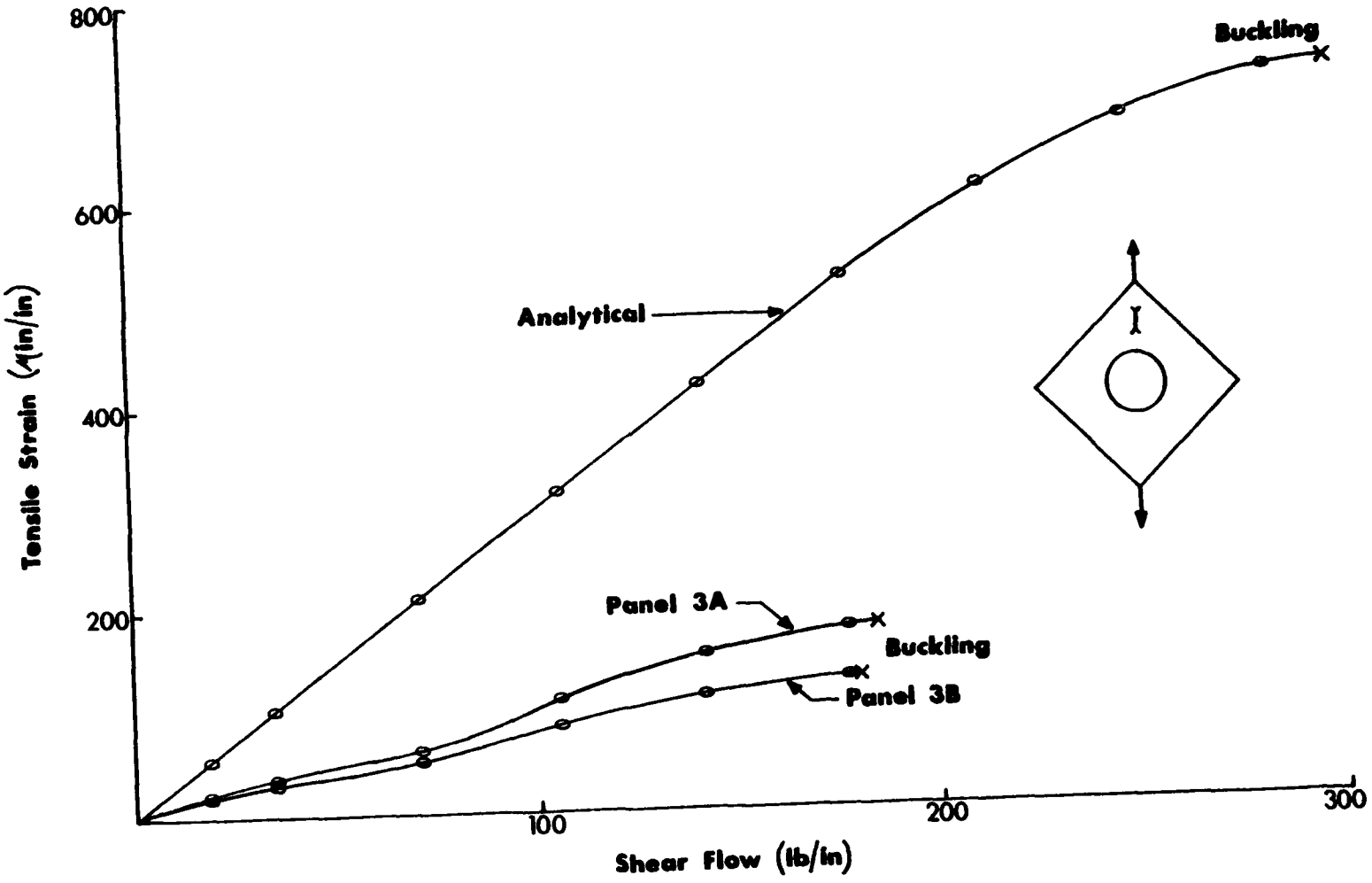

Fig. 53. Experimental and Analytical Strain on Tensile Axis for Panels with Flanged Holes

material allowables. This comparison is presented in Figure 54. Since the mode of failure for the panels with unreinforced holes was a pure, brittle fracture with fiber pullout involving no bending, the measured strain was compared to the laminate ultimate tensile strain. As shown in the figure, failure occurred for both panels shortly after exceeding the allowable strain.

The failure mode of the solid panels and the panels with flanged holes involved bending. For these panels, the measured strains on the tensile side of the layup were compared to the lamina ultimate tensile strain. Again, the correlation is reasonably good at failure. Therefore, the use of an allowable strain for a single surface layer may be satisfactory in predicting failure when bending is involved.

For both configurations 1 and 2, this measured strain relates to the first panel damage that occurs. This is not the case for the panels with flanged holes. Prior to the failure along the diagonal compression axis of these panels, a crack in the top and/or bottom of the flange occurred due to a complex state of stress at those points. However, catastrophic failure along the compression axis did occur shortly thereafter.

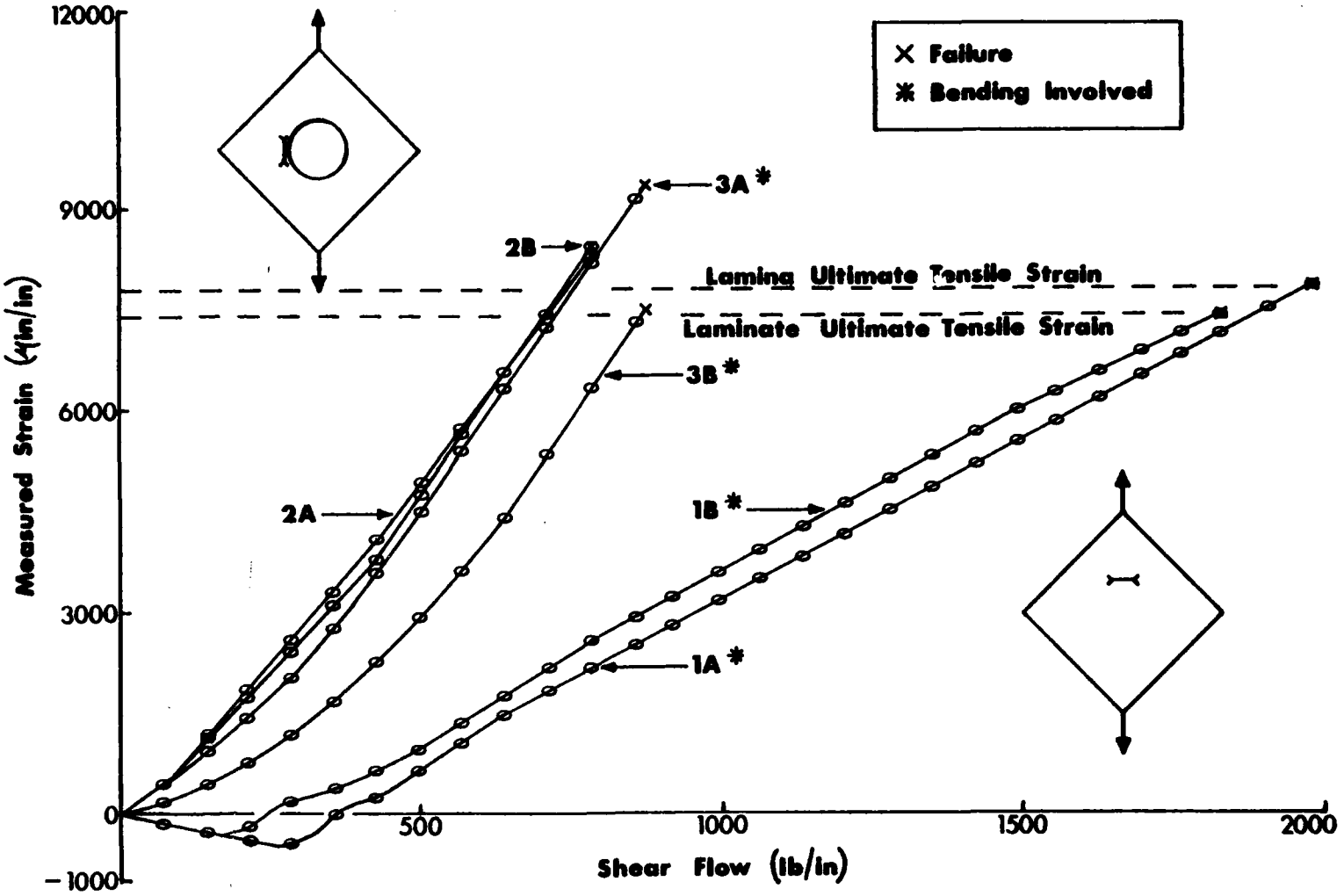

Fig. 54. Tensile Strain Near Point of Panel Failure

D. ASSESSMENT OF FLANGE-TYPE REINFORCEMENT

A 45°-flange around a cutout in a graphite/epoxy cloth panel was demonstrated to be an excellent type of reinforcement for designs in which buckling is prevented. The reduction in the load for buckling from that of a solid panel was only about five percent which is very good. The flange also functioned well in reducing stress concentrations near the edge of the hole. Figure 55 compares the experimentally-determined tangential stress distributions around one quadrant of the hole with the theoretical distribution given by Reference 13. This theoretical calculation was based on equal laminate properties in the longitudinal and transverse directions; i.e., the small differences between warp and weft in the lamina fabric were ignored. The tangential stress measured near the hole for the unreinforced panel compares well with that predicted by theory. The flange-type of reinforcement can be seen to reduce the stress concentration at the edge of the hole by approximately one-half. Of course, the stresses in the flat portion of the panel near the flange will remain high.

In contrast, the utilization of a 45°-flange in postbuckling designs is quite another matter. Although the flanged panels satisfied the criteria for the postbuckling design (see Figure 49), the compressive damage which went undetected during loading cannot be ignored. Unlike

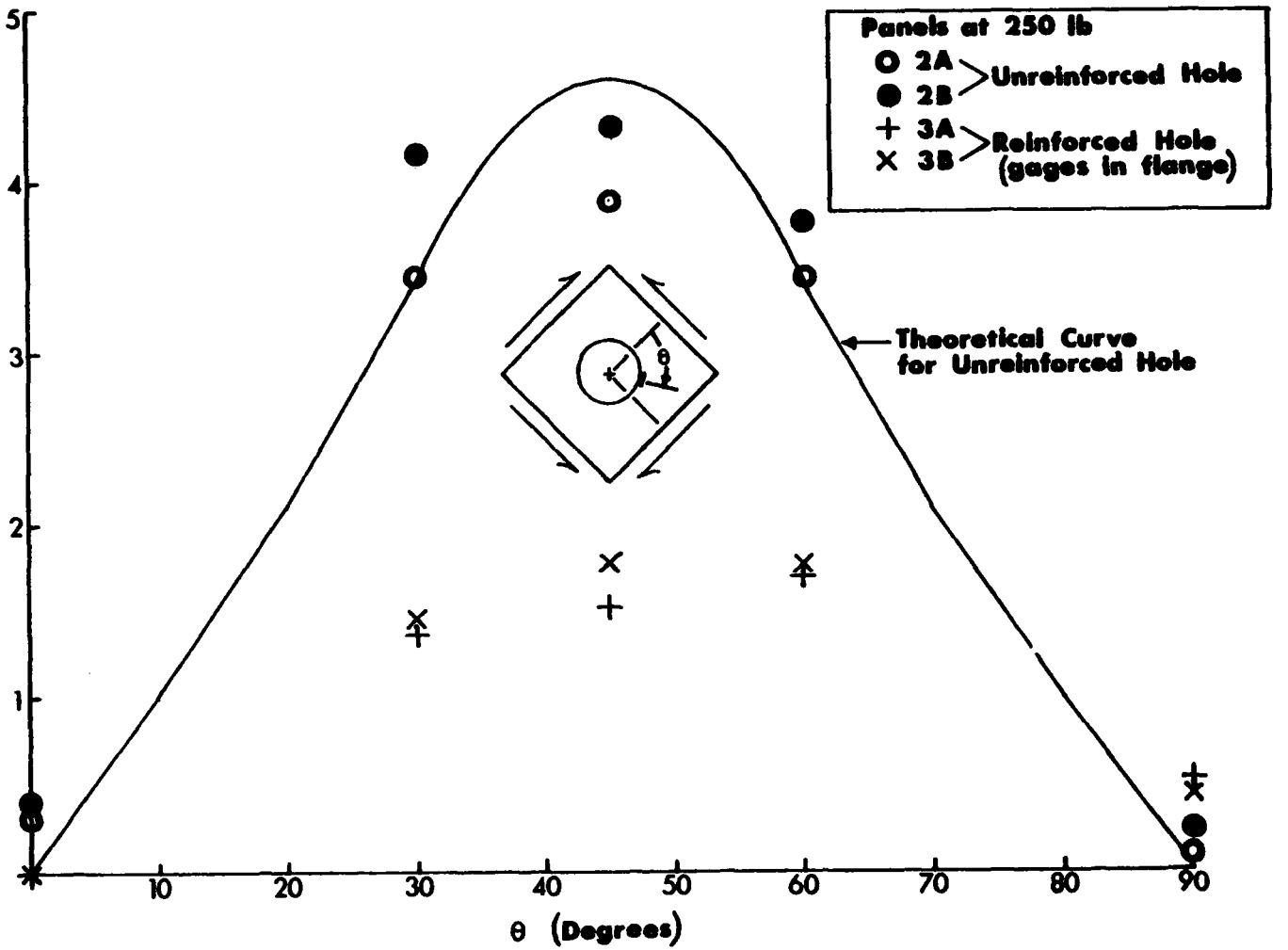

Fig. 55. Tangential Stress Distribution Around Hole

configurations 1 and 2, the compressive cracking on the surface opposite the direction of buckling was very extensive in the flanged panels. This damage could have an adverse effect on panel fatigue strength. If the failure load for the flanged panels is defined as the load where the small "crackle" sounds became numerous, then the shear flow at failure would be reduced to approximately 550 lb/in. This results in a reduction of the buckling ratio from 4.2 to 3.0, which is unsatisfactory for postbuckling designs. It should be noted, however, that even this lowered value of ultimate shear flow is 16 percent higher than an equivalent aluminum panel (see Section III).

The factor that makes the flange so attractive for reinforcing holes in non-buckling designs is the same factor which creates problems when the panel is operating in the postbuckled regime. That is, the flange acts to increase the stiffness around the hole so that buckling is delayed. Once buckling has occurred, this increased stiffness becomes an undesirable property. The flange prevents the panel from deforming in the same manner as the unreinforced-hole configuration and therefore changes the mode of failure. The problem can be isolated to the top and bottom edges of the hole. It was here that very-high local stresses were required to deform the shear panel. The area of very-high stress concentration centered around these two points produced extensive compressive damage

along the diagonal tension axis and ultimately resulted in failure of the flange. Since the effects of the flange on the web were now almost entirely removed, the panel proceeded to act as if it were unreinforced as the load was increased. The panel then collapsed in the same fashion as a panel with an unreinforced hole.

VIII. CONCLUSIONS

A. The 45°-flange reinforcement technique for lightening holes in shear webs is well-suited for use in non-buckling graphite/epoxy cloth designs.

B. A graphite/epoxy shear panel configured with a 45°-flanged lightening hole does not possess the ultimate strength required for postbuckling designs.

IX. RECOMMENDATIONS

A. A more refined finite-element model is required. This model should be designed to more closely match both the boundary conditions of the panel edges and the fixture utilized to load the panel.

B. A computer system capable of easily executing post-buckled finite-element analysis should be utilized. The results from such an analysis should then be capable of predicting the load at which the internal forces at any point surpass a failure criterion developed from material allowables.

C. A hole reinforcement technique designed for use in the postbuckling regime should be investigated.

APPENDIX A

COMPUTER CONTOUR PLOTS FOR SOLID PANEL

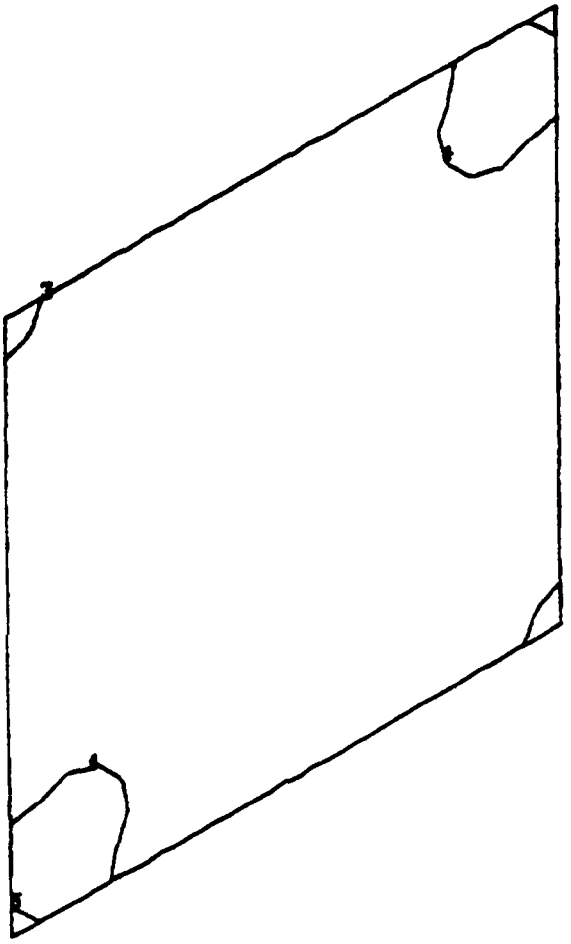

CONTOUR INDEX	
1	-1.9×10^{-8}
2	2.0×10^{1}
3	4.0×10^{1}
4	6.0×10^{1}
5	8.0×10^{1}
6	1.0×10^{2}

N_{x_1} Contours at 500 lb

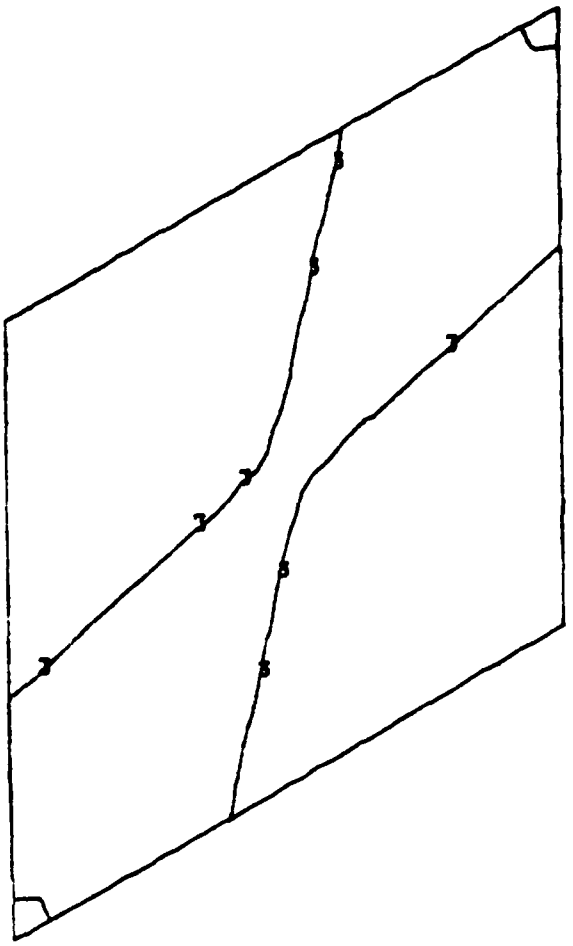

CONTOUR INDEX	
1	-3.8×10^{-8}
2	5.0×10^{1}
3	1.0×10^{2}
4	1.5×10^{2}
5	2.0×10^{2}

N_{xy} Contours at 1000 lb

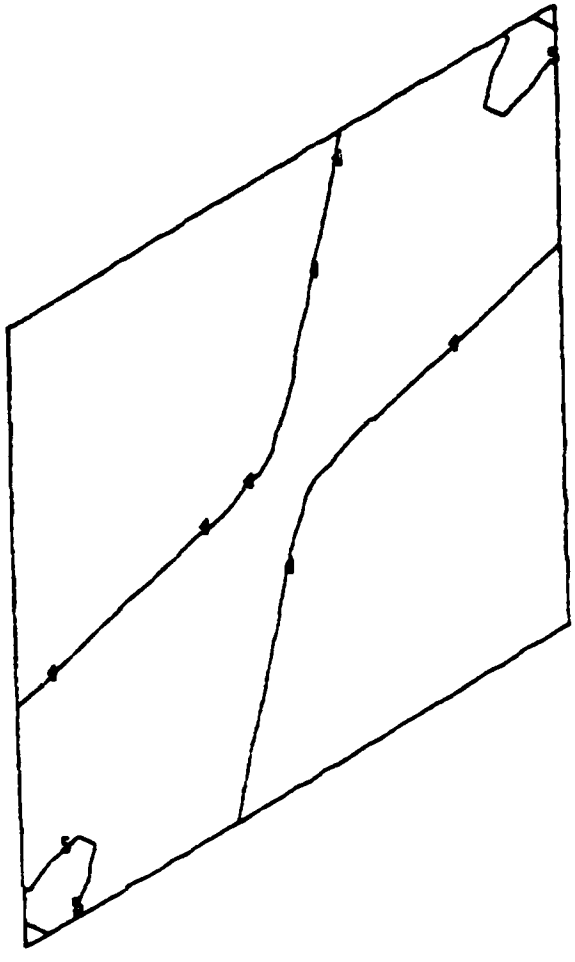

CONTOUR	INDEX
1	-3.8×10^{-8}
2	5.0×10^{1}
3	1.0×10^{2}
4	1.5×10^{2}
5	2.0×10^{2}
6	2.5×10^{2}
7	3.0×10^{2}

N_{xy} Contours at 1500 lb

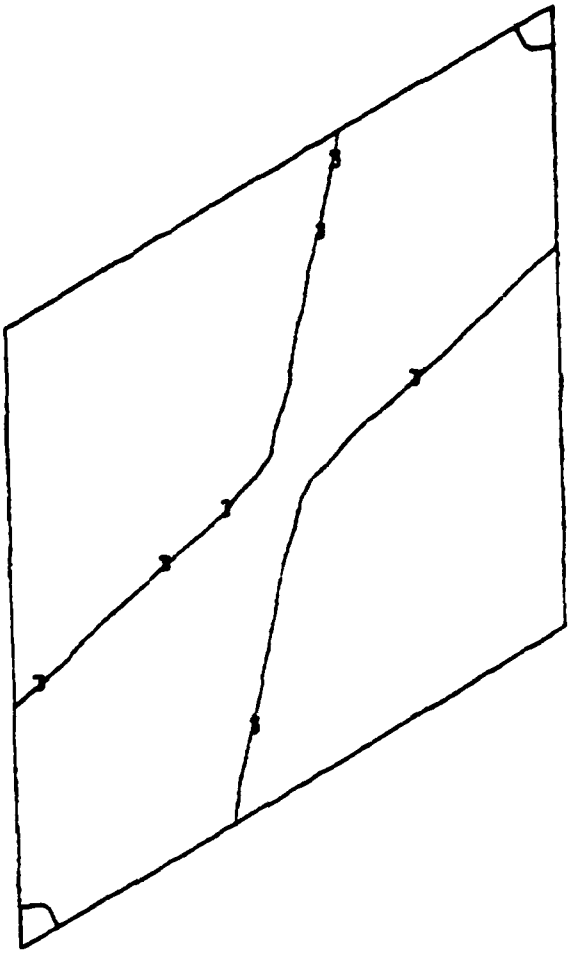

CONTOUR INDEX	
1	-7.6×10^{-8}
2	1.0×10^{2}
3	2.0×10^{2}
4	3.0×10^{2}
5	4.0×10^{2}

N_{xy} Contours at 2000 lb

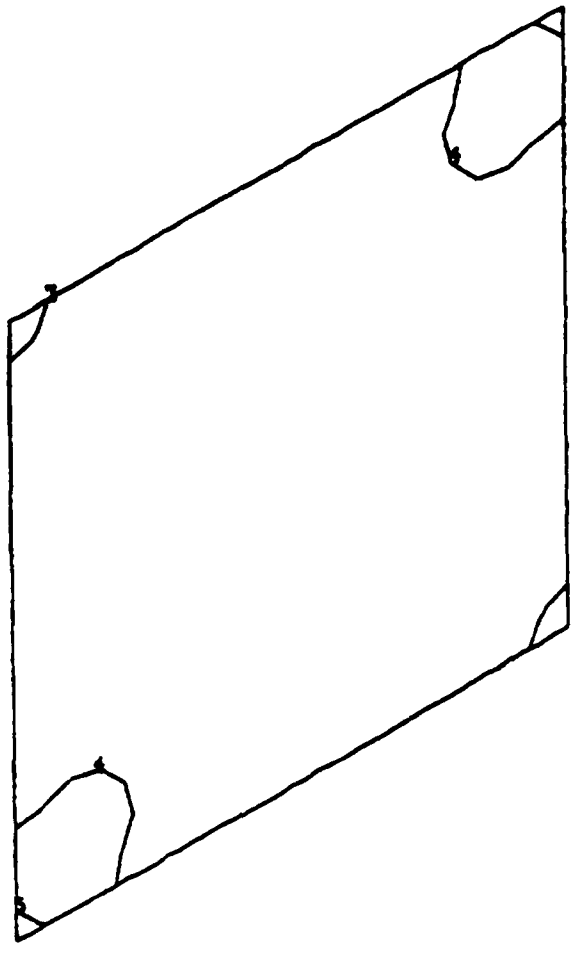

CONTOUR	INDEX
1	0.0
2	1.0×10^2
3	2.0×10^2
4	3.0×10^2
5	4.0×10^2
6	5.0×10^2

N_{xy} Contours at 2500 lb

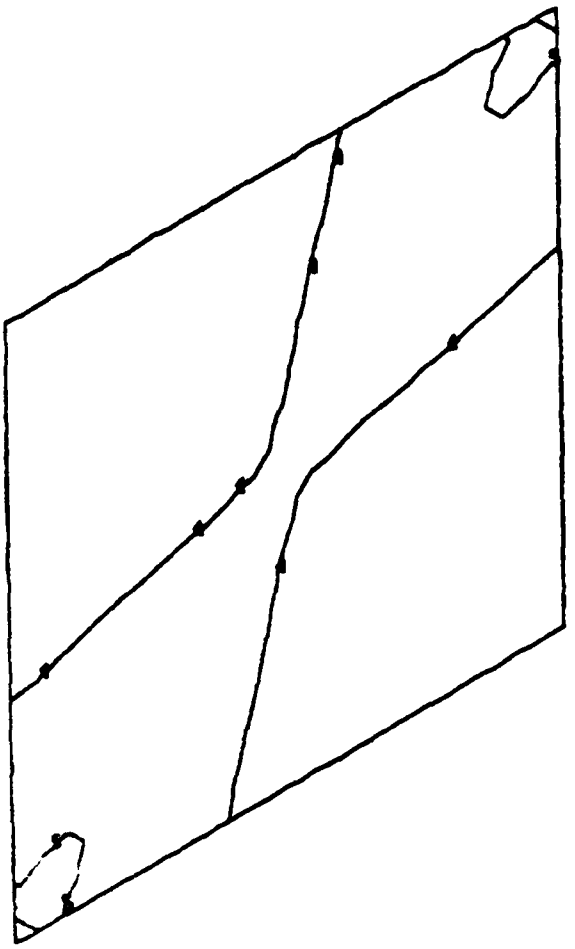

CONTOUR	INDEX
1	0.0
2	1.0×10^2
3	2.0×10^2
4	3.0×10^2
5	4.0×10^2
6	5.0×10^2
7	6.0×10^2

N_{xy} Contours at 3000 lb

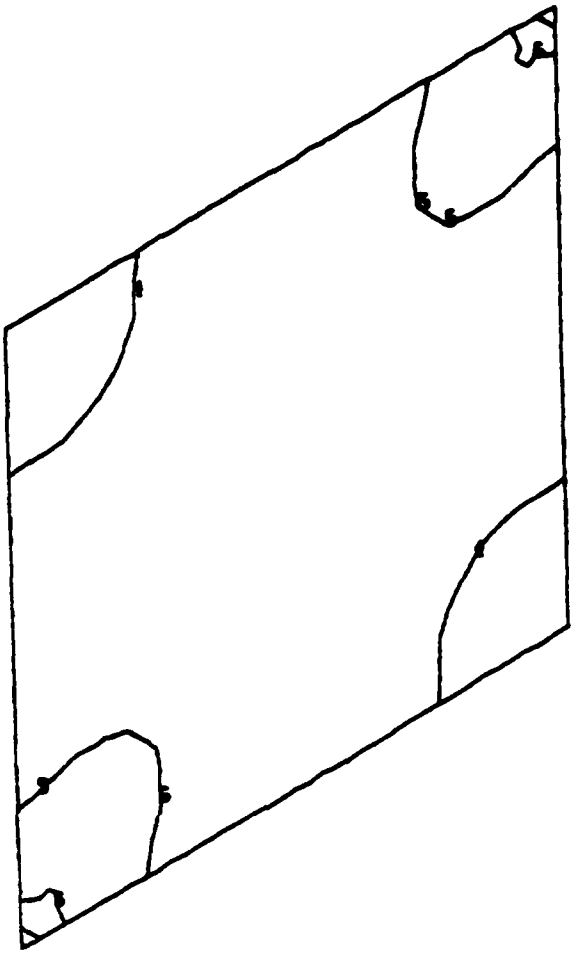

CONTOUR	INDEX
1	0.0
2	1.0×10^2
3	2.0×10^2
4	3.0×10^2
5	4.0×10^2
6	5.0×10^2
7	6.0×10^2
8	7.0×10^2

N_{xy} Contours at 3500 lb

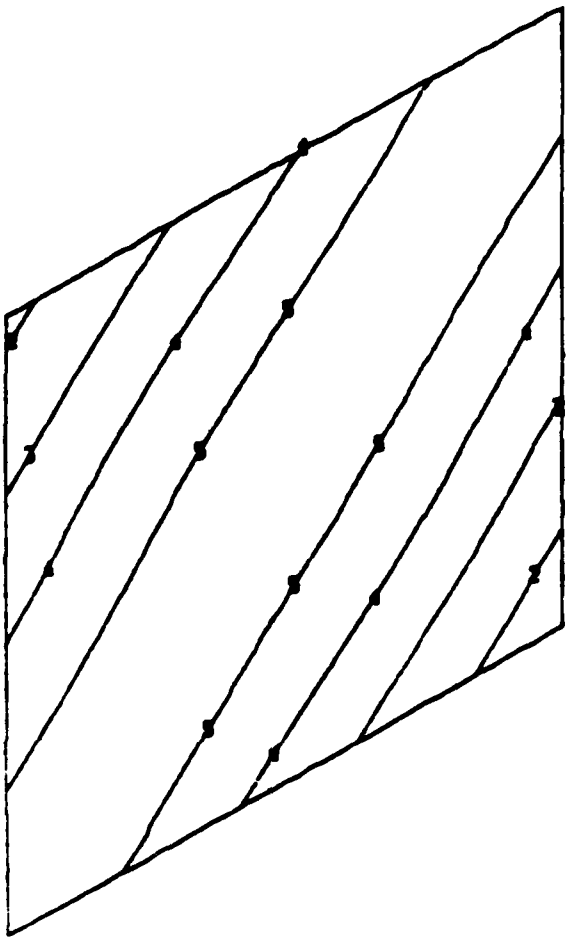

CONTOUR INDEX	
1	-5.0×10^{-9}
2	-4.0×10^{-9}
3	-3.0×10^{-9}
4	-2.0×10^{-9}
5	-10.0×10^{-10}
6	0.0

Normal Displacement Contours at 500 lb

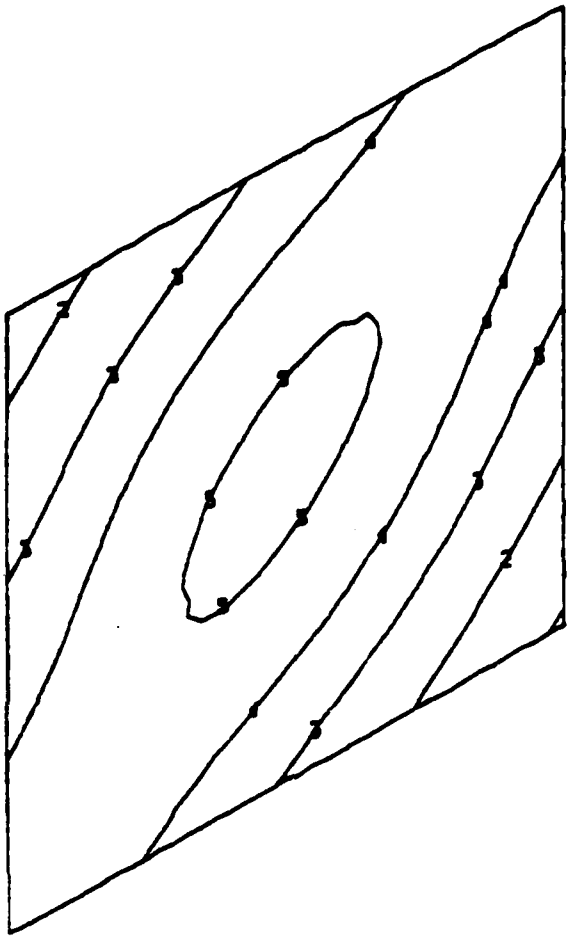

CONTOUR INDEX	
1	-8.0×10^{-9}
2	-6.0×10^{-9}
3	-4.0×10^{-9}
4	-2.0×10^{-9}
5	0.0

Normal Displacement Contours at 1000 lb

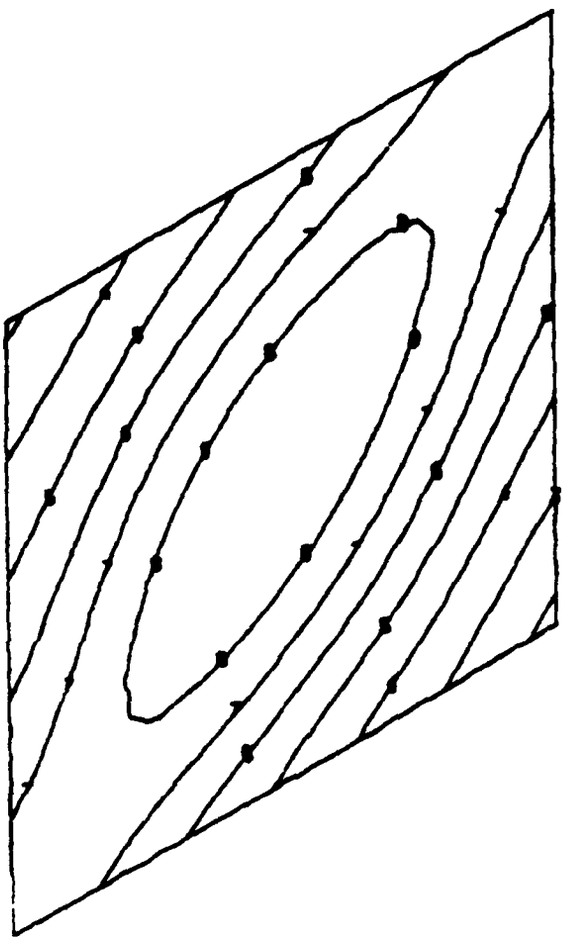

CONTOUR INDEX	
1	-1.4×10^{-8}
2	-1.2×10^{-8}
3	-10.0×10^{-9}
4	-8.0×10^{-9}
5	-6.0×10^{-9}
6	-4.0×10^{-9}
7	-2.0×10^{-9}
8	0.0
9	2.0×10^{-9}

Normal Displacement Contours at 1500 lb

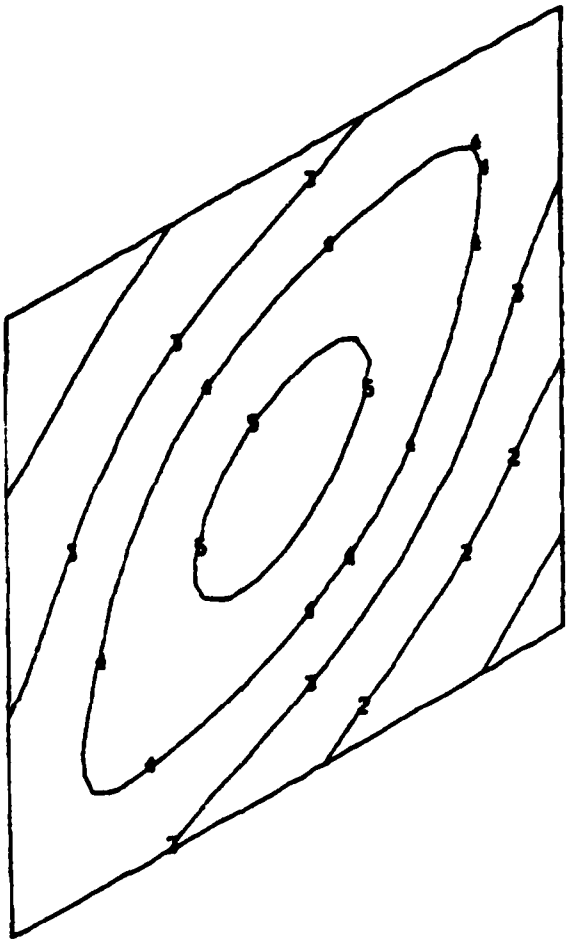

CONTOUR INDEX	
1	-1.5×10^{-8}
2	-10.0×10^{-9}
3	-5.0×10^{-9}
4	0.0
5	5.0×10^{-9}

Normal Displacement Contours at 2000 lb

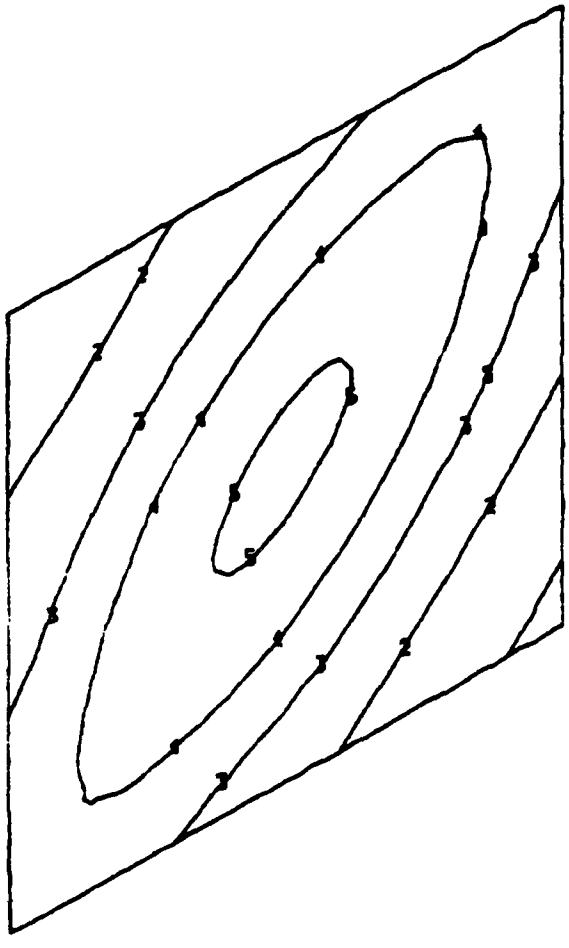

CONTOUR	INDEX
1	-3.0×10^{-8}
2	-2.0×10^{-8}
3	-10.0×10^{-9}
4	0.0
5	10.0×10^{-9}

Normal Displacement Contours at 2500 lb

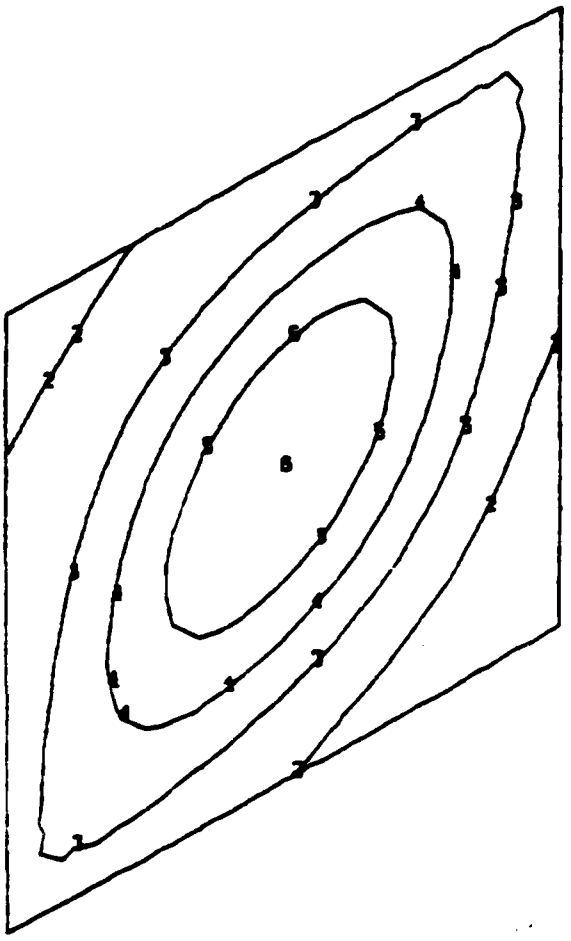

CONTOUR INDEX	
1	-4.0×10^{-8}
2	-2.0×10^{-8}
3	0.0
4	2.0×10^{-8}
5	4.0×10^{-8}
6	6.0×10^{-8}

Normal Displacement Contours at 3000 lb

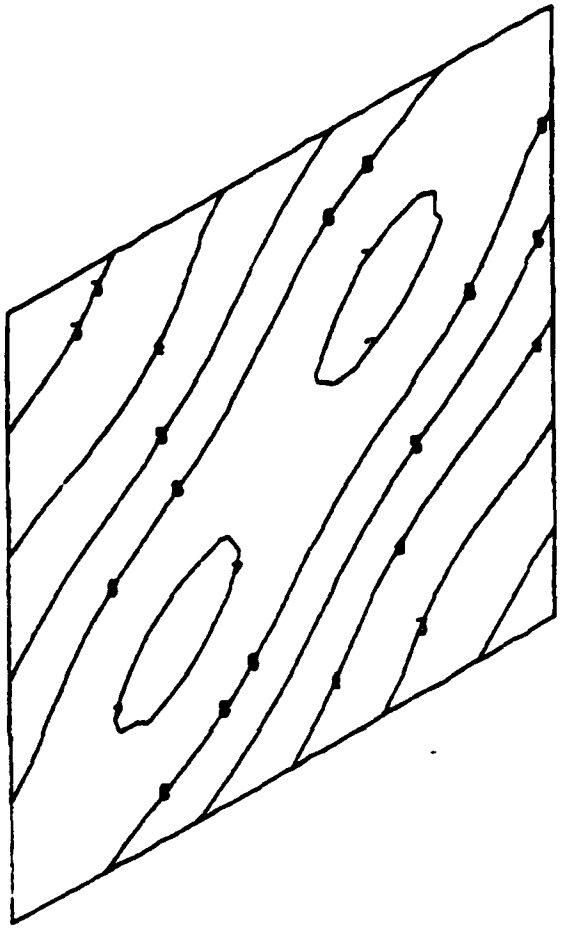

CONTOUR INDEX	
1	-3.0×10^{-7}
2	-2.5×10^{-7}
3	-2.0×10^{-7}
4	-1.5×10^{-7}
5	-10.0×10^{-8}
6	-5.0×10^{-8}
7	0.0

Normal Displacement Contours at 3500 lb

APPENDIX B

COMPUTER CONTOUR PLOTS FOR PANEL WITH UNREINFORCED HOLE

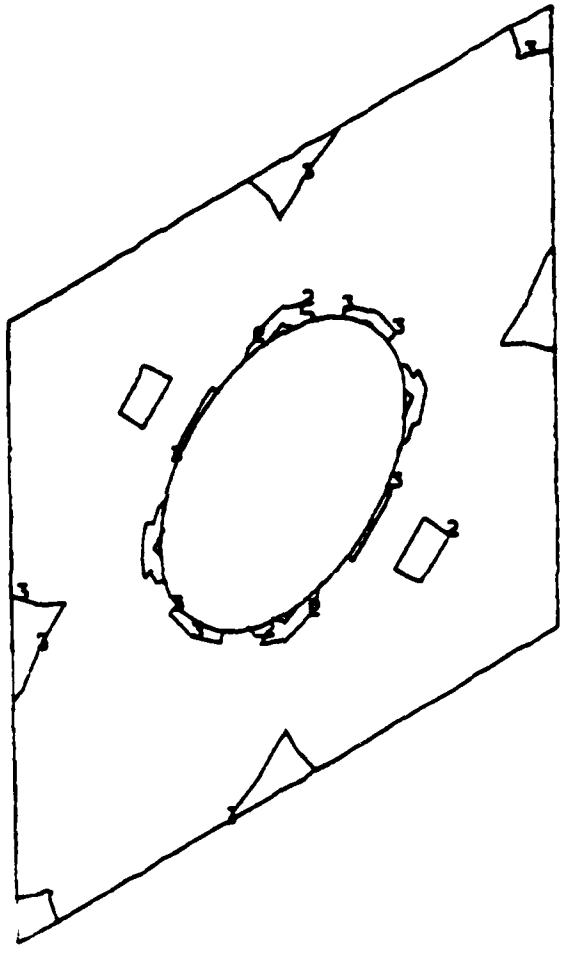

CONTOUR INDEX

1	-1.9×10^{-8}
2	2.0×10^{1}
3	4.0×10^{1}
4	6.0×10^{1}

N_{xy} Contours at 250 lb

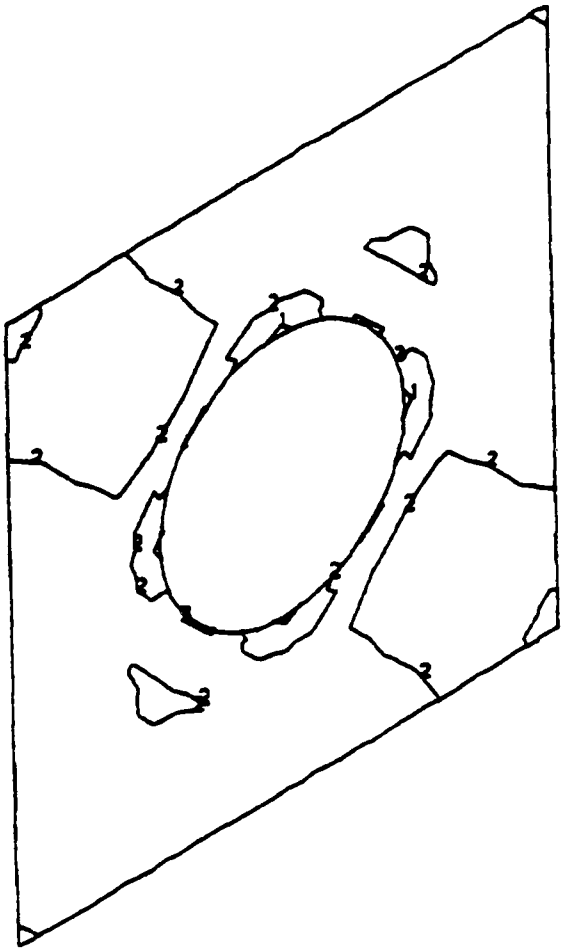

CONTOUR	INDEX
1	0.0
2	5.0×10^{1}
3	1.0×10^{2}

N_{xy} Contours at 500 lb

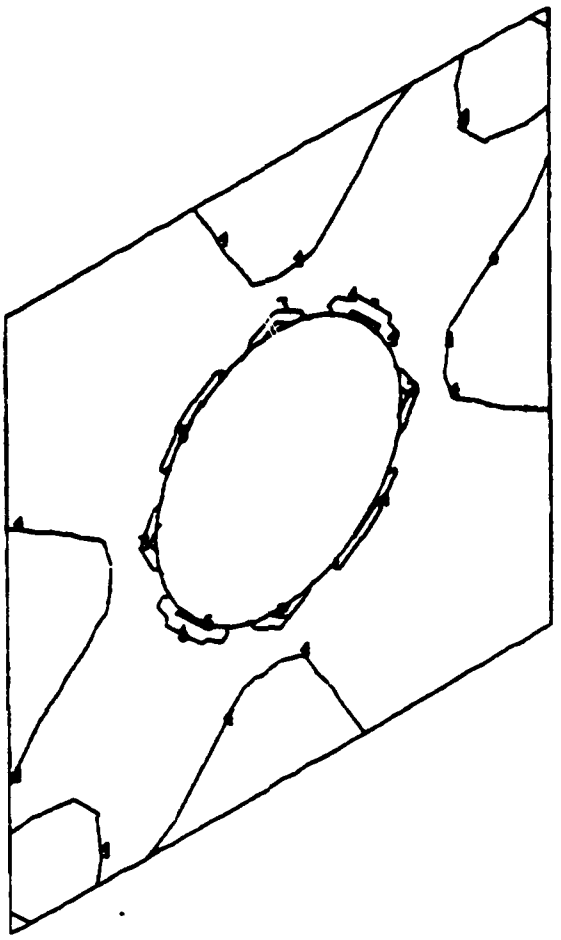

CONTOUR	INDEX
1	-5.0×10^1
2	0.0
3	5.0×10^1
4	1.0×10^2
5	1.5×10^2
6	2.0×10^2

N_{xy} Contours at 750 lb

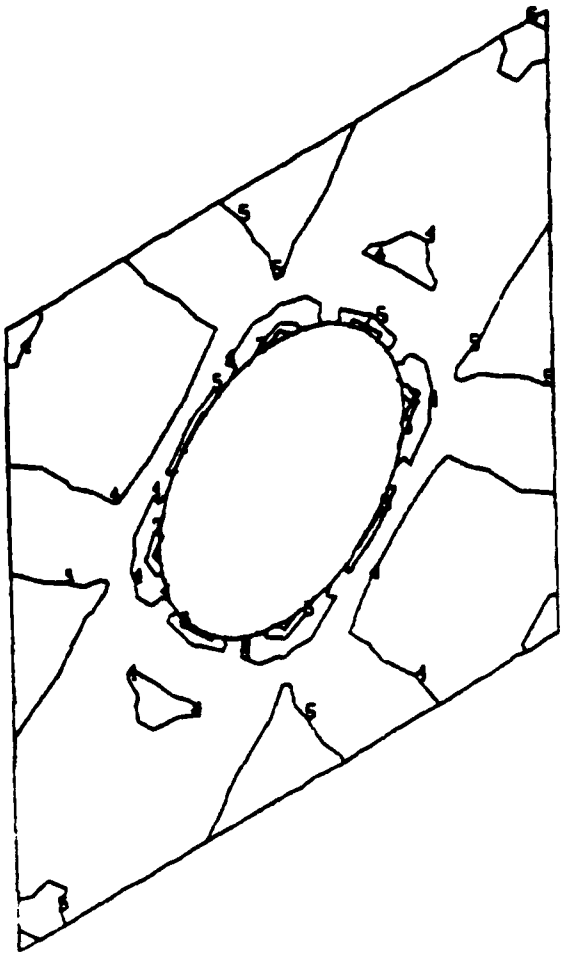

CONTOUR	INDEX
1	-5.0×10^{1}
2	0.0
3	5.0×10^{1}
4	1.0×10^{2}
5	1.5×10^{2}
6	2.0×10^{2}
7	2.5×10^{2}

N_{xy} Contours at 1000 lb

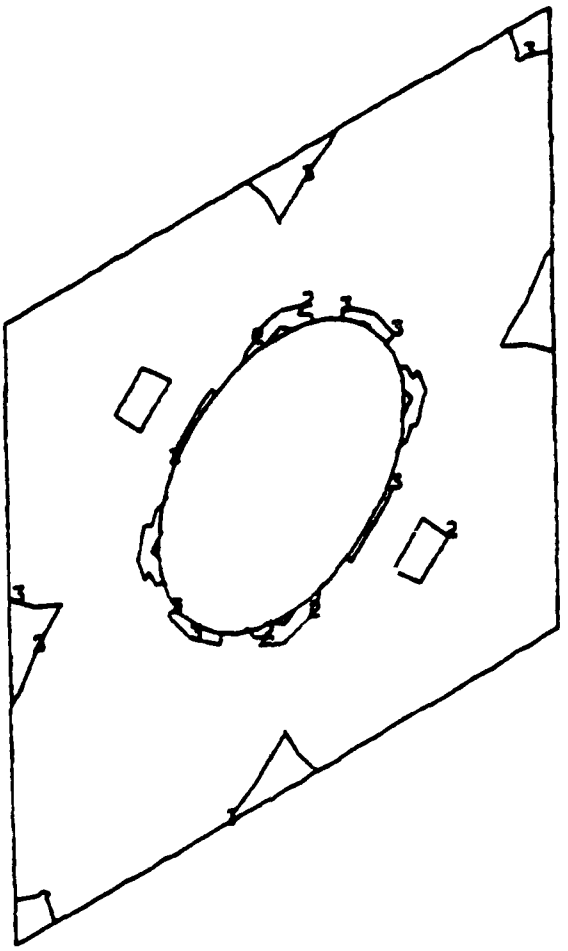

CONTOUR INDEX

1	-7.6×10^{-8}
2	1.0×10^{2}
3	2.0×10^{2}
4	3.0×10^{2}

N_{xy} Contours at 1250 lb

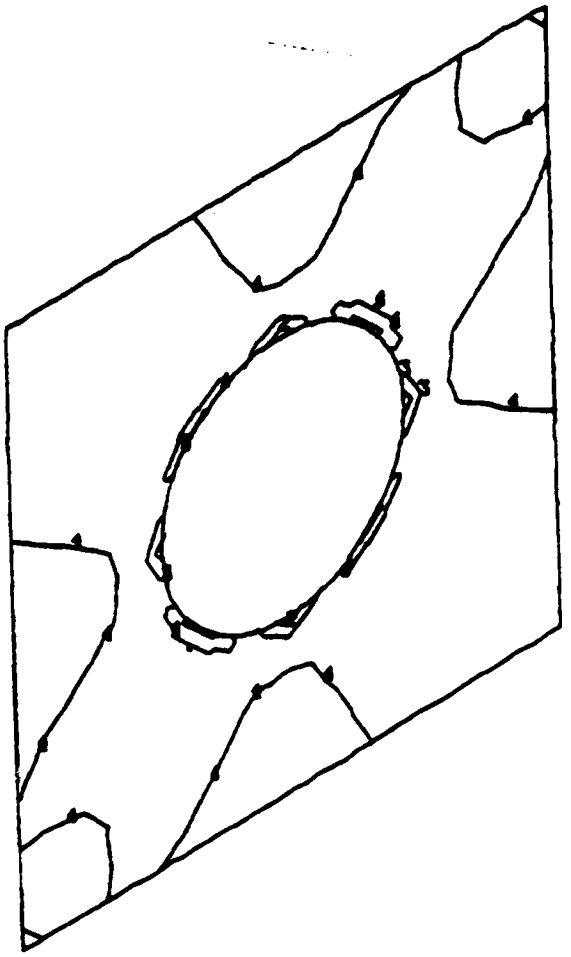

CONTOUR INDEX	
1	-1.0×10^2
2	0.0
3	1.0×10^2
4	2.0×10^2
5	3.0×10^2
6	4.0×10^2

N_{xy} Contours at 1500 lb

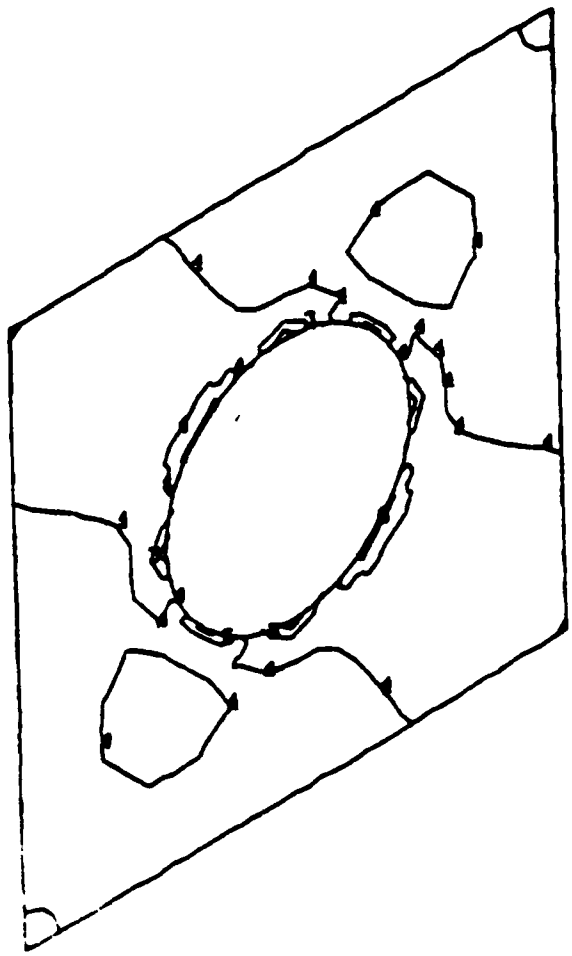

CONTOUR INDEX	
1	-1.0×10^2
2	0.0
3	1.0×10^2
4	2.0×10^2
5	3.0×10^2
6	4.0×10^2
7	5.0×10^2

N_{xy} Contours at 1750 lb

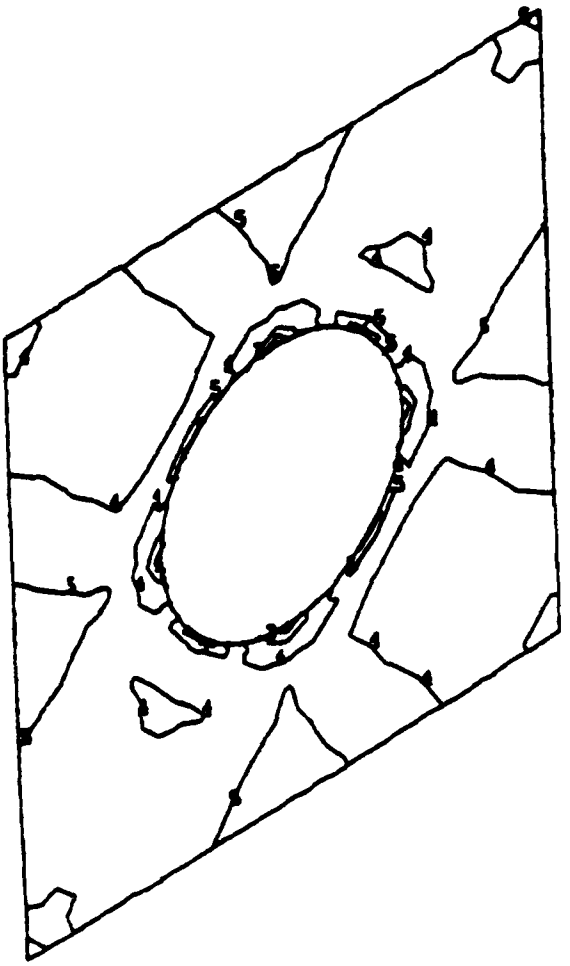

CONTOUR	INDEX
1	-1.0×10^2
2	0.0
3	1.0×10^2
4	2.0×10^2
5	3.0×10^2
6	4.0×10^2
7	5.0×10^2

N_{xy} Contours at 2000 lb

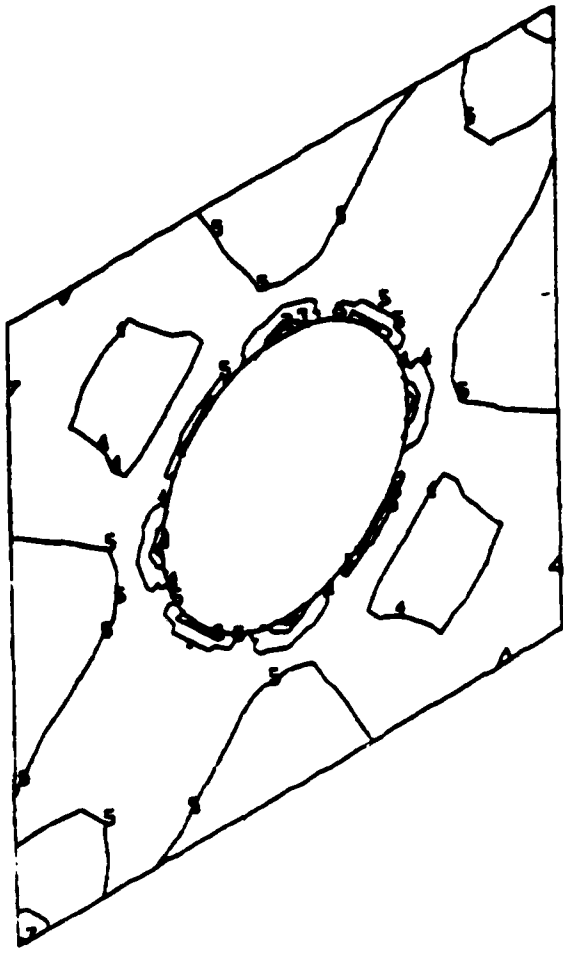

CONTOUR INDEX	
1	-1.0×10^2
2	0.0
3	1.0×10^2
4	2.0×10^2
5	3.0×10^2
6	4.0×10^2
7	5.0×10^2
8	6.0×10^2

N_{xy} Contours at 2250 lb

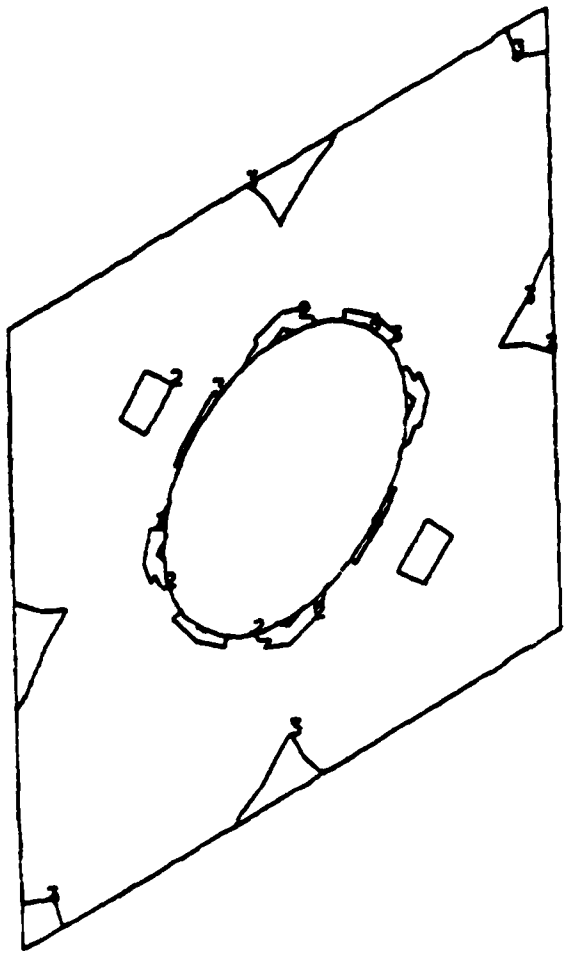

CONTOUR INDEX	
1	-1.5×10^{-5}
2	2.0×10^{2}
3	4.0×10^{2}
4	6.0×10^{2}

N_{xy} Contours at 2500 lb

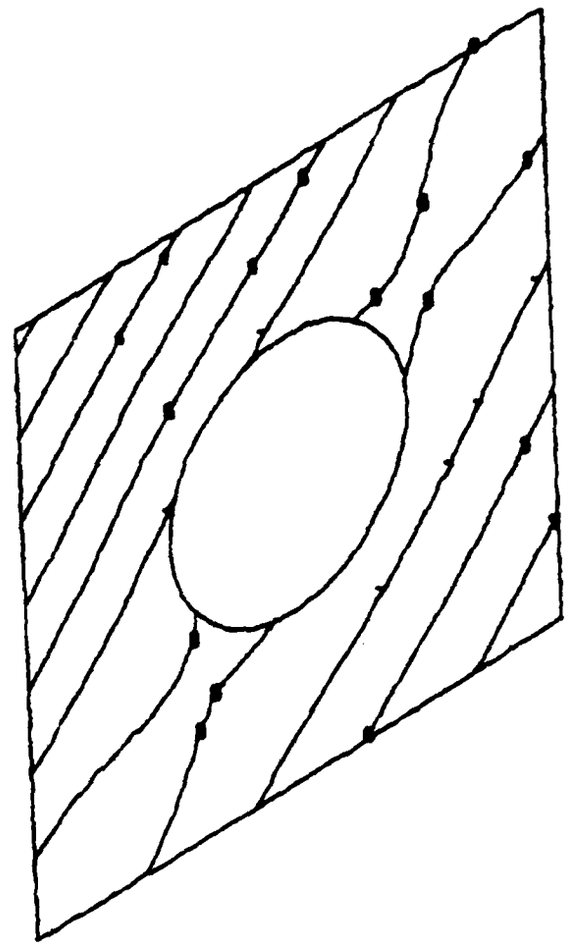

CONTOUR INDEX	
1	-4.0×10^{-9}
2	-3.5×10^{-9}
3	-3.0×10^{-9}
4	-2.5×10^{-9}
5	-2.0×10^{-9}
6	-1.5×10^{-9}
7	-10.0×10^{-10}
8	-5.0×10^{-10}
9	0.0

Normal Displacement Contours at 250 lb

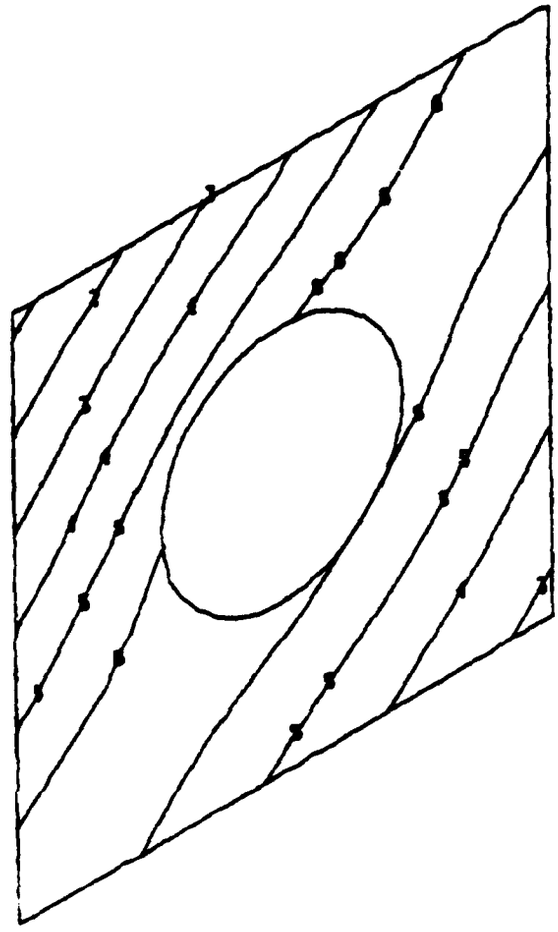

CONTOUR INDEX	
1	-6.0×10^{-9}
2	-5.0×10^{-9}
3	-4.0×10^{-9}
4	-3.0×10^{-9}
5	-2.0×10^{-9}
6	-10.0×10^{-10}
7	0.0

Normal Displacement Contours at 500 lb

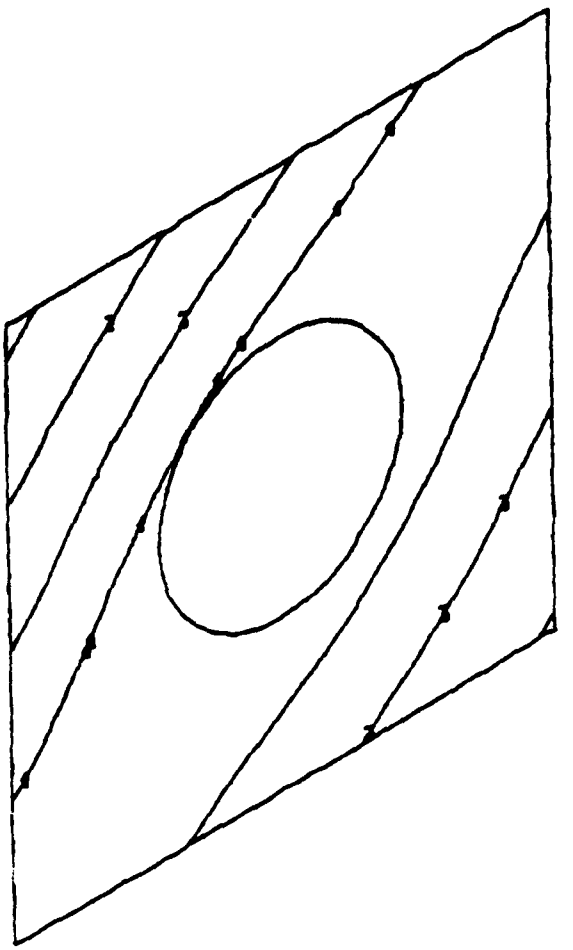

CONTOUR INDEX	
1	-8.0×10^{-9}
2	-6.0×10^{-9}
3	-4.0×10^{-9}
4	-2.0×10^{-9}
5	0.0

Normal Displacement Contours at 750 lb

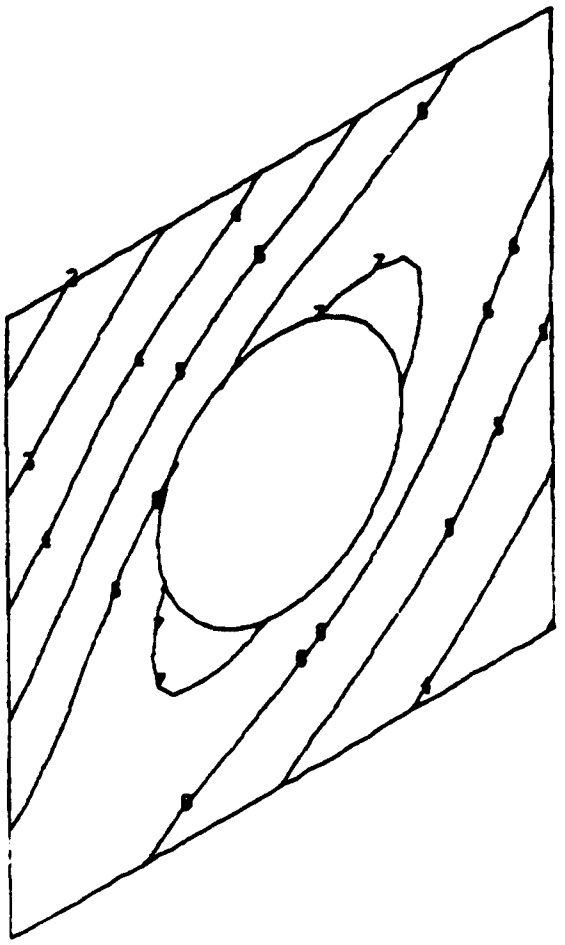

CONTOUR INDEX	
1	-1.2×10^{-8}
2	-10.0×10^{-9}
3	-8.0×10^{-9}
4	-6.0×10^{-9}
5	-4.0×10^{-9}
6	-2.0×10^{-9}
7	0.0
8	2.0×10^{-9}

Normal Displacement Contours at 1000 lb

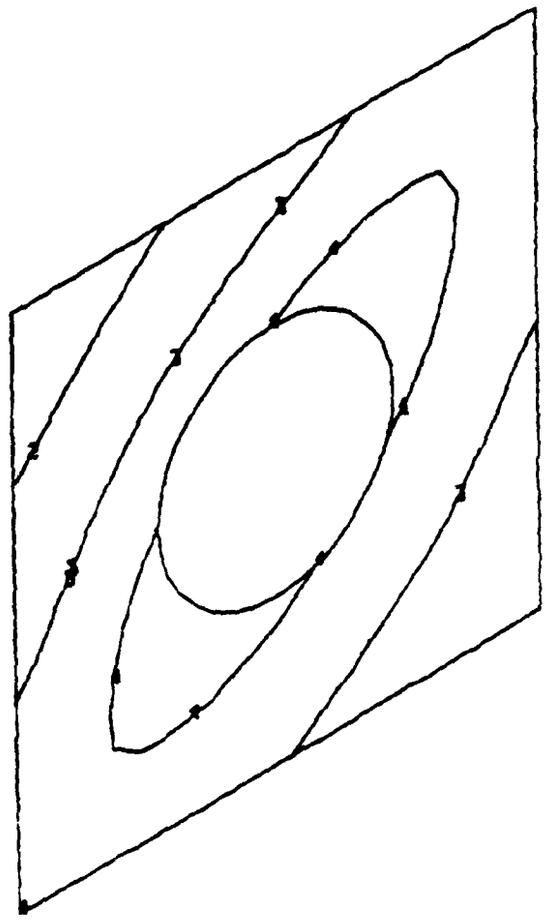

CONTOUR INDEX	
1	-1.5×10^{-8}
2	-10.0×10^{-9}
3	-5.0×10^{-9}
4	0.0

Normal Displacement Contours at 1250 lb

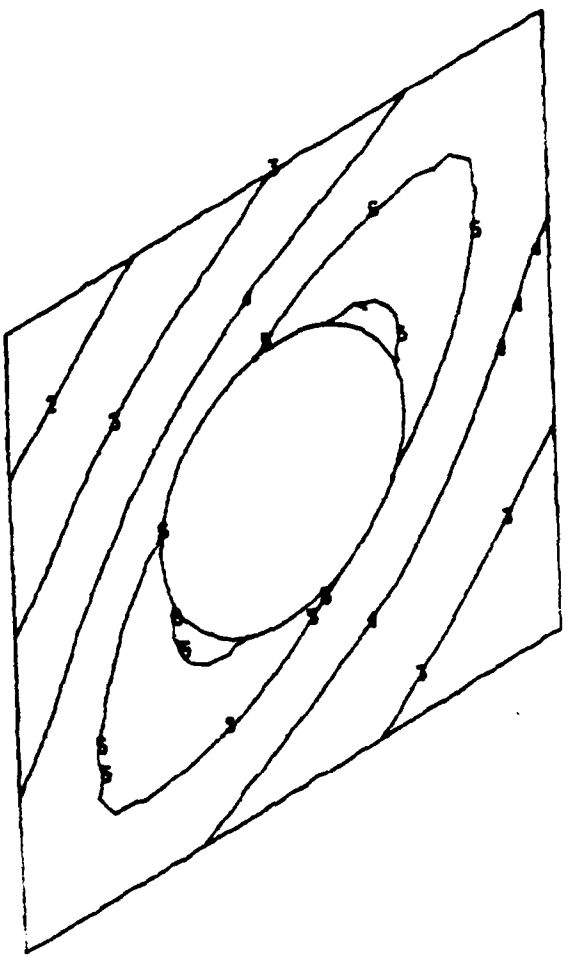

CONTOUR INDEX	
1	-2.0×10^{-8}
2	-1.5×10^{-8}
3	-10.0×10^{-9}
4	-5.0×10^{-9}
5	0.0
6	5.0×10^{-9}

Normal Displacement Contours at 1500 lb

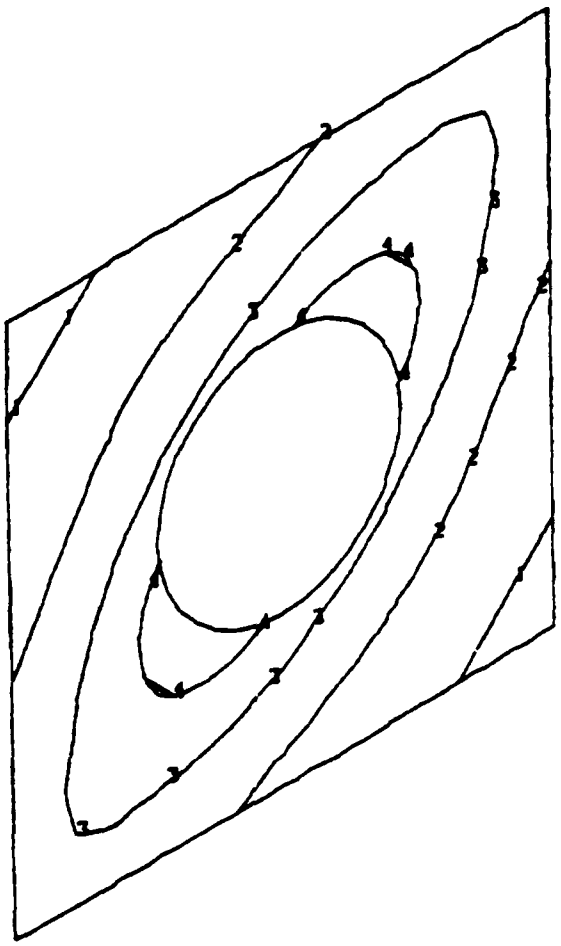

CONTOUR INDEX	
1	-2.0×10^{-8}
2	-10.0×10^{-9}
3	0.0
4	10.0×10^{-9}
5	2.0×10^{-8}

Normal Displacement Contours at 1750 lb

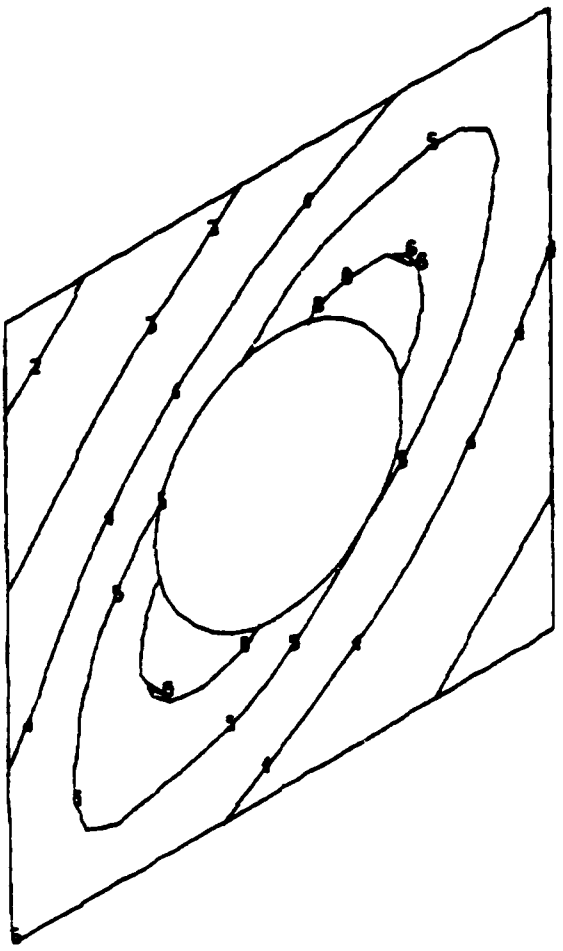

CONTOUR	INDEX
1	-8.0×10^{-8}
2	-6.0×10^{-8}
3	-4.0×10^{-8}
4	-2.0×10^{-8}
5	0.0
6	2.0×10^{-8}
7	4.0×10^{-8}

Normal Displacement Contours at 2000 lb

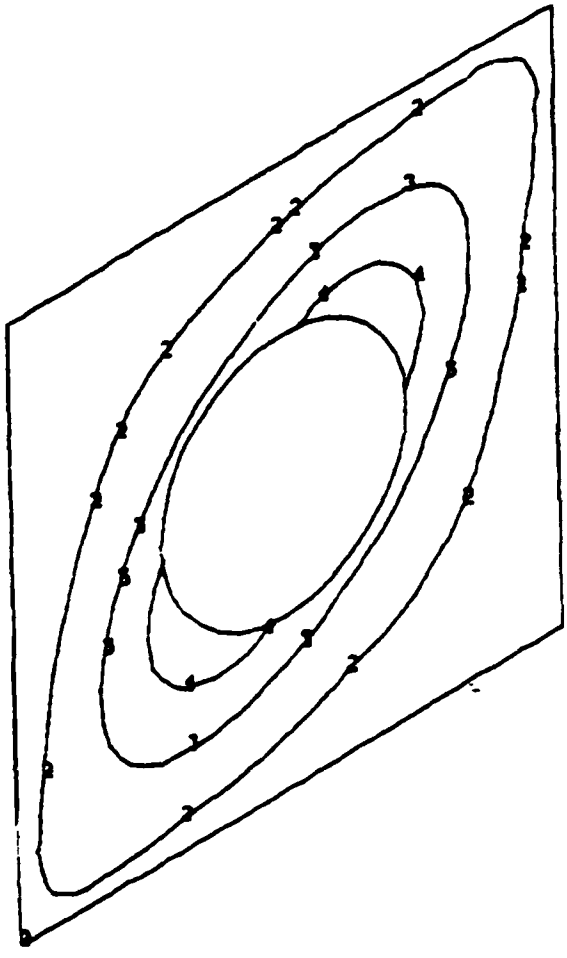

CONTOUR INDEX	
1	-5.0×10^{-8}
2	0.0
3	5.0×10^{-8}
4	10.0×10^{-8}
5	1.5×10^{-7}

Normal Displacement Contours at 2250 lb

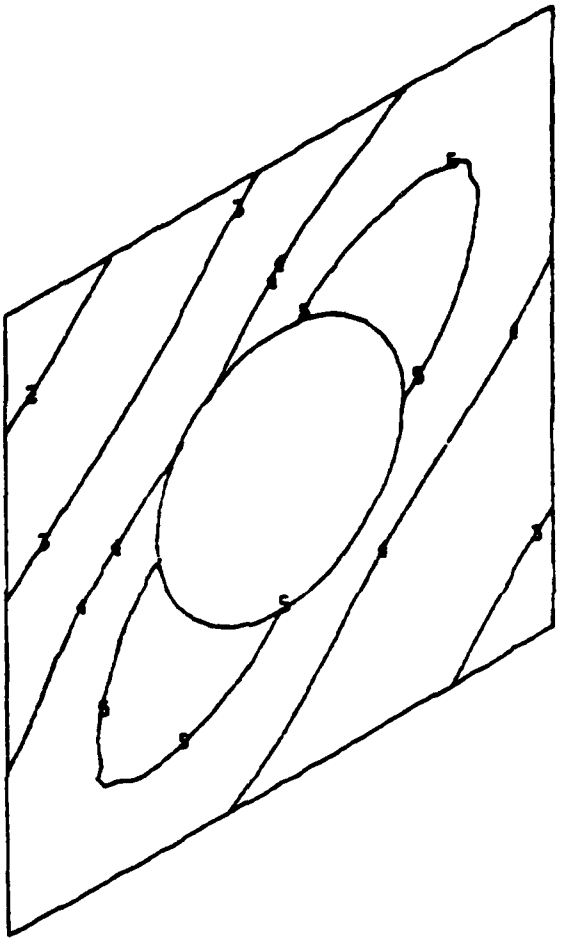

CONTOUR INDEX	
1	-8.0×10^{-7}
2	-6.0×10^{-7}
3	-4.0×10^{-7}
4	-2.0×10^{-7}
5	0.0
6	2.0×10^{-7}

Normal Displacement Contours at 2500 lb

APPENDIX C

COMPUTER CONTOUR PLOTS FOR PANEL WITH FLANGED HOLE

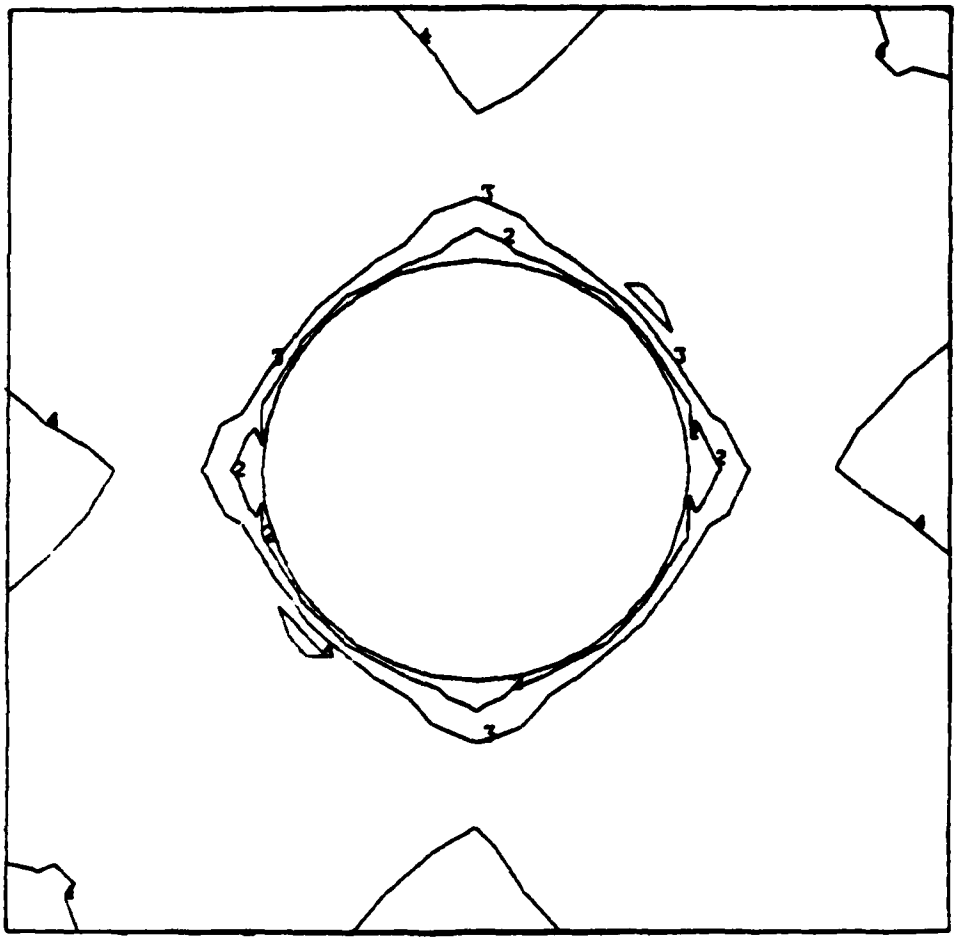

CONTOUR INDEX

1	-2.0×10^1
2	0.0
3	2.0×10^1
4	4.0×10^1
5	6.0×10^1

N_{xy} Contours at 250 lb

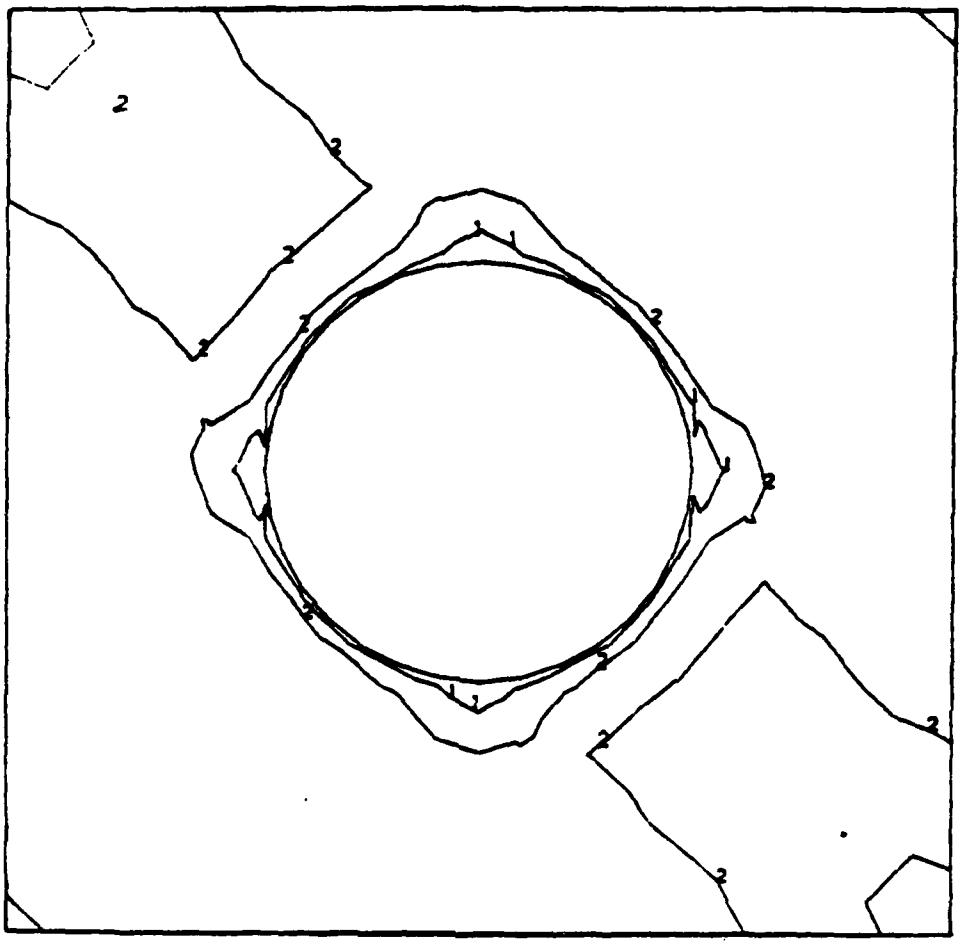

CONTOUR INDEX

1 0.0

2 5.0×10^1

3 1.0×10^2

N_{xy} Contours at 500 lb

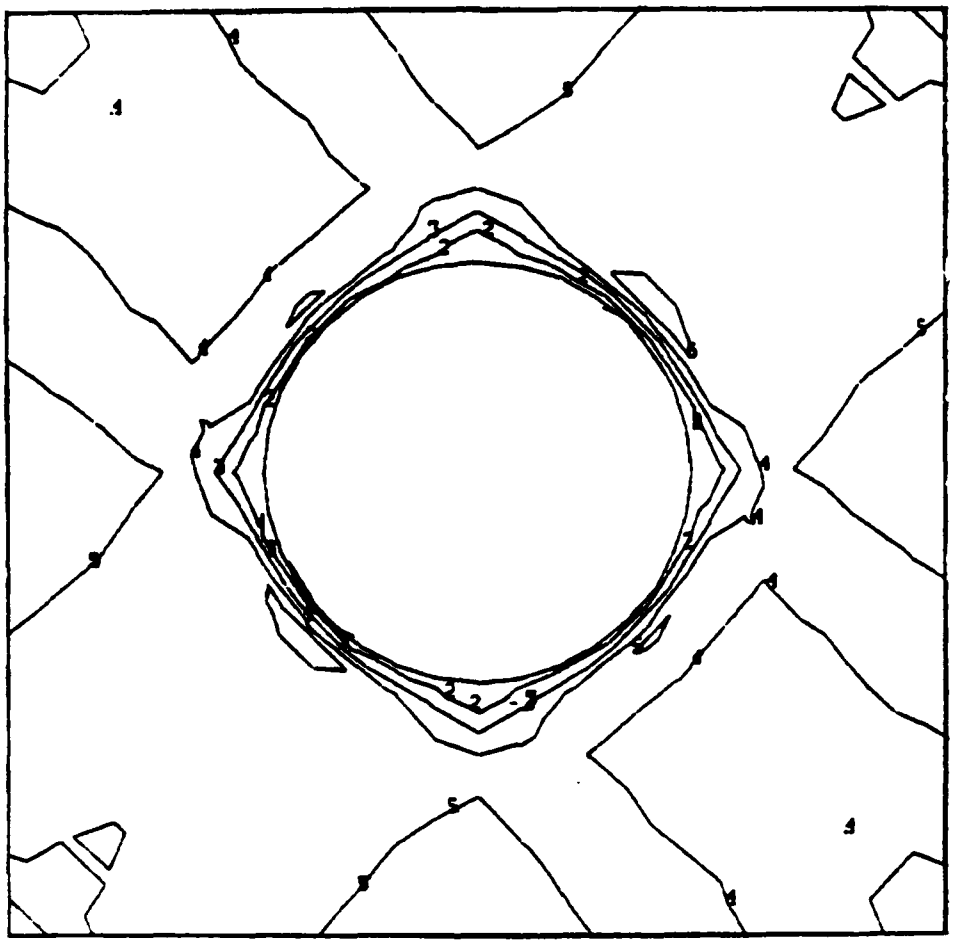

CONTOUR	INDEX
1	-5.0×10^1
2	0.0
3	5.0×10^1
4	1.0×10^2
5	1.5×10^2
6	2.0×10^2
7	2.5×10^2

N_{xy} Contours at 1000 lb

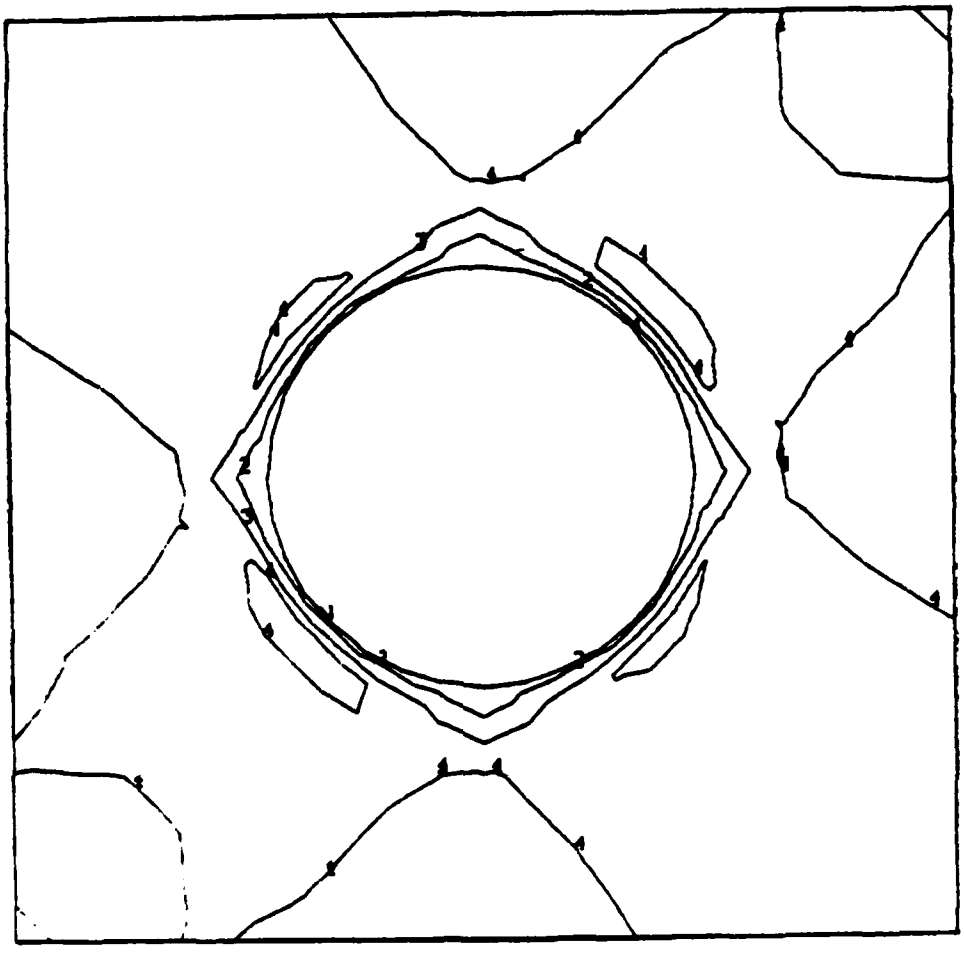

CONTOUR	INDEX
1	-1.0×10^2
2	0.0
3	1.0×10^2
4	2.0×10^2
5	3.0×10^2
6	4.0×10^2

N_{xy} Contours at 1500 lb

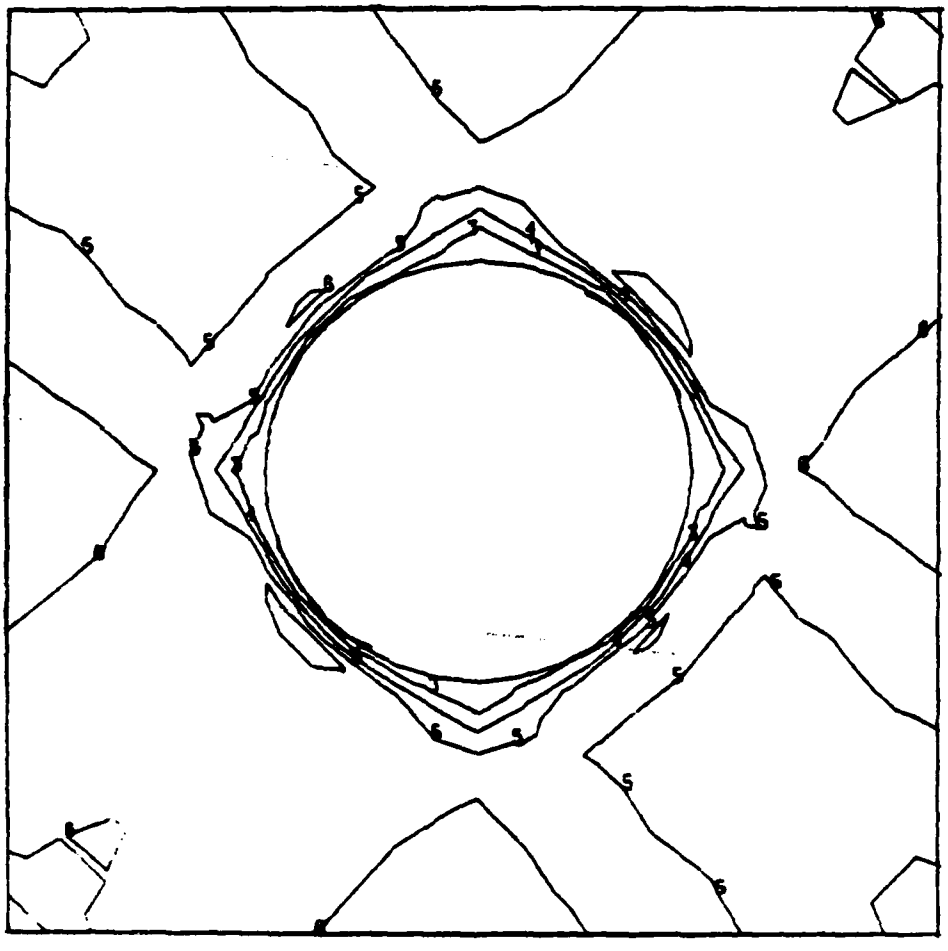

CONTOUR INDEX	
1	-2.0×10^2
2	-1.0×10^2
3	0.0
4	1.0×10^2
5	2.0×10^2
6	3.0×10^2
7	4.0×10^2
8	5.0×10^2

N_{xy} Contours at 2000 lb

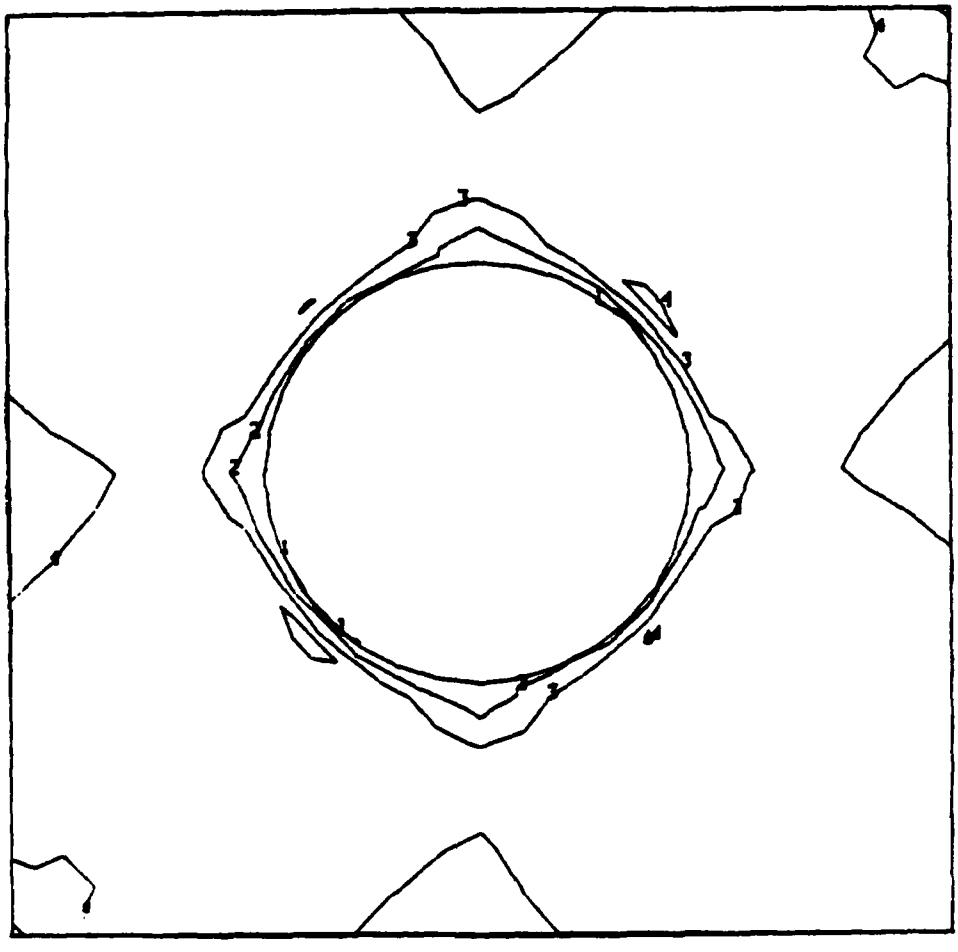

CONTOUR	INDEX
1	-2.0×10^2
2	0.0
3	2.0×10^2
4	4.0×10^2
5	6.0×10^2

N_{xy} Contours at 2500 lb

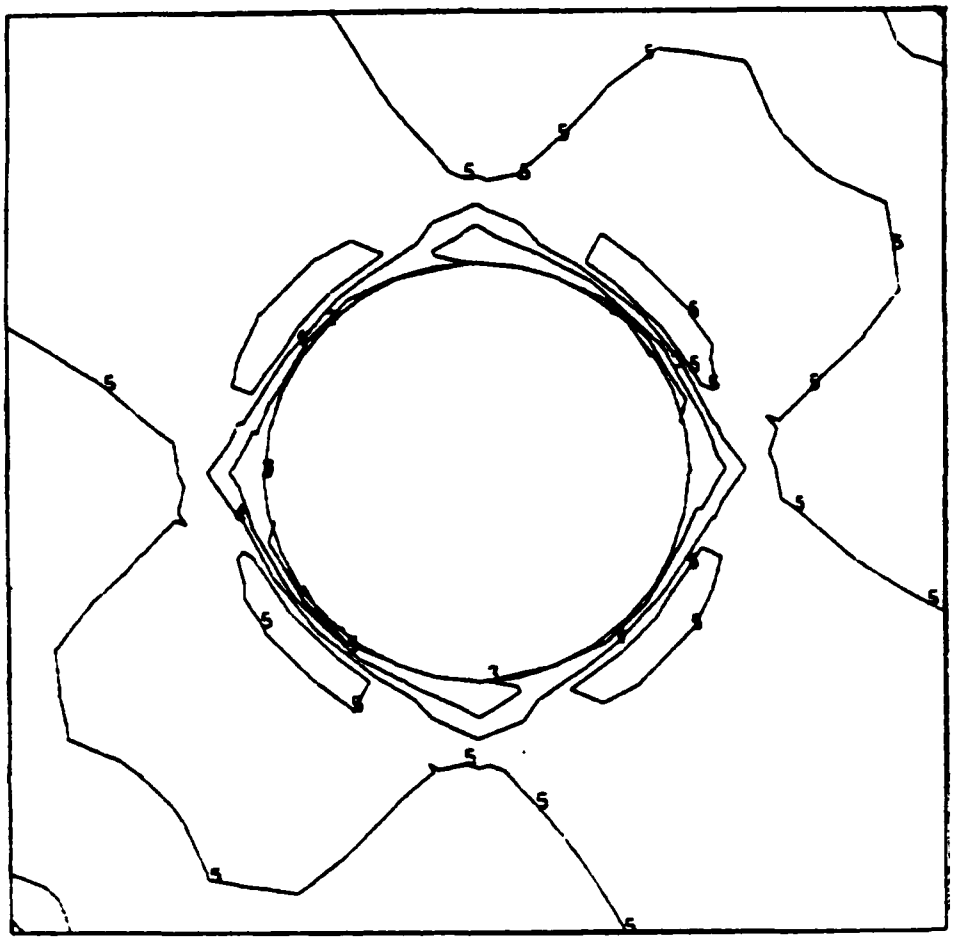

CONTOUR	INDEX
1	-4.0×10^2
2	-2.0×10^2
3	0.0
4	2.0×10^2
5	4.0×10^2
6	6.0×10^2
7	8.0×10^2

N_{xy} Contours at 3000 lb

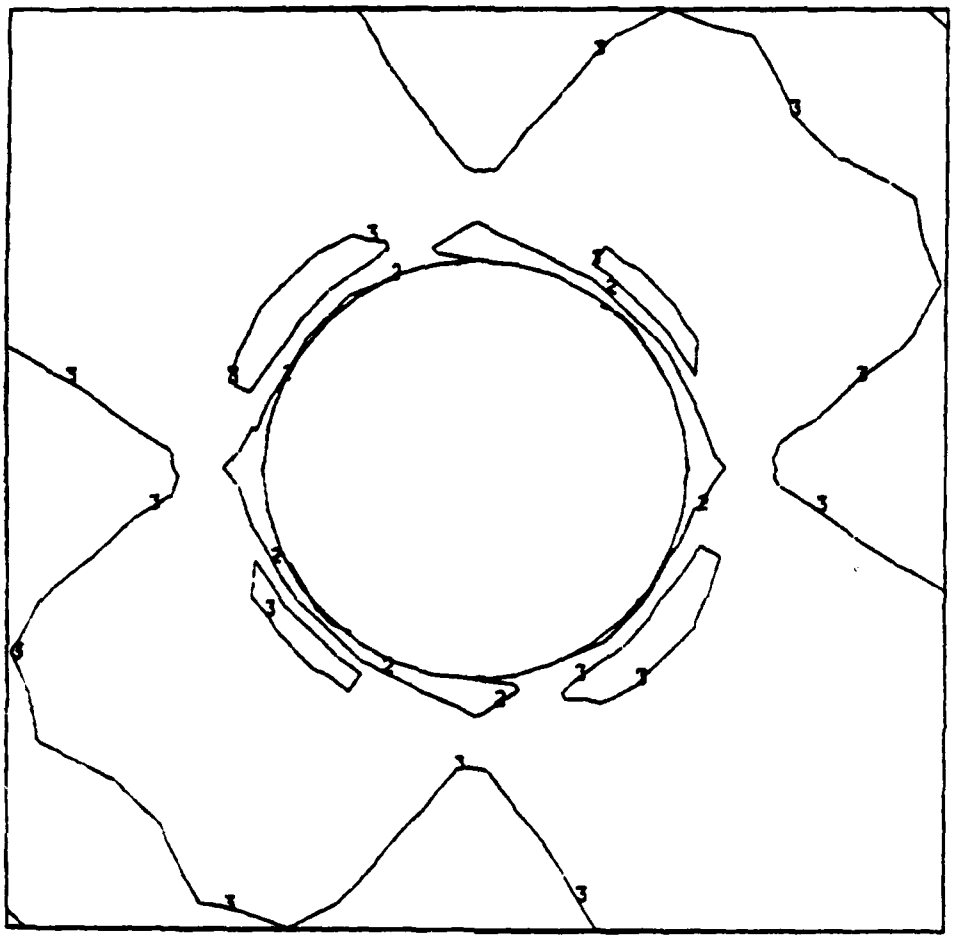

CONTOUR INDEX

1 -5.0×10^2

2 0.0

3 5.0×10^2

4 1.0×10^3

N_{xy} Contours at 3500 lb

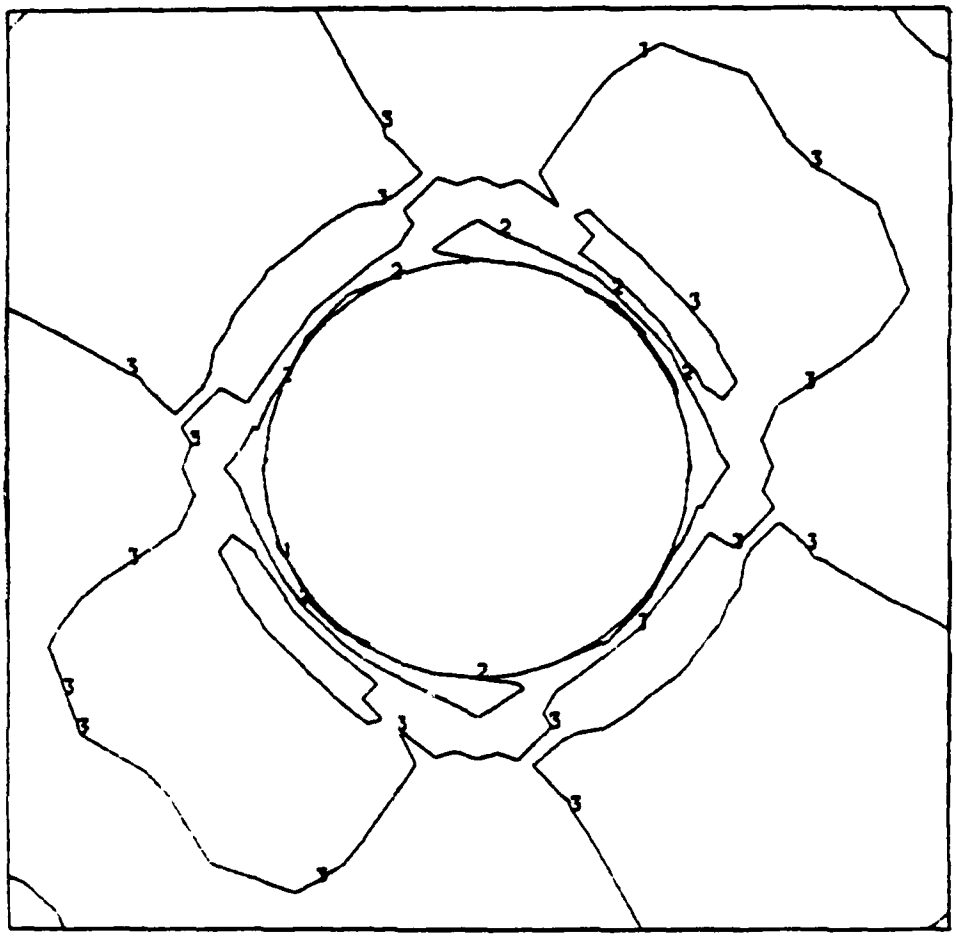

CONTOUR INDEX

1 -5.0×10^2

2 0.0

3 5.0×10^2

4 1.0×10^3

5 1.5×10^3

N_{xy} Contours at 4000 lb

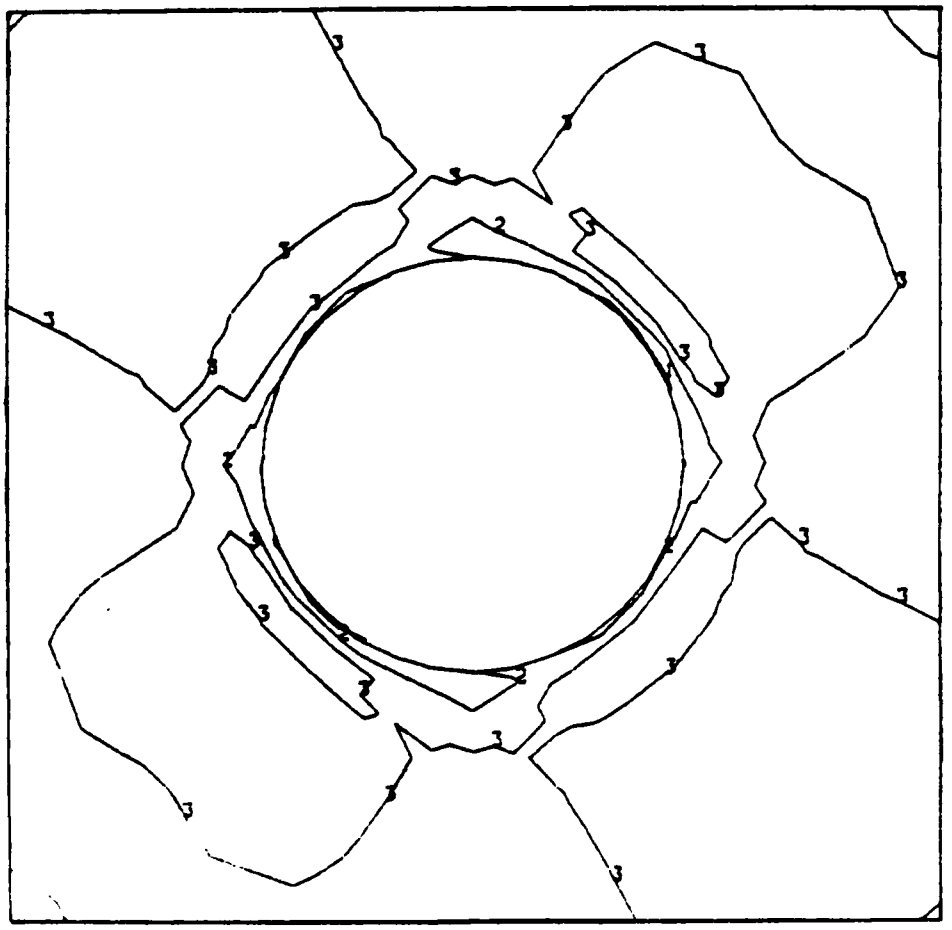

CONTOUR INDEX	
1	-5.0×10^2
2	0.0
3	5.0×10^2
4	1.0×10^3
5	1.5×10^3

N_{xy} Contours at 4250 lb

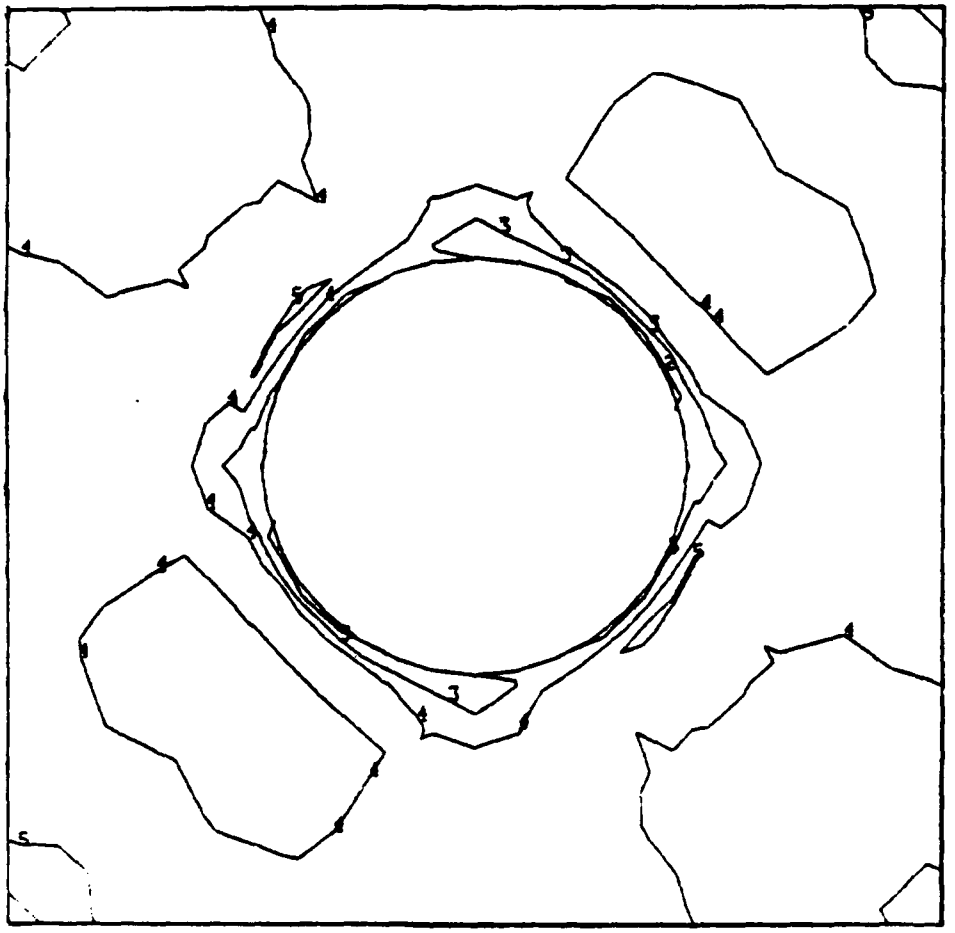

CONTOUR	INDEX
1	-1.0×10^3
2	-5.0×10^2
3	0.0
4	5.0×10^2
5	1.0×10^3
6	1.5×10^3
7	2.0×10^3

N_{xy} Contours at 4400 lb

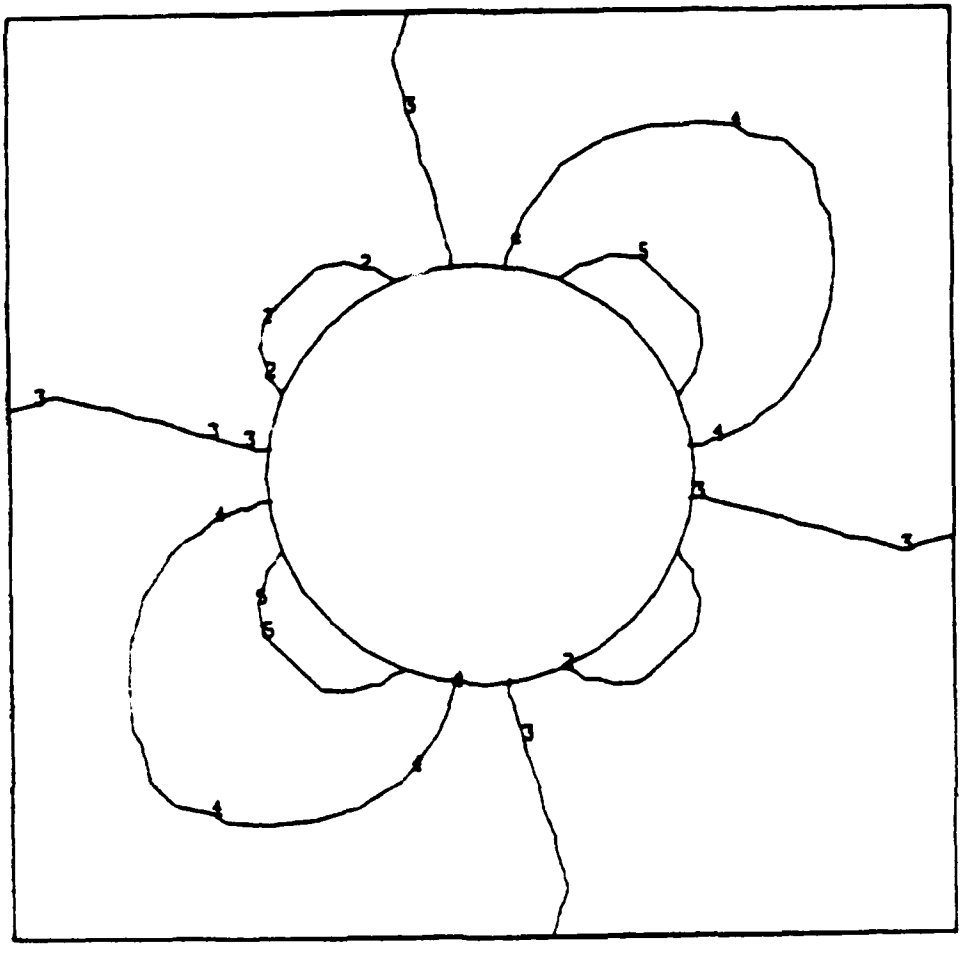

CONTOUR INDEX	
1	-1.5×10^{-3}
2	-10.0×10^{-4}
3	-5.0×10^{-4}
4	0.0
5	5.0×10^{-4}
6	10.0×10^{-4}

Normal Displacement Contours at 250 lb

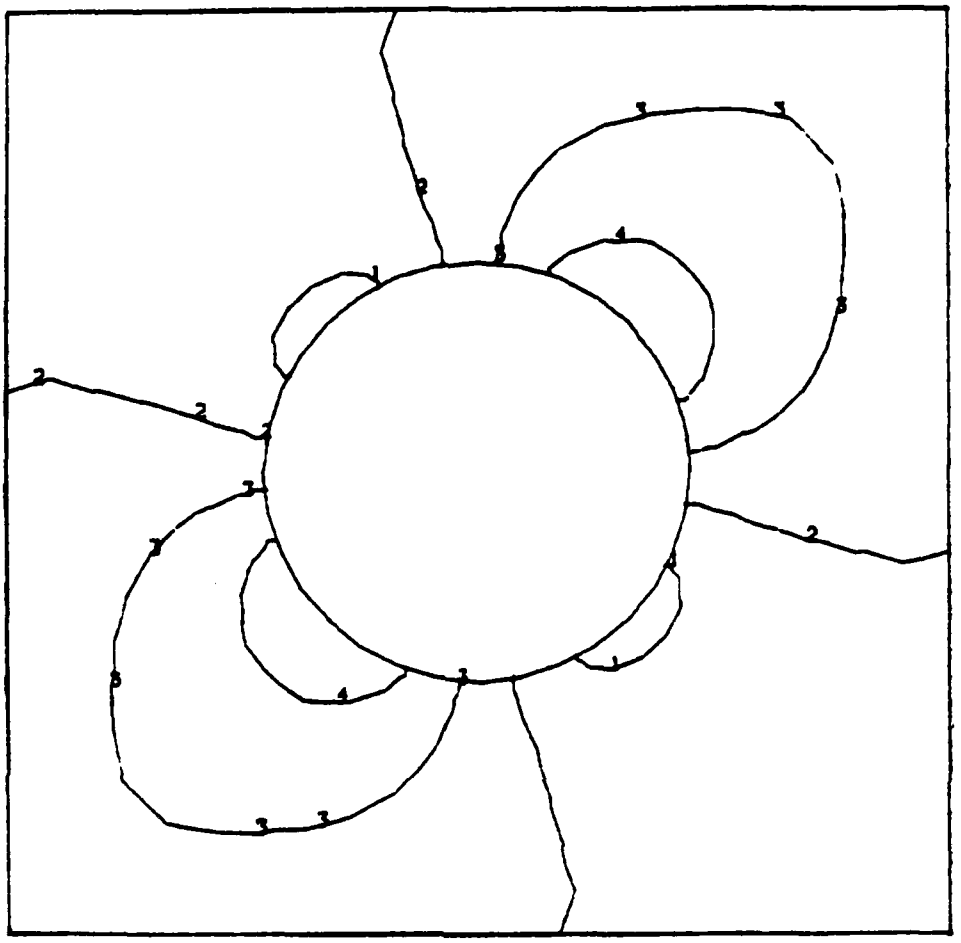

CONTOUR INDEX	
1	-2.0×10^{-3}
2	-10.0×10^{-4}
3	0.0
4	10.0×10^{-4}
5	2.0×10^{-3}

Normal Displacement Contours at 500 lb

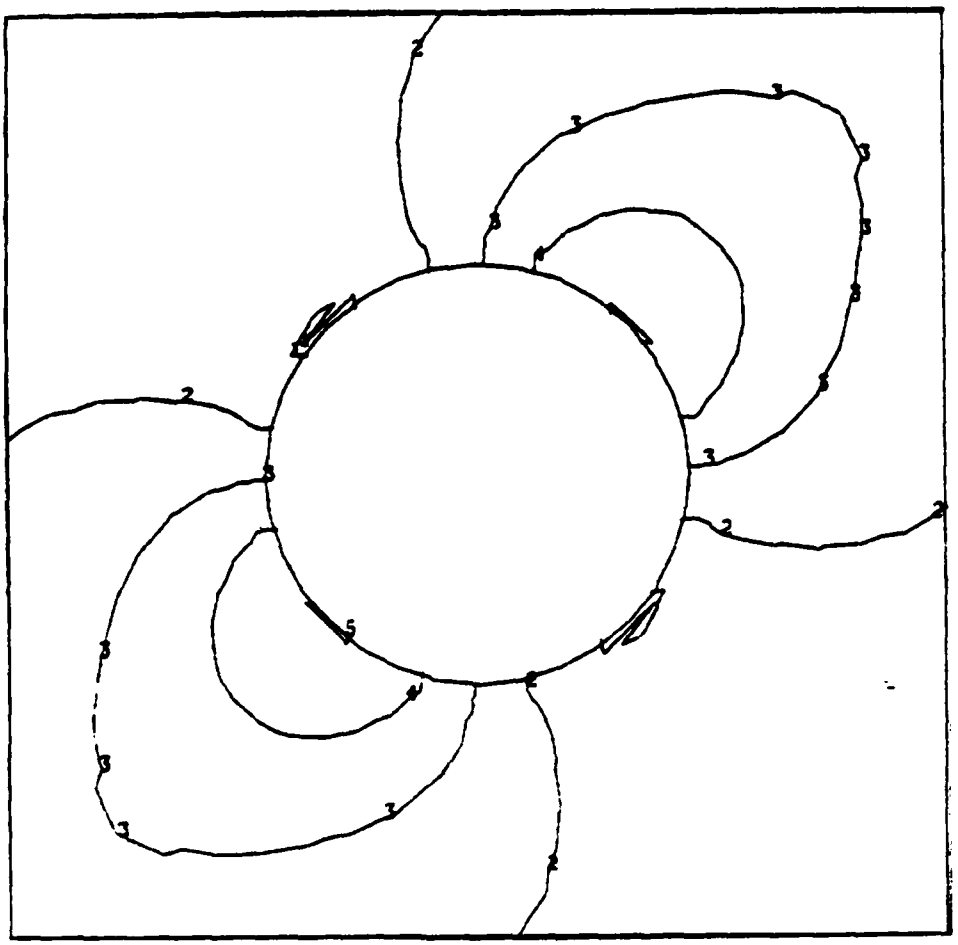

CONTOUR INDEX

1	-4.0×10^{-3}
2	-2.0×10^{-3}
3	0.0
4	2.0×10^{-3}
5	4.0×10^{-3}

Normal Displacement Contours at 1000 lb

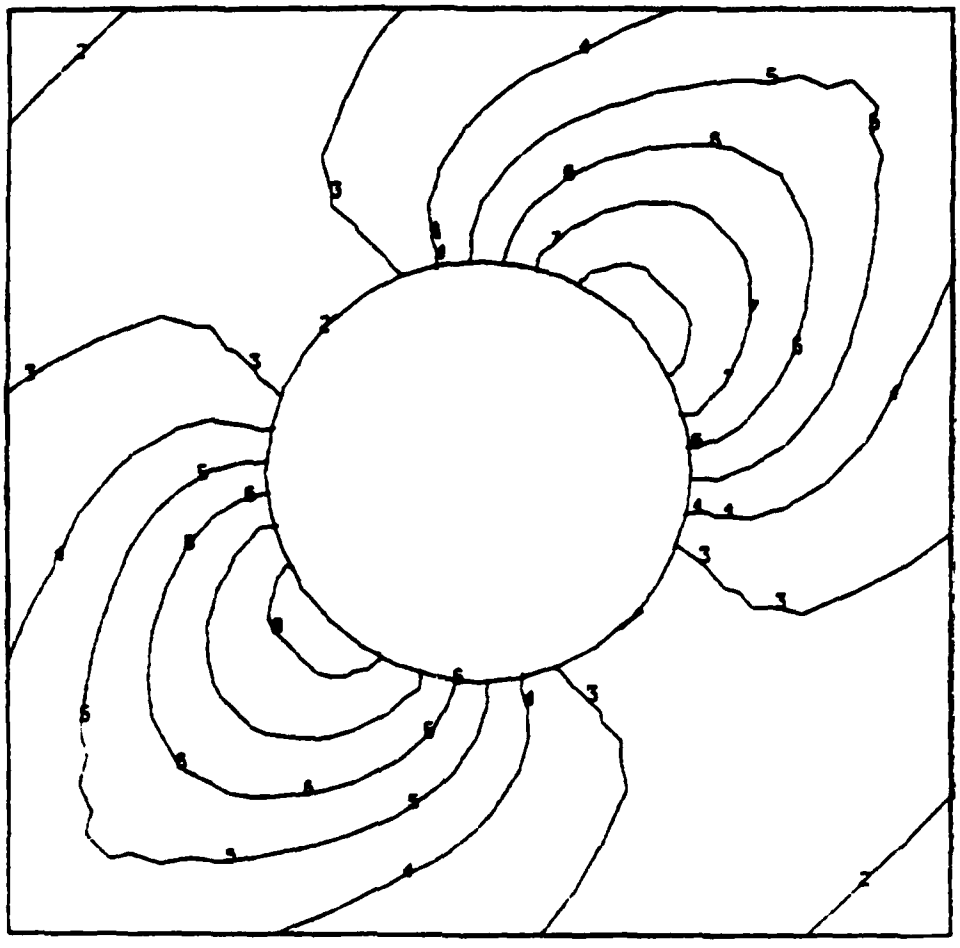

CONTOUR INDEX	
1	-8.0×10^{-3}
2	-6.0×10^{-3}
3	-4.0×10^{-3}
4	-2.0×10^{-3}
5	0.0
6	2.0×10^{-3}
7	4.0×10^{-3}
8	6.0×10^{-3}
9	8.0×10^{-3}

Normal Displacement Contours at 1500 lb

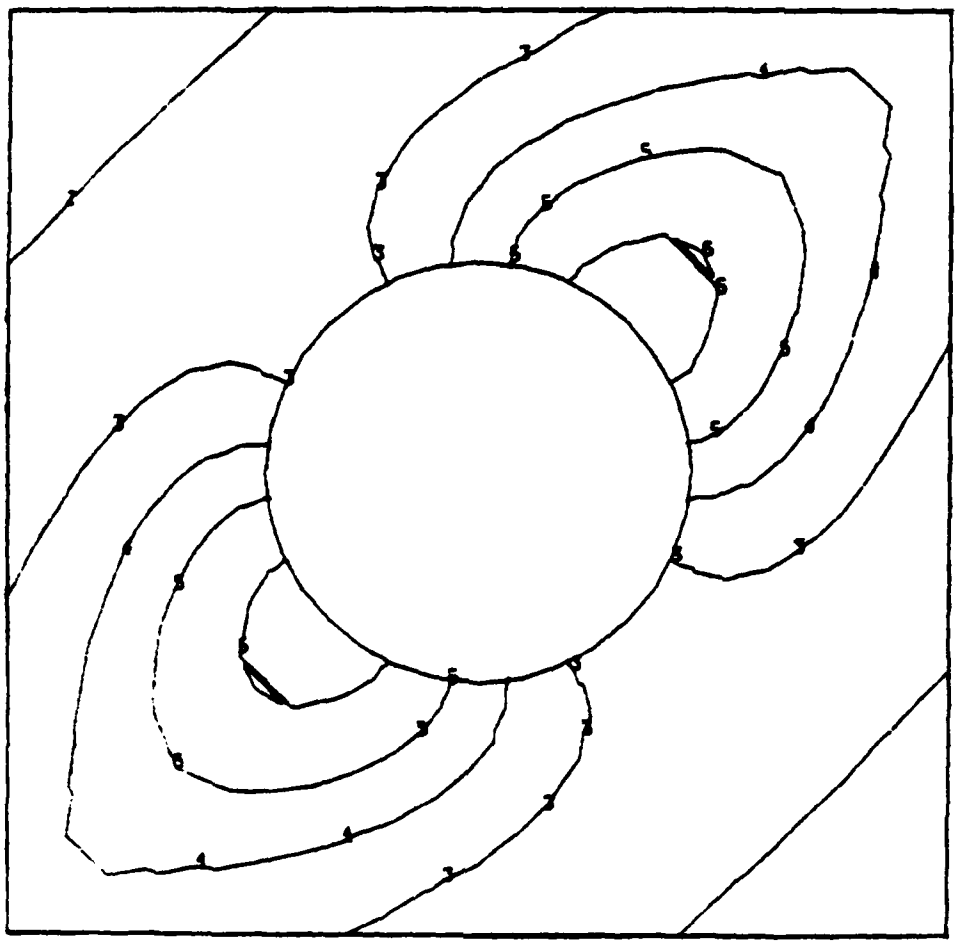

CONTOUR INDEX	
1	-1.5×10^{-2}
2	-10.0×10^{-3}
3	-5.0×10^{-3}
4	0.0
5	5.0×10^{-3}
6	10.0×10^{-3}
7	1.5×10^{-2}

Normal Displacement Contours at 2000 lb

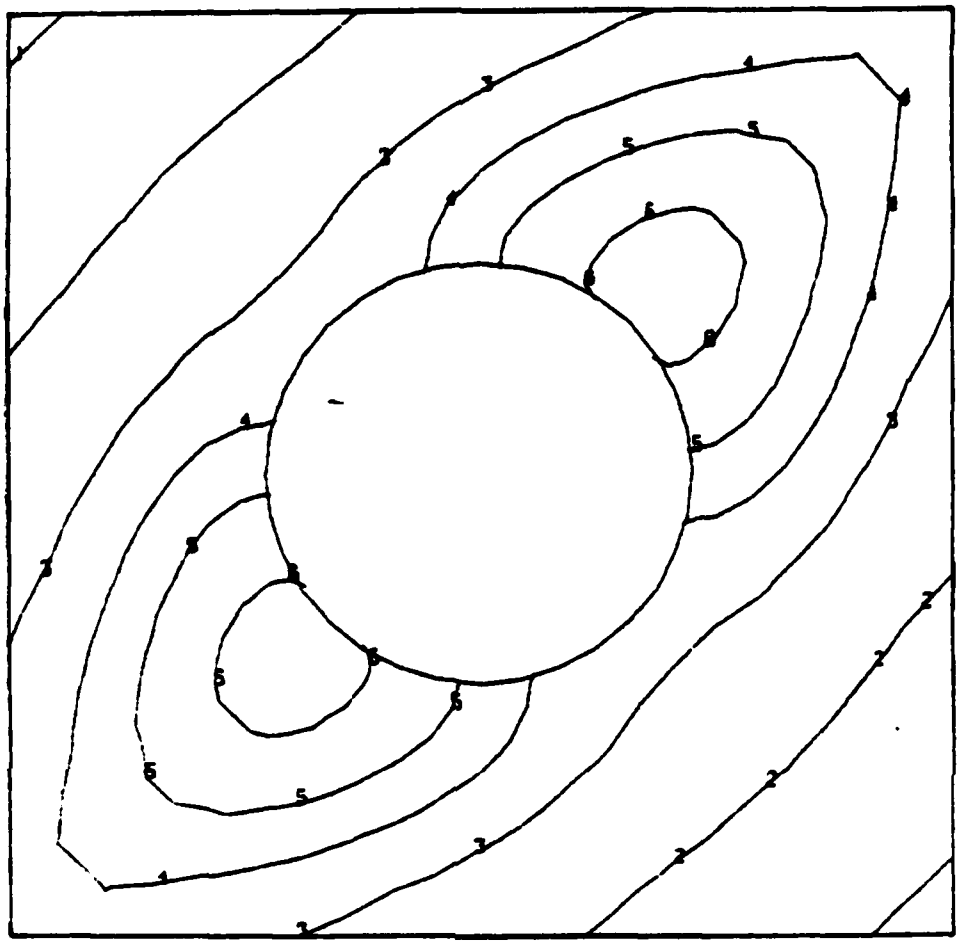

CONTOUR INDEX	
1	-3.0×10^{-2}
2	-2.0×10^{-2}
3	-1.0×10^{-2}
4	0.0
5	10.0×10^{-3}
6	2.0×10^{-2}

Normal Displacement Contours at 2500 lb

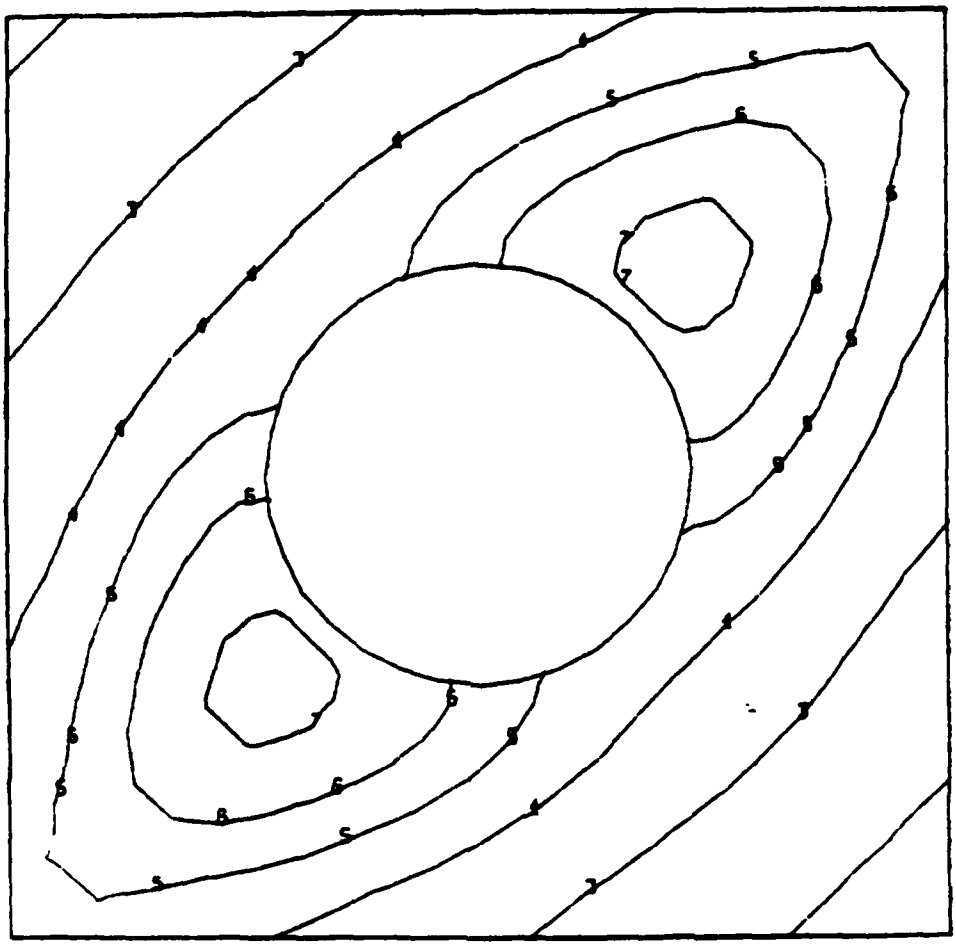

CONTOUR INDEX	
1	-8.0×10^{-2}
2	-6.0×10^{-2}
3	-4.0×10^{-2}
4	-2.0×10^{-2}
5	0.0
6	2.0×10^{-2}
7	4.0×10^{-2}

Normal Displacement Contours at 3000 lb

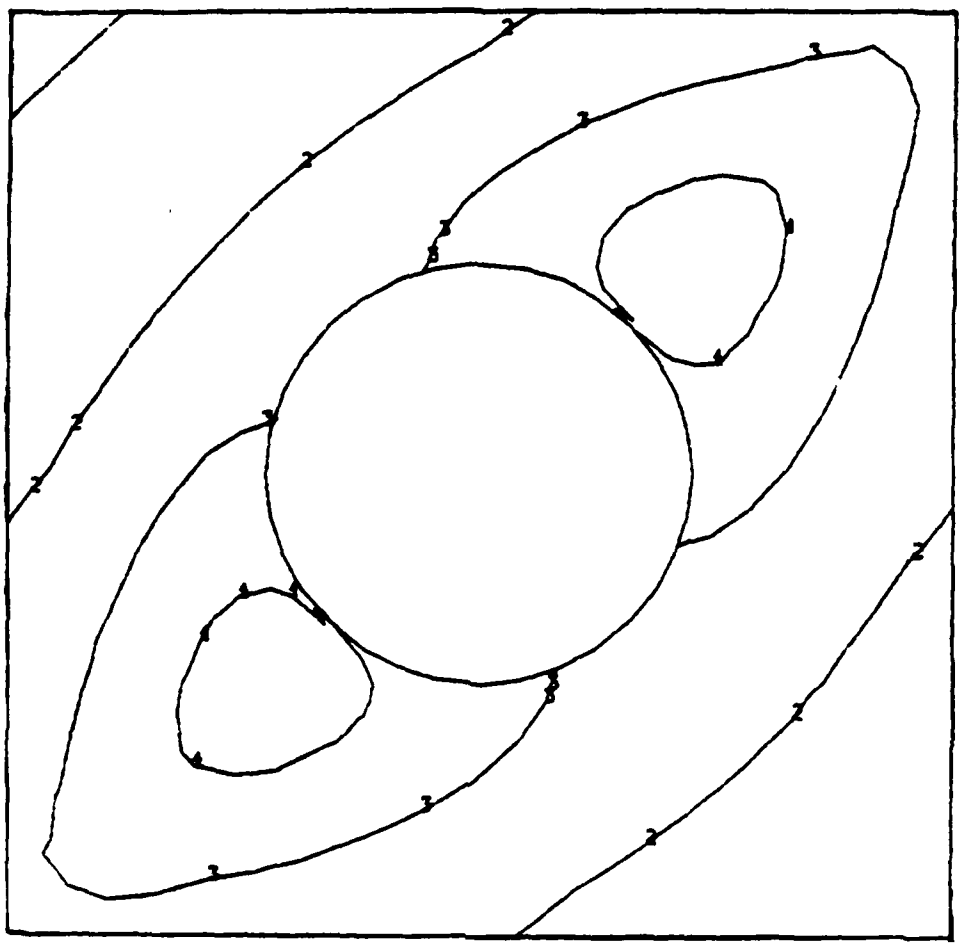

CONTOUR INDEX

1 -10.0×10^{-2}

2 -5.0×10^{-2}

3 0.0

4 5.0×10^{-2}

Normal Displacement Contours at 3500 lb

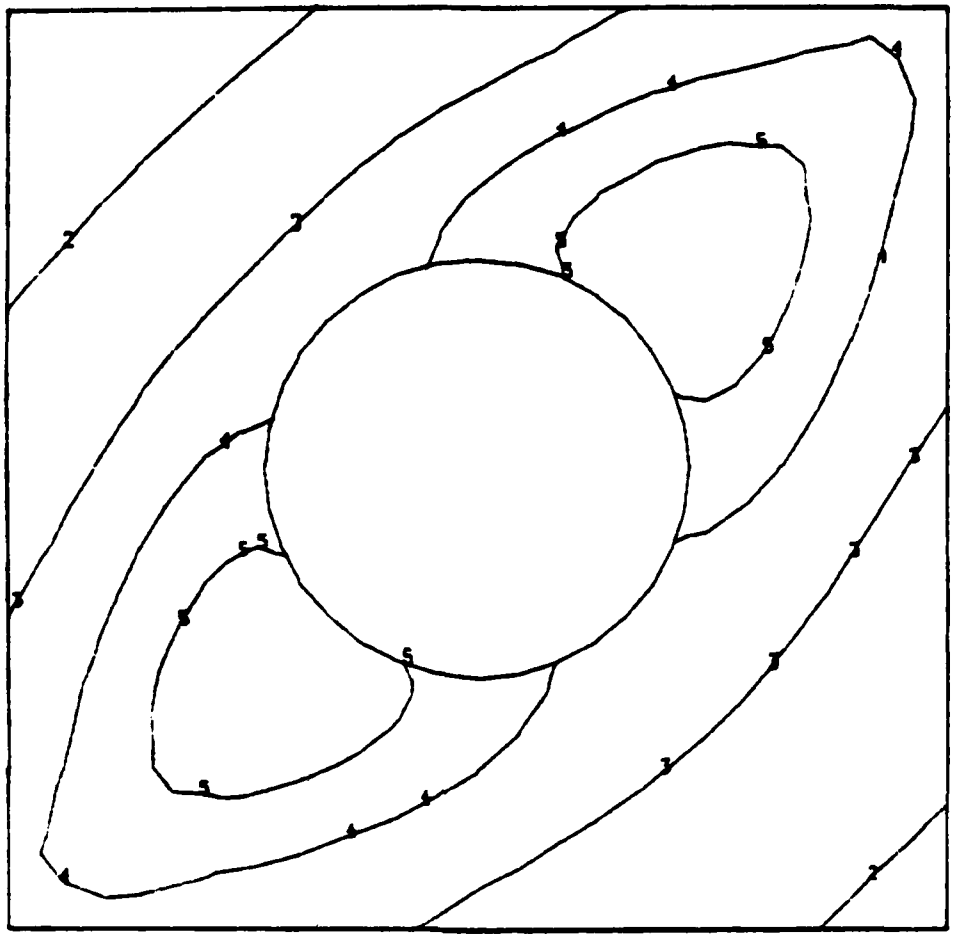

CONTOUR INDEX	
1	-1.5×10^{-1}
2	-10.0×10^{-2}
3	-5.0×10^{-2}
4	0.0
5	5.0×10^{-2}
6	10.0×10^{-2}

Normal Displacement Contours at 4000 lb

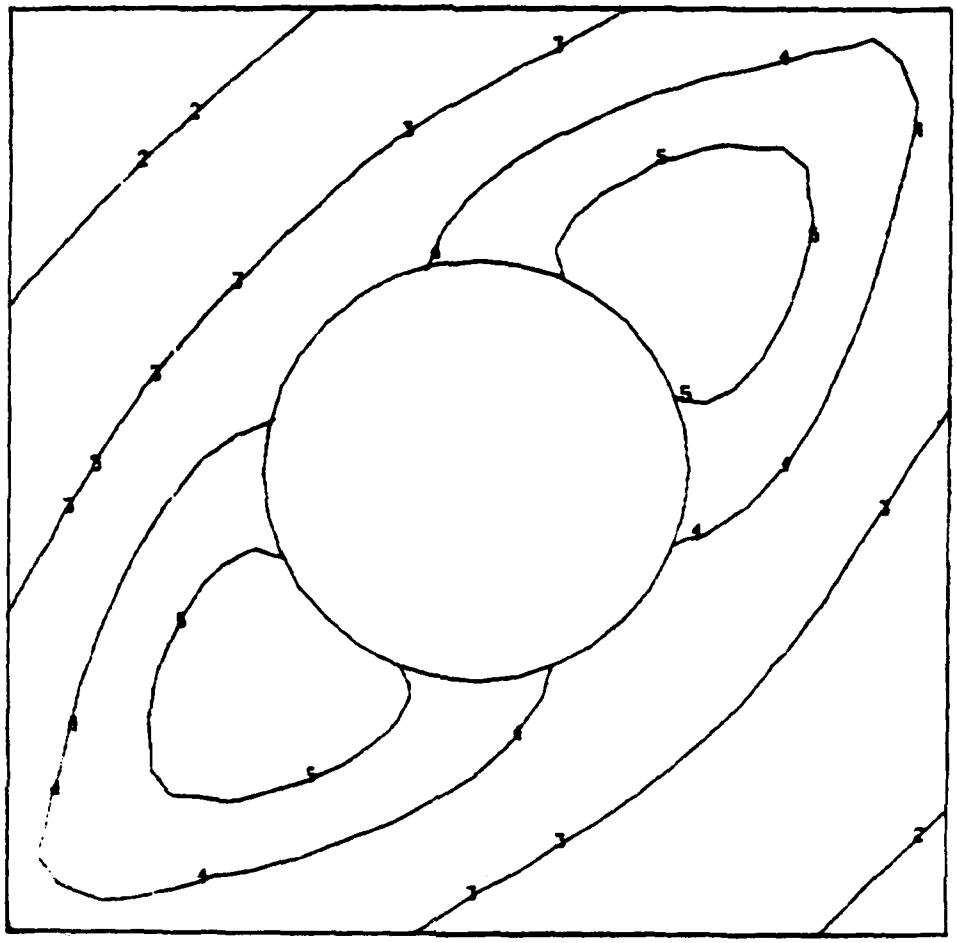

CONTOUR INDEX	
1	-1.5×10^{-1}
2	-10.0×10^{-2}
3	-5.0×10^{-2}
4	0.0
5	5.0×10^{-2}
6	10.0×10^{-2}

Normal Displacement Contours at 4250 lb

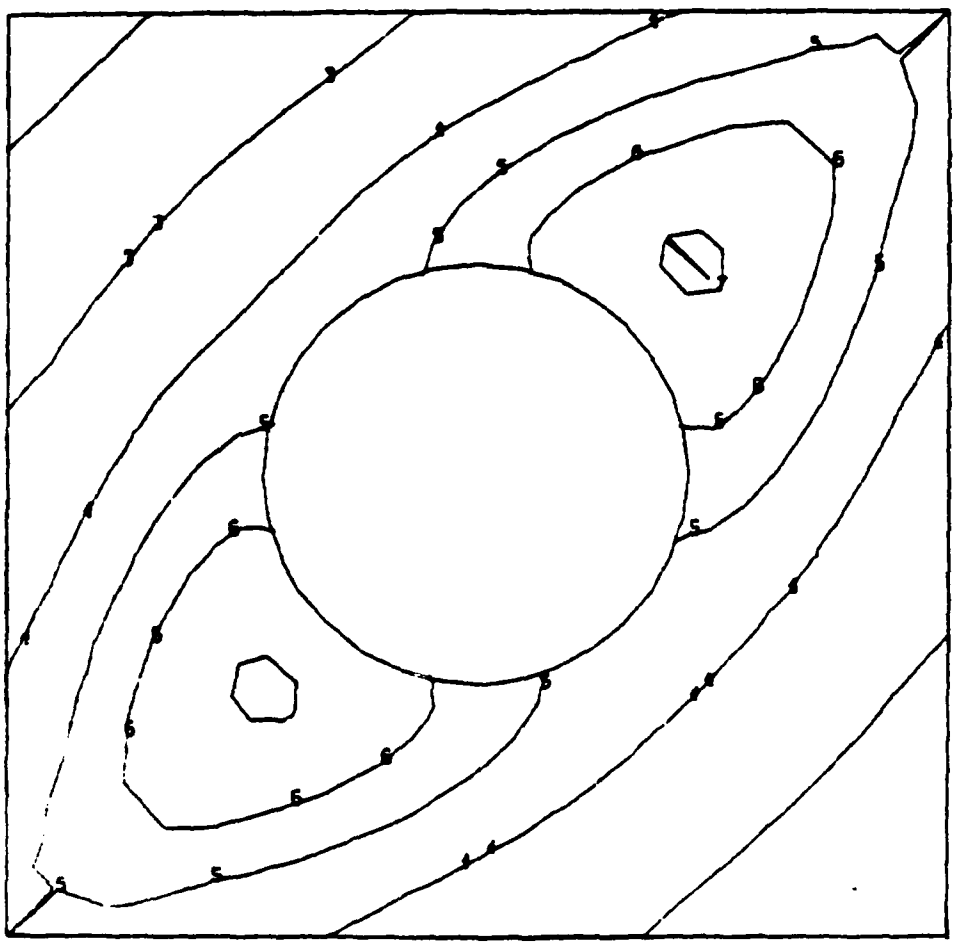

CONTOUR INDEX	
1	-2.0×10^{-1}
2	-1.5×10^{-1}
3	-1.0×10^{-1}
4	-5.0×10^{-2}
5	0.0
6	5.0×10^{-2}
7	10.0×10^{-2}

Normal Displacement Contours at 4400 lb

LIST OF REFERENCES

1. Kaminski, B. E. and Ashton, J. E., "Diagonal Tension Behavior of Boron-Epoxy Shear Panels," Journal of Composite Materials, v. 5, p. 553-558, October 1971.

2. Bhatia, N. M., "Postbuckling Fatigue Behavior of Advanced Composite Shear Panels," Proceedings of the Army Symposium on Solid Mechanics, 1976--Composite Materials, The Influence of Failure on Design, Army Materials and Mechanics Research Center Report MS 76-3, 1976.

3. Naval Air Development Center Contract Report NADC-78137-60, Post-Buckling Fatigue Behavior of Flat, Stiffened Graphite/Epoxy Panels under Shear Loading, by Lockheed Corporation, May 1981.

4. Agarwal, B. L., Postbuckling Behavior of Composite Shear Webs, presented as paper 80-0689 at AIAA/ASME/ASCE/AHS 21st Structures, Structural Dynamics and Materials Conference, Seattle, Washington, 12-14 May 1980.

5. National Advisory Committee for Aeronautics Report NACA WR L-402, The Strength and Stiffness of Shear Webs with and without Lightening Holes, by P. Kuhn, p. 2, June 1942.

6. Lockheed-California Company Report 29056, Advanced Composite Aileron, by L. Fogg, p. 6-5 to 6-14, 1979.

7. Agarwal, B. L. and Broutman, L. J., Analysis and Performance of Fiber Composites, Wiley, 1980.

8. National Advisory Committee for Aeronautics Report NACA WR L-323, The Strength and Stiffness of Shear Webs with Round Lightening Holes having 45° Flanges, by P. Kuhn, December 1942.

9. Air Force Materials Laboratory Contract Report F33615-71-C-1362, Advanced Composites Design Guide, by Rockwell International Corporation, v. II, sec. 2.2.2.2, January 1973.

10. Peery, Aircraft Structures, p. 394, McGraw-Hill, 1950.

11. Ferguson, G. H., Cyr, N. A., and Clark, R. D., DIAL Structural Analysis System User's Manual, Lockheed Missiles and Space Company, Inc., Sunnyvale, California, September 1980.

12. National Aeronautics and Space Administration Report NASA TN D-7996, Numerical Analysis and Parameter Studies of the Buckling of Composite Orthotropic Compression and Shear Panels, by J. M. Housner and M. Stein, October 1975.

13. Air Force Materials Laboratory Contract Report F33615-71-C-1362, Advanced Composites Design Guide, by Rockwell International Corporation, v. II, sec. 2.5.1.2, January 1973.

INITIAL DISTRIBUTION LIST

		No. Copies
1.	Defense Technical Information Center Cameron Station Alexandria, Virginia 22314	2
2.	Library, Code 0142 Naval Postgraduate School Monterey, California 93940	2
3.	Department Chairman, Code 67 Department of Aeronautics Naval Postgraduate School Monterey, California 93940	1
4.	Assoc. Prof. M. H. Bank, Code 034Bt Aviation Safety Programs Naval Postgraduate School Monterey, California 93940	5
5.	Lockheed Missiles and Space Company ATTN: J. A. Bailie P.O. Box 504 Sunnyvale, California 94086 via: Naval Plant Representative Office ATTN: LT M. L. Knaebel Lockheed Missiles and Space Company P.O. Box 504 Sunnyvale, California 94086	5
6.	LCDR R. J. Herman 17926 Carpintero Avenue Bellflower, California 90706	1

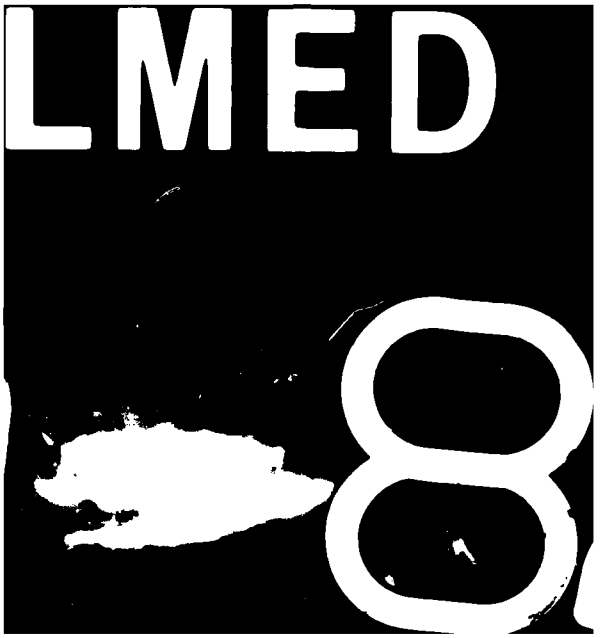
LMED
8